

**CHARACTERIZATION AND
PERFORMANCE ANALYSIS OF MULTI-
STACK VANADIUM REDOX FLOW
BATTERY**

NURIZZATI BINTI MD. NIZAM

UMP

MASTER OF SCIENCE

UNIVERSITI MALAYSIA PAHANG

UNIVERSITI MALAYSIA PAHANG

DECLARATION OF THESIS AND COPYRIGHT

Author's Full Name : NURIZZATI BINTI MD NIZAM

Date of Birth : 24TH SEPTEMBER 1992

Title : CHARACTERIZATION AND PERFORMANCE ANALYSIS
OF MULTI-STACK VANADIUM REDOX FLOW BATTERY

Academic Session : SEM 2 2018/2019

I declare that this thesis is classified as:

- CONFIDENTIAL (Contains confidential information under the Official Secret Act 1997)*
- RESTRICTED (Contains restricted information as specified by the organization where research was done)*
- OPEN ACCESS I agree that my thesis to be published as online open access (Full Text)

I acknowledge that Universiti Malaysia Pahang reserves the following rights:

1. The Thesis is the Property of Universiti Malaysia Pahang
2. The Library of Universiti Malaysia Pahang has the right to make copies of the thesis for the purpose of research only.
3. The Library has the right to make copies of the thesis for academic exchange.

Certified by:

(Student's Signature)

(Supervisor's Signature)

920924-05-5004
New IC/Passport Number
Date:

Associate Prof. Ts. Dr. Mohd
Rusllim Bin Mohamed
Name of Supervisor
Date:

NOTE : * If the thesis is CONFIDENTIAL or RESTRICTED, please attach a thesis declaration letter.

SUPERVISOR'S DECLARATION

I hereby declare that I have checked this thesis and in my opinion, this thesis is adequate in terms of scope and quality for the award of the degree of Master of Science.

(Supervisor's Signature)

Full Name : TS. DR. MOHD RUSLLIM BIN MOHAMED

Position : ASSOCIATE PROFESSOR

Date :



UMP

STUDENT'S DECLARATION

I hereby declare that the work in this thesis is based on my original work except for quotations and citations which have been duly acknowledged. I also declare that it has not been previously or concurrently submitted for any other degree at Universiti Malaysia Pahang or any other institutions.

(Student's Signature)

Full Name : NURIZZATI BINTI MD NIZAM

ID Number : MEE15008

Date :



UMP

CHARACTERIZATION AND PERFORMANCE ANALYSIS OF MULTI-STACK
VANADIUM REDOX FLOW BATTERY

The logo of the University of Malaysia Pahang (UMP) is a shield-shaped emblem. It features a central white vertical band. The left side of the shield is light blue, and the right side is a darker blue. At the top, there is a yellow diamond shape with a light blue ring around it. The text 'NURIZZATI BINTI MD NIZAM' is centered on the white band.

NURIZZATI BINTI MD NIZAM

Thesis submitted in fulfillment of the requirements
for the award of the degree of
Master of Science

UMP

Faculty of Electrical & Electronics Engineering

UNIVERSITI MALAYSIA PAHANG

AUGUST 2019

ACKNOWLEDGEMENTS

I am grateful to Allah SWT, the most powerful and the most merciful for His blessing of giving me this opportunity to complete this project successfully. Not to forget, Peace and Prayers for the Prophet, Muhammad s.a.w.

My sincere appreciation to the project's supervisor, Prof. Madya Ts. Dr. Mohd Rusllim Bin Mohamed for his guidance, patience and support throughout this project completion.

I also wish to thank the laboratory assistance, for all the cooperation and help during the project completion at laboratories and also a few seniors who provided guidance throughout completing this project.

Lastly, I would like to reserve my special thanks to my family, especially to my beloved parents Encik Md Nizam Bin Ab Aziz and Puan Noorlaily Binti Nahar for their unconditional love and continuous support physically, mentally and emotionally. Not forgotten, thanks to my dearest friends whom always gave me their full support and useful advice along the way to finish up this project. Their presences indeed assist me indirectly.



UMP

ABSTRAK

Teknologi penyimpanan tenaga adalah teknologi yang menguruskan sistem bekalan kuasa elektrik demi menjana tenaga dan penjimatan kos bagi syarikat pengeluar utiliti dan pengguna. Kuasa angin, solar, dan kuasa hidroelektrik adalah diantara contoh sumber yang boleh diperbaharui dan ianya digunakan sebagai tenaga alternatif dan tenaga simpanan untuk bekalan kuasa elektrik. Bateri Aliran Redoks (RFB) adalah sistem elektrokimia yang boleh menukar dan menyimpan tenaga berulang kali dalam skala yang besar. Bateri Aliran Redoks Vanadium (VRFB) adalah salah satu teknologi penyimpanan tenaga yang perlu diberikan perhatian disebabkan oleh keupayaannya menyingkir masalah pencampuran elektrolit yang berlaku dalam kalangan Bateri Aliran redoks yang lain. Berkongsi prinsip yang sama untuk menyimpan tenaga luaran seperti sel bahan bakar, RFB mempunyai kelebihan iaitu membalikkan tindak balas elektrokimia dalam sel secara elektrik. Baru-baru ini, banyak penyelidikan mengenai VRFB telah difokuskan di bawah ujian lapangan, peringkat demonstrasi dan penyiasatan masalah – masalah kebocoran oleh getah disekeliling sel, membran, bahan karbon dan pemasangan didalam pembinaan sel, tetapi maklumat mengenai pembinaan sel, pencirian eksperimen, penyediaan elektrolit, dan sistem keseluruhan di bawah kajian masih minima. Projek ini memfokuskan kepada pencirian dan analisis prestasi untuk linierasi VRFB oleh saiz permukaan sel yang berbeza iaitu 25 cm², 56.25 cm² dan 100 cm². Prestasi unit sel berkenaan dengan kecekapan voltan di bawah parameter yang berbeza (kepadatan arus elektrik, kadar aliran elektolit, jumlah elektrolit, suhu sel, keliangan elektrod dan kekonduksian membran) dibentangkan bersama dengan penentuan linearasi sel sambil mengekalkan kecekapan coulombik pada nilai optimumnya iaitu 90%. Sel yang berbeza saiz permukaan mempamerkan ciri – ciri yang berbeza di bawah operasi parameter yang berbeza. Reka bentuk sel terbaik untuk projek ini adalah bagi saiz elektrod 100 cm² pada ketumpatan arus elektrik 50 mA/cm², kadar aliran elektrolit 0.17 cm³/s, jumlah elektrolit 10 cm³, suhu sel 288.15 K, keliangan elektrod 0.94 epsilon dan konduktiviti membran sebanyak 15 S/m. Hubungan antara saiz elektrod VRFB yang pelbagai dianalisis dan dibincangkan untuk mencipta teori-teori bagi linearasi di mana kajian mendapati bahawa terdapat hubungan linear antara ketumpatan arus elektrik, kadar aliran elektrolit, suhu sel dan nilai keliangan elektrod dengan saiz sel yang sama manakala tiada hubungan linear antara jumlah elektrolit dan nilai kekonduksian membran dengan saiz sel yang sama. Akhir sekali, cadangan untuk penambahbaikan sistem dibincangkan.

ABSTRACT

Energy storage technology is a technology that manages power supply system to create energy and cost saving for utilities and consumers. Wind power, solar, and hydroelectric power are examples of renewable resources and are used as an alternative energy and energy storage for power supply. Redox Flow Battery (RFB) is an electrochemical system that could repeatedly convert and store energy in large scale. Vanadium Redox Flow Battery (VRFB) is one of the noteworthy energy storage due to the fact that it eliminates the cross contamination of electrolyte problem that occurs in other redox flow battery. Sharing the same principle of storing the energy externally as fuel cells, RFB has the advantage of being able to electrically reverse the electrochemical reaction within the cell. Much of the emphasis of recent research on vanadium redox flow battery (VRFB) has been focused under field testing, demonstration stage and the investigation of leakage problem caused by rubber seal, membrane, carbon felt and fitting in construction, but information on construction, experimental characterization, electrolyte preparation, and overall systems under study is still minimal. This project focuses on the characterization and performance analysis for linearity of a multi-stack VRFB for different cell stack sizes of 25 cm², 56.25 cm² and 100 cm². The unit cell performance with respect to voltage efficiency under different performance parameters (current density, flow rates, volume of electrolytes, temperature of cell, electrode porosity and membrane conductivity) are presented along with the cell linearity findings while keeping the coulombic efficiency at its optimum value of 90%. The cell stack exhibits different characteristics under different operating parameters. The best cell design for this project is for the electrode size of 100 cm² at current density of 50 mA/cm², flow rate of 0.17 cm³/s, electrolyte volume of 10 cm³, cell temperature of 288.15 K, electrode porosity of 0.94 epsilon and membrane conductivity of 15 S/m. The relation between the size of electrodes in multi-stack VRFB is also analysed and discussed to develop theories for linearity in which it is found that there exists a linear relationship between different current density, flow rate, temperatures of cell and electrode porosity value with the same cell stack size but no linear relationship between different volume of electrolytes and membrane conductivity values with the same cell stack size. Ultimately, suggestion for system improvement is highlighted.

The logo for UMP (Universiti Malaysia Perlis) is a large, stylized letter 'M' composed of four triangles meeting at the center. The top-left triangle is light blue, the top-right is light green, the bottom-left is light purple, and the bottom-right is light teal. The letters 'UMP' are written in a bold, white, sans-serif font across the center of the 'M'.

TABLE OF CONTENT

DECLARATION	
TITLE PAGE	
ACKNOWLEDGEMENTS	ii
ABSTRAK	iii
ABSTRACT	iv
TABLE OF CONTENT	v
LIST OF TABLES	viii
LIST OF FIGURES	x
LIST OF SYMBOLS	xiii
LIST OF ABBREVIATIONS	xiv
CHAPTER 1 INTRODUCTION	1
1.1 Chapter Overview	1
1.2 Introduction	1
1.3 Problem Statement	6
1.4 Objectives	7
1.5 Contribution	7
1.6 Scope of Project	7
1.7 Thesis Outline	8
CHAPTER 2 LITERATURE REVIEW	10
2.1 Chapter Overview	10
2.2 Energy Storage Research	10

2.2.1	Energy Storage Comparison	11
2.2.2	Battery Storage Technologies	13
2.3	Overview of Redox Flow Battery	15
2.3.1	Vanadium RFB	17
2.4	Design Consideration of VRFB	19
2.4.1	Cell Structure	19
2.4.2	Cell Characterization	24
2.5	Performance Parameter of VRFB	28
2.6	Linearity Study	29
2.7	Simulation Method for VRFB	34
2.8	Chapter Conclusion	36
CHAPTER 3 METHODOLOGY		37
3.1	Chapter Overview	37
3.2	Flow Process	37
3.3	Design and dimension of the cell	39
3.4	Interfaces and application mode of COMSOL Multiphysics	42
3.5	Modelling of VRFB	43
3.6	Model Assumption	46
3.7	Chapter Conclusion	46
CHAPTER 4 RESULTS AND DISCUSSION		47
4.1	Chapter Overview	47
4.2	Results and discussion	47
4.3	Results and Analysis of VRFB Modelling	48
4.3.1	Current Density	48

4.3.2	Flow Rates	56
4.3.3	Volume of Electrolytes	64
4.3.4	Temperature of cell	70
4.3.5	Electrode Porosity	77
4.3.6	Membrane Conductivity	84
4.4	Chapter Conclusion	91
CHAPTER 5 CONCLUSION		93
5.1	Chapter Overview	93
5.2	Conclusion	93
5.3	Recommendation	95
REFERENCES		97
APPENDIX A		104
APPENDIX B		106
APPENDIX C		108

A large, semi-transparent watermark of the Ump logo is centered on the page. The logo consists of a shield-like shape with a yellow diamond at the top, a white center, and teal and blue sections at the bottom. The letters 'UMP' are written in white across the bottom of the shield.

UMP

LIST OF TABLES

Table 2.1	Characteristics comparison of energy storage. Adapted from (Dekka, Ghaffari, & Venkatesh, 2015), (H. Chen, Ngoc, Yang, Tan, & Li, 2009), (Schaber, Christopher & Mazza, Patrick & Hammerschlag, 2004) & (International Energy Agency, 2014)	12
Table 2.2	Comparison between several battery technologies. Adapted from (Dekka et al., 2015), (H. Chen et al., 2009), (Rosin & Tallinn, 2012) & (Luo, Wang, Dooner, & Clarke, 2015)	14
Table 3.1	Full dimension of component in VRFB cell	41
Table 4.1	Voltage efficiency of VRFB for different current density applied at different electrode size	50
Table 4.2	Simulation data for different current densities applied at different electrode sizes in a specific time.	51
Table 4.3	Linearity equations and fitting goodness for 25 cm ² of VRFB cell.	52
Table 4.4	Linearity equations and fitting goodness for 56.25 cm ² of VRFB cell.	53
Table 4.5	Linearity equations and fitting goodness for 100 cm ² of VRFB cell.	54
Table 4.6	Voltage efficiency of VRFB for different flow rates applied at different electrode sizes.	59
Table 4.7	Simulation data for different flow rates applied at different electrode sizes in a specific time.	60
Table 4.8	Linearity equations and fitting goodness for 25 cm ² of VRFB cell	61
Table 4.9	Linearity equations and fitting goodness for 56.25 cm ² of VRFB cell.	62
Table 4.10	Linearity equations and fitting goodness for 100 cm ² of VRFB cell	66
Table 4.11	Voltage efficiency of VRFB for different volumes of electrolyte applied at different electrode sizes.	66
Table 4.12	Simulation data for different volumes of electrolyte applied at different electrode sizes at a specific time.	67
Table 4.13	Linearity equations and fitting goodness for 25 cm ² of VRFB cell.	68
Table 4.14	Linearity equations and fitting goodness for 56.25 cm ² of VRFB cell.	68
Table 4.15	Linearity equations and fitting goodness for 100 cm ² of VRFB cell.	69
Table 4.16	Voltage efficiency of VRFB for different temperatures of cell applied at different electrode sizes.	73

Table 4.17	Simulation data for different temperatures of cell applied at different electrode sizes in a specific time.	74
Table 4.18	Linearity equations and fitting goodness for 25 cm ² of VRFB cell.	74
Table 4.19	Linearity equations and fitting goodness for 56.25 cm ² of VRFB cell.	75
Table 4.20	Linearity equations and fitting goodness for 100 cm ² of VRFB cell.	76
Table 4.21	Voltage efficiency of VRFB for different electrode porosities applied at different electrode sizes.	80
Table 4.22	Simulation data for different electrode porosities applied at different electrode sizes at a specific time.	81
Table 4.23	Linearity equations and fitting goodness for 25 cm ² of VRFB cell.	82
Table 4.24	Linearity equations and fitting goodness for 56.25 cm ² of VRFB cell.	82
Table 4.25	Linearity equations and fitting goodness for 100 cm ² of VRFB cell.	83
Table 4.26	Voltage efficiency of VRFB for different membrane conductivities applied on different electrode sizes.	87
Table 4.27	Simulation data for different membrane conductivities applied at different electrode sizes in a specific time.	88
Table 4.28	Linearity equations and fitting goodness for 25 cm ² of VRFB cell.	89
Table 4.29	Linearity equations and fitting goodness for 56.25 cm ² of VRFB cell.	90
Table 4.30	Linearity equations and fitting goodness for 100 cm ² of VRFB cell.	90

LIST OF FIGURES

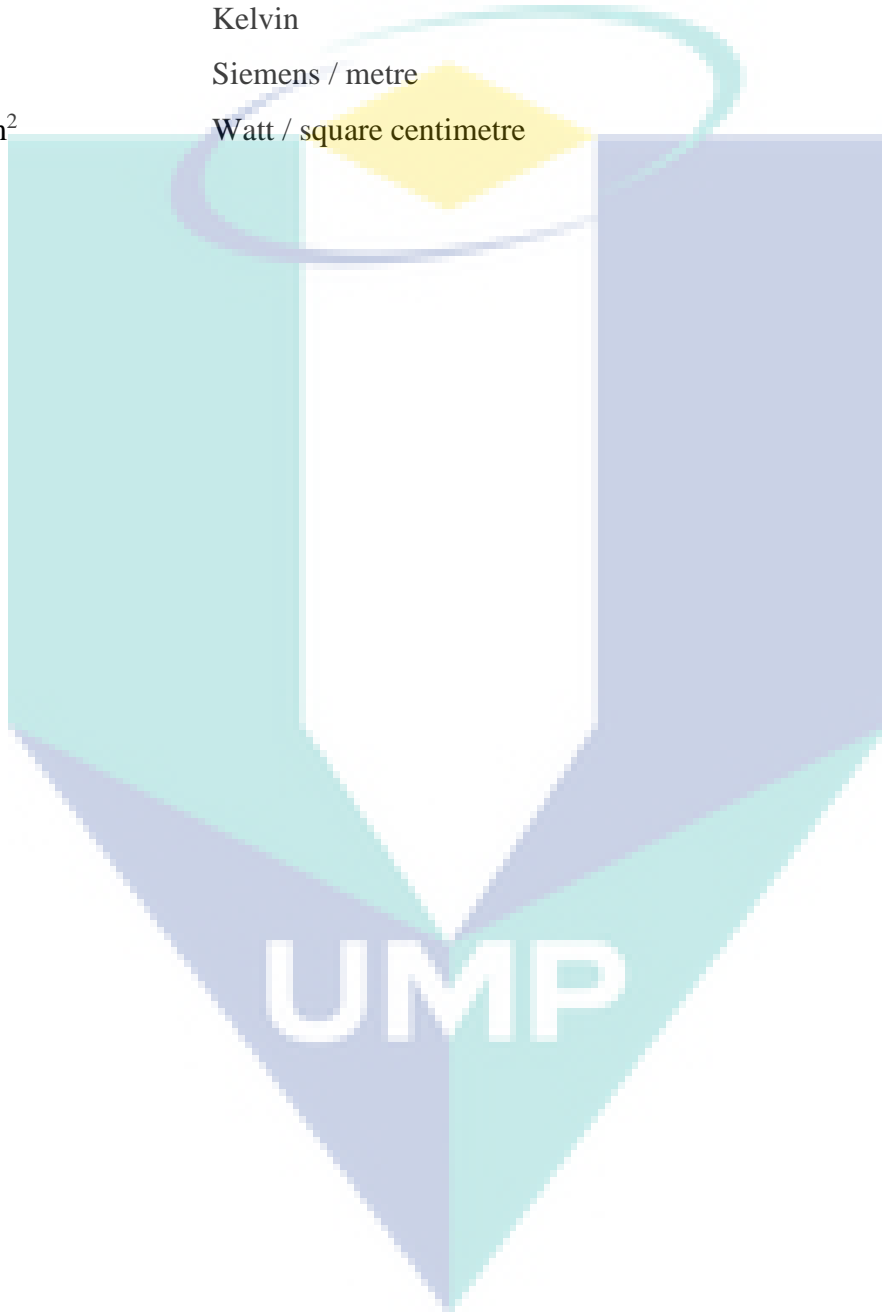
Figure 2.1	Electricity storage installed capacity in 2012 (MW). Adapted from (Abbas A. Akhil, Georgianne Huff, Aileen B. Currier, Benjamin C. Kaun & Stella Bingqing Chen, Andrew L. Cotter, Dale T. Bradshaw, 2013)	11
Figure 2.2	VRFB configuration. Adapted from (Barsukov, 2013)	18
Figure 2.3	The structure of 25 cm ² VRFB cell. Adapted from (Boaventura et al., 2018)	23
Figure 3.1	Flow Process of the project	39
Figure 3.2	Components of battery design	40
Figure 3.3	Full diagram of geometry drawing with different size of electrodes (side view)	40
Figure 3.4	Full diagram of geometry drawing with different size of electrodes (front view)	41
Figure 4.1	Cell voltage vs. time representing charge – discharge characteristics of a 25 cm ² VRFB under controlled current density (50, 75 and 100 mA/cm ²) for 10 cm ³ volume of electrolyte at constant linear flow rate of 0.17 cm ³ /s, temperature of 298.15 K, electrode porosity of 0.94 and membrane conductivity of 15 S/m.	49
Figure 4.2	Cell voltage vs. time representing charge – discharge characteristics of a 56.25 cm ² VRFB under controlled current density (50, 75 and 100 mA/cm ²) for 10 cm ³ volume of electrolyte at constant linear flow rate of 0.17 cm ³ /s, temperature of 298.15 K, electrode porosity of 0.94 and membrane conductivity of 15 S/m.	49
Figure 4.3	Cell voltage vs. time representing charge – discharge characteristics of a 100 cm ² VRFB under controlled current density (50, 75 and 100 mA/cm ²) for 10 cm ³ volume of electrolyte at constant linear flow rate of 0.17 cm ³ /s, temperature of 298.15 K, electrode porosity of 0.94 and membrane conductivity of 15 S/m.	50
Figure 4.4	Relationship trend between cell voltage vs. different cell stack size (25, 56.25 and 100 cm ²) for current density of 50, 75 and 100 mA/cm ² .	55
Figure 4.5	Cell voltage vs. time representing charge – discharge characteristics of a 25 cm ² VRFB under 100 mA/cm ² current density.	56
Figure 4.6	Cell voltage vs. time representing charge – discharge characteristics of a 25 cm ² VRFB at controlled flow rate (0.17, 0.50 and 0.83 cm ³ /s) for 10 cm ³ volume of electrolyte at constant temperature of 298.15 K, current density of 50 mA/cm ² , electrode porosity of 0.94 and membrane conductivity of 15 S/m.	57

Figure 4.7	Cell voltage vs. time representing charge – discharge characteristics of a 56.25 cm ² VRFB at controlled flow rate (0.17, 0.50 and 0.83 cm ³ /s) for 10 cm ³ volume of electrolyte at constant temperature of 298.15 K, constant current density of 50 mA/cm ² , electrode porosity of 0.94 and membrane conductivity of 15 S/m.	58
Figure 4.8	Cell voltage vs. time representing charge – discharge characteristics of a 100 cm ² VRFB at controlled flow rate (0.17, 0.50 and 0.83 cm ³ /s) for 10 cm ³ volume of electrolyte at constant temperature of 298.15 K, current density of 50 mA/cm ² , electrode porosity of 0.94 and membrane conductivity of 15 S/m.	58
Figure 4.9	Relationship trend between cell voltage vs. different cell stack size (25, 56.25 and 100 cm ²) for flow rate of 0.17, 0.50 and 0.83 cm ³	63
Figure 4.10	Cell voltage vs. time representing charge – discharge characteristics of a 25 cm ² VRFB at controlled volume of electrolyte (10, 20, 30, 40 and 50 cm ³) at constant flow rate of 0.17 cm ³ /s, temperature of 298.15 K, current density of 50 mA/cm ² , electrode porosity of 0.94 and membrane conductivity of 15 S/m.	64
Figure 4.11	Cell voltage vs. time representing charge – discharge characteristics of a 56.25 cm ² VRFB at controlled volume of electrolyte (10, 20, 30, 40 and 50 cm ³) at constant flow rate of 0.17 cm ³ /s, temperature of 298.15 K, current density of 50 mA/cm ² , electrode porosity of 0.94 and membrane conductivity of 15 S/m.	65
Figure 4.12	Cell voltage vs. time representing charge – discharge characteristics of a 100 cm ² VRFB at controlled volume of electrolyte (10, 20, 30, 40 and 50 cm ³) at constant flow rate of 0.17 cm ³ /s, temperature of 298.15 K, current density of 50 mA/cm ² , electrode porosity of 0.94 and membrane conductivity of 15 S/m.	65
Figure 4.13	Relationship trend between cell voltage vs. different cell stack size (25, 56.25 and 100 cm ²) for volume of electrolyte of 10, 30 and 50 cm ³ .	70
Figure 4.14	Cell voltage vs. time representing charge – discharge characteristics of a 25 cm ² VRFB under controlled temperatures (288.15, 293.15 and 298.15 K) for 10 cm ³ volume of electrolyte at constant linear flow rate of 0.17 cm ³ /s, current density of 50 mA/cm ² , electrode porosity of 0.94 and membrane conductivity of 15 S/m.	71
Figure 4.15	Cell voltage vs. time representing charge – discharge characteristics of a 56.25 cm ² VRFB under controlled temperatures (288.15, 293.15 and 298.15 K) for 10 cm ³ volume of electrolyte at constant linear flow rate of 0.17 cm ³ /s, current density of 50 mA/cm ² , electrode porosity of 0.94 and membrane conductivity of 15 S/m.	71
Figure 4.16	Cell voltage vs. time representing charge – discharge characteristics of a 100 cm ² VRFB under controlled temperatures (288.15, 293.15 and 298.15 K) for 10 cm ³ volume of electrolyte at constant linear flow rate of 0.17 cm ³ /s, current density of 50	

	mA/cm ² , electrode porosity of 0.94 and membrane conductivity of 15 S/m.	72
Figure 4.17	Relationship trend between cell voltage vs. different cell stack size (25, 56.25 and 100 cm ²) for temperature of cell of 288.15, 293.15 and 298.15 K.	77
Figure 4.18	Cell voltage vs. time representing charge – discharge characteristics of a 25 cm ² VRFB at controlled electrode porosity (0.92, 0.93 and 0.94) with constant flow rate of 0.17 cm ³ /s, volume of 10 cm ³ , temperature of 298.15 K, membrane conductivity of 15 S/m and current density of 50 mA/cm ² .	78
Figure 4.19	Cell voltage vs. time representing charge – discharge characteristics of a 56.25 cm ² VRFB at controlled electrode porosity (0.92, 0.93 and 0.94) with constant flow rate of 0.17 cm ³ /s, volume of 10 cm ³ , temperature of 298.15 K, membrane conductivity of 15 S/m and current density of 50 mA/cm ² .	78
Figure 4.20	Cell voltage vs. time representing charge – discharge characteristics of a 100 cm ² VRFB at controlled electrode porosity (0.92, 0.93 and 0.94) with constant flow rate of 0.17 cm ³ /s, volume of 10 cm ³ , temperature of 298.15 K, membrane conductivity of 15 S/m and current density of 50 mA/cm ² .	79
Figure 4.21	Relationship trend between cell voltage vs. different cell stack size (25, 56.25 and 100 cm ²) for electrode porosity of 0.92, 0.93 and 0.94.	84
Figure 4.22	Cell voltage vs. time representing charge – discharge characteristics of a 25 cm ² VRFB at controlled membrane conductivity (5, 10 and 15 S/m) with constant flow rate of 0.17 cm ³ /s, volume of 10 cm ³ , temperature of 298.15 K, electrode porosity of 0.94 and current density of 50 mA/cm ² .	85
Figure 4.23	Cell voltage vs. time representing charge – discharge characteristics of a 56.25 cm ² VRFB at controlled membrane conductivity (5, 10 and 15 S/m) with constant flow rate of 0.17 cm ³ /s, volume of 10 cm ³ , temperature of 298.15 K, electrode porosity of 0.94 and current density of 50 mA/cm ² .	85
Figure 4.24	Cell voltage vs. time representing charge – discharge characteristics of a 100 cm ² VRFB at controlled membrane conductivity (5, 10 and 15 S/m) with constant flow rate of 0.17 cm ³ /s, volume of 10 cm ³ , temperature of 298.15 K, electrode porosity of 0.94 and current density of 50 mA/cm ² .	86
Figure 4.25	Relationship trend between cell voltage vs. different cell stack size (25, 56.25 and 100 cm ²) for membrane conductivity of 5, 10 and 15 S/m.	91

LIST OF SYMBOLS

mA/cm^2	Mill ampere / square centimetre
cm^3/s	Cubic centimetre / second
cm^3	Cubic centimetre
K	Kelvin
S/m	Siemens / metre
W/cm^2	Watt / square centimetre



LIST OF ABBREVIATIONS



VRFB	Vanadium redox flow battery
EIA	Energy Information Administration
IEO2013	International Energy Outlook 2013
RFB	Redox flow battery
DOD	Depth of discharge
UNSW	University of New South Wales
GW	Gigawatt
SMES	Superconducting Magnetic Energy Storage
LA	Lead Acid
NaS	Sodium Sulphur
Li-ion	Lithium ion
Zn-Br	Zinc Bromine
SOC	State of Charge
MATLAB	Matrix Laboratory
ODE	Ordinary Differential Equations
RK	Runge – Kutta
DAE	Differential Algebraic Equation
EIS	Electrochemical Impedance Spectroscopy
MSA	Measurement System Analysis
PEMFC	Proton Exchange Membrane Fuel Cells

CHAPTER 1

INTRODUCTION

1.1 Chapter Overview

This chapter covers the introduction to characterization and performance comparison of multi stack vanadium redox flow battery (VRFB). In the introduction section, several facts and figures regarding the world energy demand and the basis of redox flow battery are discussed. Problem statement, objectives, contribution, scope of project, and thesis outline are also presented in this chapter.

1.2 Introduction

Energy is one of the most important driving forces for a nation to develop as it is used in almost all section in daily life which includes all sector such as telecommunication, transportation, agriculture, and industrial activities that influences the economic growth. The worldwide energy demand is continuously growing day by day and according to the forecasts of the U.S. Energy Information Administration (EIA), the consumption of energy around the world is expected to increase by 56% between the year of 2010 and 2040 (U.S. Energy Information Agency, 2013). United Nations also predicted that world population will grow from 6.7 billion in the year of 2011 to 8.7 billion by 2035 which will result on an increase for energy demand substantially over that period of time (“World Energy Needs and Nuclear Power,” 2015).

A convenient source of energy is electricity and it can be generated through a number of ways. One of the ways is by using a primary energy sources which is fossil fuels. Fossil fuel is a type of non-renewable energy where some examples of it consists of coal, oil and natural gas. It also plays a vital role in global electricity generation. In 2012

alone, fossil fuels accounted for 87% of primary energy consumption worldwide (Milena Gonzales and Matt Lucky, 2013). Even in some countries such as Malaysia, the energy produced is more dependent towards fossil fuel sources where in the year of 2009, almost 94.5% of its electricity generation came from fossil fuels (Shafie, Mahlia, Masjuki, & Andriyana, 2011).

Although the fossil fuels reserve will last for the next decades, it is still limited in supply and it might not be able to cover the increasing global consumption of energy in the future. Besides that, in terms of environmental issue, there will be changes in climates due to the increase in the atmospheric carbon dioxide content as generation of electricity is one of the major sources of carbon dioxide emissions to atmosphere due to burning of fossil fuels (“Climate Change – The Science,” 2014). Thus, with the depletion of fossil fuel and growing of electricity demands globally, researchers has begun looking at other possibilities to ensure future energy security (General Dr. Mohamed ElBaradei, 2014).

According to International Energy Outlook 2013 (IEO2013), since the early 2000s, the high price of fossil fuels combines with concerns about environmental effects of greenhouse gas emission resulted in researchers interest in developing alternatives for fossil fuels specifically towards renewable energy sources and nuclear power (U.S. Energy Information Agency, 2013). However, there only exists limited prospects for nuclear power, ultimately, to only four unresolved problems which are: environmental and health issues, higher lifetime overall costs, and has perceived adverse safety. Other unresolved challenges include the long-term management of radioactive wastes and its proliferation is such that nuclear power entails potential security risks, notably the possible misuse of commercial or associated nuclear facilities (Massachusetts Institute of Technology, 2003).

Therefore, renewable energy is projected to be the fastest-growing source of generation of electricity with increasing percentage of 2.5% each year from 11% of total energy consumption in 2010 to 15% in 2040 (U.S. Energy Information Agency, 2013). In the meanwhile, as reported by David Fessler (Fessler, 2015), renewable energy sources now generate about 28% of the global electricity, up from 25% in 2013 and it is the first time in 40 years that global carbon emission has stabilized despite an increase in the energy consumption annually. This shows that an increase in renewable energy usage and

improvements in energy efficiency are responsible for this. Thus, it becomes clear that future clean energy supply can only be guaranteed through the increase usage of renewable energy sources.

However, since the sun is not always shining and the wind is not always blowing in any desirable location, there has been an increased call for researchers to deploy a new technology called energy storage system to store the energy produced by the renewable energy resources (Denholm, Ela, Kirby, & Milligan, 2010). The other reason on why this new technology is introduced is also due to intermittent and creating fluctuation along with non-dispatchable problem in electricity generation caused by renewable energy (Parasuraman, Mariana, Menictas, & Skyllas-kazacos, 2013).

In particular, energy storage is a system that provides an alternative problem solving in the generation balancing and power consumptions (European Commission Directorate-General for Energy, 2013). It can also be said that the system has become a modern demand with a high increase of alternative resources. Energy storage technology functions as a load leveller where it levels the power load by storing power during off – peak hours and later discharging it during peak hours (Shigematsu, 2011). Among the energy storage technologies being explored and developed today, battery energy storage technology is considered to be the most viable one compared to the others.

As there are many types of battery energy storage being introduced, one of it that has gained the most attention is the redox flow battery (RFB). RFB is a type of electrochemical energy storage system that stores energy in the form of two solutions made up of different redox couples. It has many technical merits compared to other energy storage systems as they represent an outstanding union of energy efficiency, life cycle costs and capital cost (Prifti, Parasuraman, Winardi, Lim, & Skyllas-Kazacos, 2012). Above all, the most attractive features of this technology are its flexibility and scalability, high round-trip efficiency, fast responsiveness, independent sizing of power and energy, high depth of discharge (DOD), long durability, and also reducing the environmental impact. All of these allow wide ranges of operational powers and discharge times to takes place, making RFB ideal for aiding electricity generation from renewable sources (Alotto, Guarnieri, & Moro, 2014).

Redox flow battery, which is fit for wide scale energy storage, has currently been developed at numerous organizations around the world (Shigematsu, 2011). In the early-mid 1970s, Thaller (L.H. Thaller, 1974) had done the earliest work regarding the redox flow cell. Since then, several groups around the world have evaluated the concept of RFB but there are major problems encountered by few types of redox flow batteries such as iron/titanium, iron/chromium, and polysulfide bromine where cross mixing of electrolytes occurs due to usage of distinct redox couple species in each of reservoir tank and also lacking of development for an ideal cell membrane (Prifti et al., 2012). Regardless of that, the redox flow battery is attractive for electric vehicle applications as it is rechargeable either conventionally or with mechanical refuelling at appropriate refuelling station.

In University of New South Wales (UNSW), Maria Skyllas Kazacos and her co-workers have pioneered the vanadium redox flow battery (VRFB). The vanadium overcome the problems encountered by the other redox couple by introducing the similar electrolyte solution in both half-cells of the battery, thus preventing problem of cross mixing between electrolytes in the cell. Furthermore, vanadium has a potential to be explored as it has a long life cycle and about 80% of energy efficiency has been achieved with the VRFB developed in large installation where it reaches the performance requirement for wide scale energy storages (Zeng, Zhao, An, Zhou, & Wei, 2015). Much of the significance of recent research on VRFB has focused on enhancing the performance of the battery and its leakage problem. Research has also been made in order to improve the efficiency of battery such as by the concentration of electrolyte or materials of cell. There are also a few solutions proposed for the leakage problem made by several researchers.

In the meanwhile, several prototypes of VRFBs have been successfully applied worldwide, and the technology is swiftly progressing towards commercialization. While much advance has been achieved during the last several years, the performance of VRFBs still needs to be upgraded in terms of their efficiency (voltage, coulombic and energy) to afford low-cost operation of the cells in a long-term. Some researchers had pointed out regarding the performance of VRFB by only analysing one unit cell of VRFB whereas other researchers only highlighted on few issues regarding VRFB such as electrolyte concentration, electrode thickness, material of membrane, leakage problem in cell stack and also battery performance regarding compartment shape. Since VRFB is very flexible

in terms of its energy and power scalability to suit different application in energy usage, several researches have been done on this topic.

However, there is little to no discussion on the linearity relationship of the electrode compartment towards energy, power and performance efficiency of the VRFB even with all the mentioned advantages of easily scalable characteristic of VRFB. The only mention was by Mohamed's (Mohamed, Leung, & Sulaiman, 2015) previous research where it was assumed that there is a linear relationship of the electrode compartments by using faradays law of electrolysis. Since the assumption was made without a proof, the performance analysis of the Multi-Stack VRFB based on different size of electrode compartments with different operating parameters (current density, flow rate, volume of electrolyte, temperature of cell, electrode porosity and membrane conductivity) are analysed by using a simulation on COMSOL Multiphysics software. Different values of current densities (50 mA/cm^2 , 75 mA/cm^2 and 100 mA/cm^2), flow rates ($0.17 \text{ cm}^3/\text{s}$, $0.50 \text{ cm}^3/\text{s}$ and $0.83 \text{ cm}^3/\text{s}$), volume of electrolytes (10 cm^3 , 20 cm^3 , 30 cm^3 , 40 cm^3 and 50 cm^3), temperature (288.15 K , 293.15 K and 298.15 K), electrode porosity (0.92 , 0.93 and 0.94) and membrane conductivity (5 S/m , 10 S/m and 15 S/m) are used throughout this project. Thus, under the operating parameters, results for the efficiency of voltage are analysed.

On the other hand, this research is also intended to prove the linearity assumption made previously regarding Multi-Stack VRFB between different sizes of electrodes and its performance parameters of cell voltage during charging and discharging process. The Multi-Stack refers to the difference in sizing of the cell stack that is used. This project uses different sizes of the electrode compartments which are 5 cm , 7.5 cm and 10 cm which makes up a total area of 25 cm^2 , 56.25 cm^2 and 100 cm^2 . The relationship between all the operating parameters and the different sizes of electrode compartments can determine whether it is linear or not by calculating the data achieved from the charge and discharge graph through manual calculation, and after that analysing the equation obtained based on the arithmetic sequence.

1.3 Problem Statement

The utilization of RFB has become a major issue as it has been internationally acknowledged by UNSW as the most favourable technology for new energy storage application currently. With various cells and batteries that were established and commercialized, research for VRFB is still very much on-going with no standardization taking place, which implies that a research for performance characterization for the cell is essential. A better understanding of VRFB performance under different operating parameters such as flow rate and current densities are crucial to be analysed through some modification and characterization.

Previously, researchers only mentioned the thickness of electrode, membrane material, concentration of the electrolyte and leakage problem. Some other recent studies also only discussed regarding the performance of the battery in terms of the shape of the compartment. Furthermore, latest study about the flow rate (Hsieh, Leu, Wu, & Chen, 2014) summed up that at a higher electrolyte flow rate, the battery has a larger discharge depth. The research on different flow rates was not conducted properly using Multi-Stack VRFB, hence the experiment on different values of flow rate is investigated in this project which might improve the performance of the VRFB.

Besides that, based on Mohamed's previous research (Mohamed, 2013), it was assumed that there is a linear relationship of the electrode compartments by using faradays law of electrolysis. However, it should be noted that there is no specific research done to prove the assumption. Furthermore, based on the literature, there is no direct proof that its assumption could be true. Therefore, it is the major intention of this work to validate the linearity of the electrode compartments and its operational performances whether it is linear or non-linear. The result of the relationship of parameter could lead to the finalization on the Figure of Merit based on voltage, coulombic and energy efficiency and hence, the battery standardization could take place and eventually be the benchmark for the VRFB performance.

1.4 Objectives

The main objectives of this project are:

1. To model charging and discharging characteristic of VRFB by using COMSOL Multiphysics software.
2. To analyse VRFB performance in terms of voltage efficiency with the influence of different stack size of electrode compartment at different operating parameters.
3. To investigate the relationship pattern or trend between different size of electrode compartments and the different operating parameters whether it is linear or not.

1.5 Contribution

For this project, the contribution can be seen in terms of determining the VRFB characterization and its performance comparison. There is a need to develop a relationship between different sizes of electrode compartments since there is still a gap would be filled. The major intention of this work is to validate the relationship of the electrode compartment size and its operational performances whether it is linear or not. Thus, under the operating parameters which are current density, flow rate, temperature of cell, volume of electrolyte, electrode porosity and membrane conductivity, results for the efficiency of voltage is analysed. Following from there, through the result, an equation can be created to check if there exists any linear relationship between them or not. The significance of linearity in this project is so that the battery could be scalable in order to suite various applications. Finally, all those operating parameters are selected to be studied due to its tendency to affect the battery efficiency based on previous research done before and it is mentioned further in the literature review section.

1.6 Scope of Project

The aim of this project is to investigate the characterization and performance comparison of Multi-Stack VRFB. The word stack refers to the cell compartment while the word multi-stack refers to different sizes of electrode compartments being used in this project which are 5 cm, 7.5 cm and 10 cm which results in 25 cm², 56.25 cm² and 100 cm² of total area in the cell compartment, respectively. In simulating Multi-Stack VRFB

with different sizes of electrode compartments, the operating parameters at different values of current density, flow rates, volume of electrolyte, temperature, electrode porosity and membrane conductivity are used to obtain the voltage efficiency results.

Different values of current densities of 50 mA/cm^2 , 75 mA/cm^2 and 100 mA/cm^2 , flow rates of $0.17 \text{ cm}^3/\text{s}$, $0.50 \text{ cm}^3/\text{s}$ and $0.83 \text{ cm}^3/\text{s}$, electrolytes volume of 10 cm^3 , 20 cm^3 , 30 cm^3 , 40 cm^3 and 50 cm^3 , cell temperature of 288.15 K , 293.15 K and 298.15 K , electrode porosity of 0.92 , 0.93 and 0.94 and membrane conductivity of 5 S/m , 10 S/m and 15 S/m are chosen in order to simulate the charge and discharge graph throughout this project, as referred to the data used from previous research and also due to the existence of a few limitations in COMSOL Multiphysics itself. The limitation includes the parameter values that can be in a certain range of number only and if the number is out of the range, it will result in an error as the maximum iteration number is reached or the convergence issue occurs by that time.

Besides that, for mesh window, only mapped component is chosen under the predefined distribution type so that a high resolution mapping is obtained in the porous electrode. For defining the function window, Nernst Equation is used due to its usage in determining the electrical potential of a chemical reaction and to describe the membrane transport phenomena for ionic diffusion. Last but not least, there is also another limitation in this project where the coulombic efficiency throughout the simulation is assumed to be 90% as referred to its optimum efficiency based on references thus, only voltage efficiency will be analysed throughout this project. Finally, the efficiency of battery will be analysed by using the calculation theory. By comparing the voltage efficiency results, it is assumed to prove that the size of electrode compartment influences the efficiency of the battery.

1.7 Thesis Outline

This thesis consists of five chapters which explain and discuss the development of a Multi-Stack Vanadium Redox Flow Battery (VRFB), to determine the experimental characteristics of VRFB. The content of each chapter can be outlined as follows:

Chapter 1 basically explains the title of the project and introduces the idea for this project. Problem statement, objectives, contribution and scope of project is also stated in order to develop this project.

Chapter 2 provides an overview of the chapter and also the literature review, background and relevant issues from the past research related to this project. All the parameters investigated by previous researchers have been mentioned and considered in this chapter.

Chapter 3 describes on the research methodology of this project to achieve the objectives of the experiment. The methodologies explained consists of the flow process of the project, the simulation design of different sizes of the electrodes by using COMSOL Multiphysics software and the analysis of the design when combining different physics option to simulate the VRFB process.

Chapter 4 presents the result and discussion on this project which were obtained through the simulation of VRFB. All the data and information collected were explained for every different sizes of electrode based on each different operating parameter.

Chapter 5 provides a general conclusion based on the results obtained. The recommendations for further development of this project are highlighted and the project limitations are stated.



UMP

CHAPTER 2

LITERATURE REVIEW

2.1 Chapter Overview

In this chapter, the basic knowledge related to different technologies for energy storage is described. An overview of VRFB is also discussed further along with its characteristics. Lastly, the design consideration is mentioned along regarding its cell structure and cell characterization.

2.2 Energy Storage Research

Energy storage that stores electricity is not a new concept. In 2012, according to Bloomberg New Energy Finance database, there are more than 128 GW installed capacity amounted worldwide (Abbas A. Akhil, Georgianne Huff, Aileen B. Currier, Benjamin C. Kaun & Stella Bingqing Chen, Andrew L. Cotter, Dale T. Bradshaw, 2013). However, 99% of the global installed capacity has been restricted to only one technology which is the pumped hydro storage as shown in Figure 2.1.

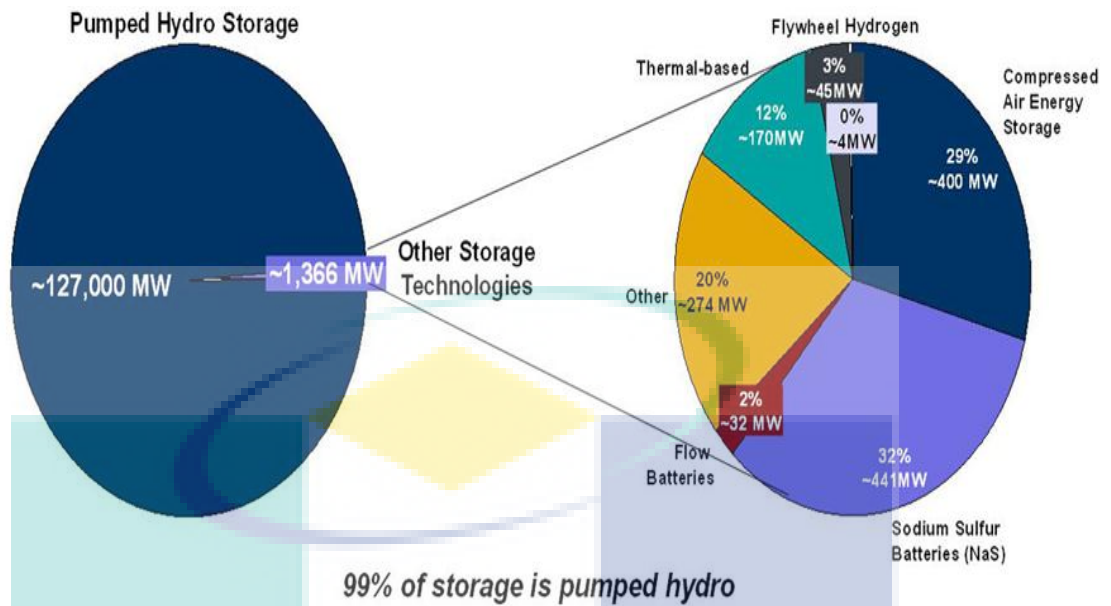


Figure 2.1 Electricity storage installed capacity in 2012 (MW).

Source: Abbas A. Akhil et al., (2013).

If an efficient and economic energy storage is implemented on a large scale in the current power infrastructure, it could bring about some of the significant changes in the power industry in decades. Besides that, reliability and dynamic stability of the power system could be improved with energy storage by providing stable, plentiful energy reserves that are less susceptible to varying fuel prices or shortages and require little ramp time (Verma, Gambhir, & Goyal, 2013).

Electrical energy is difficult to store unlike liquid or gaseous energy carriers and they must usually be converted into another form of energy incurring its conversion losses. Despite that, many energy storage technologies that rely on mechanical, electrochemical, thermal, electrical or chemical energy have been developed in recent decades. Most of them are currently at the early deployment phases where capital requirements and risks are at their highest.

2.2.1 Energy Storage Comparison

There are a few types of energy storage available worldwide which can be categorized to electrochemical, mechanical, thermal, chemical and electrical energy storage where each has their own advantages and disadvantages. Examples of mechanical

energy storage are compressed air, pumped hydroelectric and flywheel while example of chemical energy storage is hydrogen fuel cell. On the other hand, batteries are example of electrochemical energy storage while sensible heat storage is the example of thermal energy storage.

In addition to that, examples of electrical energy storage are supercapacitor, and Superconducting Magnetic Energy (SMES). Several studies affiliated to the use of energy storage in power systems are still ongoing and many researchers have seen new potential and more benefits in long and short-term storage devices based on the newest developments in technology of storage. Table 2.1 below summarizes the characteristics of some notable storage technologies.

Table 2.1 Characteristics comparison of energy storage. Adapted from

Storage technology	Power rating	Efficiency	Discharge time	Life time (years)	Technology status	Capital cost (\$/kW)
Pumped Hydro electric	100 – 5000 MW	70 – 80 %	Hours – Days	40 – 60	Mature	600 – 2000
Compressed Air	5 – 300 MW	85 %	Hours – Days	20 – 40	Mature	400 – 800
Flywheel	0 – 250 kW	89 %	Seconds – Minutes	15	Developing	250 – 350
Batteries	30 kW– 15 MW	60 – 80 %	Seconds – Hours	5 – 20	Developing	300 – 2500
Super Capacitor	0 – 300 kW	86 %	Seconds – Minutes	500 – 5000	Developing	100 – 300
SMES	100 kW– 10 MW	21 %	Seconds	20 above	Developing	200 – 300

Source: Dekka, Ghaffari, & Venkatesh, (2015), H. Chen, Ngoc, Yang, Tan, & Li, (2009), Schaber, Christopher & Mazza, Patrick & Hammerschlag, (2004) & International Energy Agency, (2014).

Pumped hydroelectric has high efficiency, can be used as long-term storage and is widely used, however, it has a large capital cost to begin with and requires a significant land area with a specific topography to build it. For compressed air, it is the clean and sustainable type of energy storage, has high reliability and also can be used in long-term storage but the drawback for this system is that it has a large capital and operating costs.

In the meanwhile, flywheel has an advantage in terms of possessing very high efficiency and is successfully commercialize compared to the other energy storage system, but the disadvantages are it can only be used as a short-term storage, has a large capital cost and also larger in size where it is only suitable for stationary purpose.

On the other hand, although super capacitor has a long cyclic life and is small in size, it is limited in power range and is only suitable for short term storage. While SMES can offer a quick response, the downside is that it has needs for refrigeration, has a large capital cost and low overall efficiency. Therefore, batteries are claimed to offer a promising alternative and are well suited for many applications compared to all the mentioned energy storage above as it provides flexibility, has a quick response and offers environmental benefits to electricity power system despite its weakness on the efficiency dependent on electrochemistry and has a high capital cost.

2.2.2 Battery Storage Technologies

Battery storage technology is one of the mature energy storage system available. There are two types of batteries storage available which are flow batteries and secondary batteries. Secondary batteries comprised of two electrodes (positive and negative) immersed in liquid, paste or solid electrolyte together which allows chemical reaction to take place while for flow batteries, it consists of one or more electrolytes species that is stored in tanks and physically divided by an ion exchange membrane. As the electrolyte gets pumped in and out of the cell stack, it undergoes redox reaction where the chemical energy in the electrolyte is converted into electrical energy. The reaction is reversible enabling the battery to be charged, discharged and recharged (H. Chen et al., 2009).

The examples of secondary batteries are Lead Acid (LA), Sodium Sulphur (NaS), and Lithium ion (Li-ion), whereas examples of flow batteries are Zinc – Bromine flow battery (Zn-Br) and Vanadium Redox Flow Battery (VRFB). Batteries offer flexibility in

terms of sizing, while providing a quick response. It also has environmental benefits, so it is ideally suited for electrical energy storage applications. Besides that, batteries also offer a few benefits to the electricity utility such as enhancing the system stability as it can respond very fast to load changing situation and accepts third-party power or co-generated power. Table 2.2 below compares several battery technologies available for energy storage.

Table 2.2 Comparison between several battery technologies.

Storage Technology	Power rating	Efficiency	Cycle Lifetime	Suitable storage duration	Capital cost (\$/kW)
Lead Acid	0 – 20 MW	82 %	2000 cycles	Minutes – Days	300 – 600
Sodium-Sulphur (NaS)	50 kW – 8 MW	90 %	2500 cycles	Seconds – Hours	1000 – 3000
Lithium-Ion (Li-Ion)	0 – 100 kW	98 %	11000 cycles	Minutes – Days	1200 – 4000
Zinc-Bromine (Zn-Br)	50 kW – 2 MW	75 %	2000 cycles	Hours - Months	700 – 2500
Vanadium (VRFB)	30 kW – 3 MW	85 %	14000 cycles	Hours - Months	600 – 1500

Source: Dekka et al., (2015), H. Chen et al., (2009), Rosin & Tallinn, (2012) & Luo, Wang, Dooner, & Clarke, (2015).

For Lead acid, it can be summarized that it has a high cost and maintenance requirement and is used in short term applications. On the other hand, Sodium-Sulphur battery is temperature sensitive but has a combined use for power quality and peak shaving. For Lithium-ion, it has a high cost, only limited to lower power range, can only be used in short term applications and has a quick response, whereas Zinc-bromine battery is highly scalable and suitable to be used in medium- and long-term applications. For VRFB, it is highly scalable, cost effective, and suitable for medium- and long-term applications.

2.3 Overview of Redox Flow Battery

The knowledge on the redox reaction in electrochemistry is important for an understanding of redox flow batteries as it stores energy in solution containing dissimilar redox couple to charge and discharge the battery through reversible conversion between electrical and chemical energy (Shah & Walsh, 2008). In RFB, the energy capacity of the system is directly proportional to the volume of electrolyte tank and reactant concentration while the power output varies depending on the cell stack size. The most notable benefits of RFB is that their power and energy are not coupled together like any other battery systems since its electrolyte and electroactive materials are stored externally (Wei Wang, Qingtao Luo, Bin Li, Xiaoliang Wei, Liyu Li, 2013).

Redox flow battery cell concept was first introduced by Thaller for more than 40 years. It is suitable for many applications such as load levelling, peak shaving, suitable for large scale utility application, reserve electricity supplies for emergency backup, uninterruptible power supplies, power supply for electric vehicles and also as integrating storage to be coupled with renewable power sources (Mohamed et al., 2015). In RFB, all the electro-active materials are dissolved in a liquid electrolyte. The separation between the energy and power requirement makes it possible to design the system to have optimal delivery properties and power acceptance without needing to maximize the energy density (Hasan, 2014). RFB can be divided into several types which are Soluble Lead Acid RFB, Bromide Polysulphide RFB, Zinc Bromide RFB, Iron Chromium RFB, Zinc/Cerium RFB, Vanadium Bromide RFB and Vanadium RFB. These RFBs are significantly different from each other due to their redox potential and electrolytes, except all of them have the same net chemical redox reactions.

Soluble lead acid battery consists of two half-cell where the cathode is made of PbO_2 while the anode is made of Pb . The sulphuric acid acts as the supporting electrolyte. Differing from other redox flow battery, soluble lead acid only requires a single electrolyte and it operates without the separator or membrane which can significantly minimize the cost and design complexity of batteries as reported by Ponce et al. (Le & Walsh, 2006). Soluble lead acid has small daily self-discharge rate, fast response time and very low capital cost as mentioned by C. P Zhang (Walsh & Zhang, 2011). However, this type of RFB suffers from certain limitation mainly due to the low cycling time and low energy density. Besides that, the performance of the soluble lead acid RFB is weak when operating in low temperature and this problem would eventually increase the thermal management cost of the system.

For Bromide Polysulphide RFB, it is one of the RFB technology that employs sulphide as anode and bromide as cathode. The low cost electrolyte species sodium-bromide and sodium-polysulfide are used as electrolytes (Zhao, Zhang, Zhou, & Yi, 2005) while the electrode is separated by a cation exchange membrane. On the other hand, Polysulphide Bromide RFB are independent in scaling-up the energy capacity and power, deep-discharge capability and long life. The main disadvantage of this RFB is that it is facing the cross contamination problem, hence proper electrolyte management is required to enhance the energy efficiency of battery as stated by Zhou et al. (H. Zhou, Zhang, Zhao, & Yi, 2006).

Zinc Bromide batteries from different manufacturers have different energy densities. The electrolyte is composed of zinc bromide salt that is dissolved in water. It has good energy densities and efficiencies, high cell voltage, low cost of reactant and high degree of reversibility. Poulikkas et al. mentioned that in the positive electrode, during charging process, the bromide is converted to bromine and at the negative electrode, the metallic zinc is plated from the electrolyte solution (Poullikkas, 2017). It is also stated that the drawback is zinc bromide's electrodes are high in cost, the material easily corrodes due to the electroplating of zinc and it has a low cycle life. Moreover, the Zn/Zn^{2+} ion species reacts quicker than the bromine/bromide couple causing the polarization to occur.

Iron-chromium RFB system stores energy by employing an aqueous solution of $\text{Fe}^{2+}/\text{Fe}^{3+}$ and $\text{Cr}^{2+}/\text{Cr}^{3+}$ redox couples. Similar to other types of RFB, the energy and

power ratings for this battery are independent of each other. Besides that, it was once considered as promising battery system due to the production of high value electrochemical potential which is 1.18V. Nonetheless, it suffers from cross contamination problem due to diffusion on the cations across the membrane. For zinc cerium RFB, it has a successful operation result in the high current density as high as 500mA (Le & Walsh, 2006). Unfortunately, it prohibits zinc electrodeposition which results in extreme hydrogen evolution process and leads to lower efficiency of charge (Shi, 2014). Lastly, for Vanadium bromide, the energy density produced is used for electrical vehicles thus, it will be useless unless a high energy is produced.

Regardless of all the other types of RFB mentioned above, there have been several studies in the literature reporting the major drawback of the system which is the cross contamination of redox couple. Therefore, in 1980s, Skyllas Kazacoz and co-workers pioneered the first vanadium redox flow battery (VRFB) that holds all the merits of other types of RFB (Wei Wang, Qingtao Luo, Bin Li, Xiaoliang Wei, Liyu Li, 2013). Since then, VRFB is the only secondary battery that is most developed and reached commercial fruition to date (Skyllas Kazacos M, Chakrabarti MH, Hajimolona SA, Mjalli FS, 2011). The main features of VRFB typically consists of cell stacks that store electrolytes along with the electrode which provides a place for oxidation-reduction reaction to take place.

2.3.1 Vanadium RFB

The VRFB configuration is shown in Figure 2.2 below. It is made up of two tank of electrolyte filled with the electrolytes of V(II)/V(III) and V(IV)/V(V) in supporting acid solution, respectively, battery stack and electric pumps. The electrolytes are pumped into the battery stack which generates electrochemical reaction to occur. An ionic membrane in the stack separates the cell as well as electrolytes into anodic and cathodic. The VRFB system is the only redox flow battery using ions of the similar metal in both electrolyte tanks, which removes electrolyte cross-mixing as experienced by other redox couple in redox flow battery. The state of charge (SOC) can be measured continuously; therefore, the capacity residual in the battery can be read instantly. By the use of tapping cells in the battery, it can be charged at one voltage and discharged at another while also sustaining an external load if required (Huang, Li, Liu, Tan, & Chen, 2008).

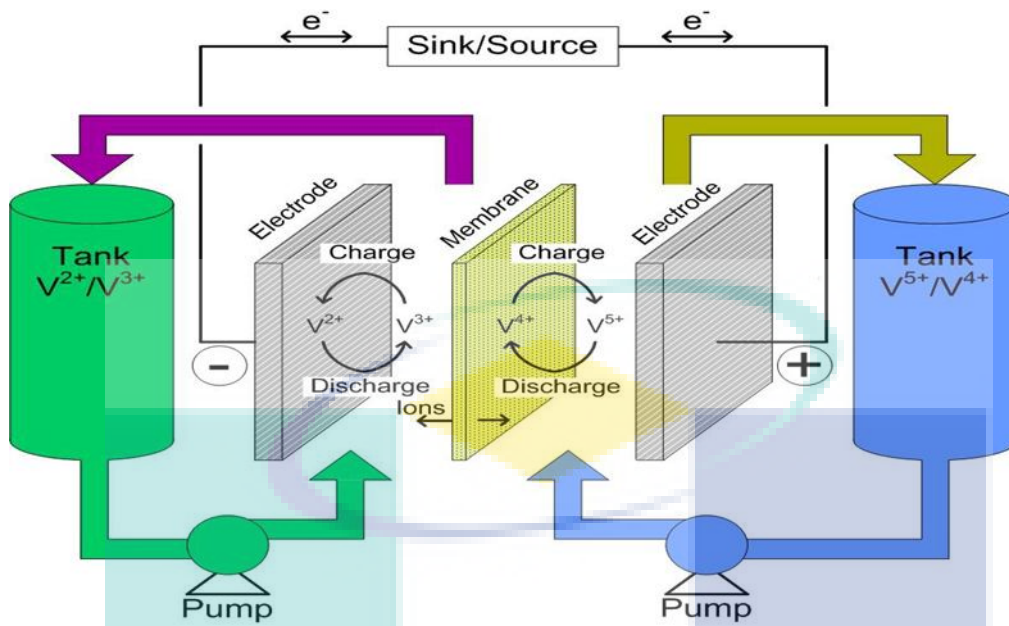


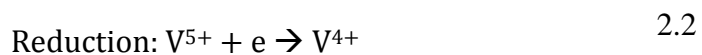
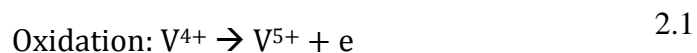
Figure 2.2 VRFB configuration.

Source: Barsukov, (2013).

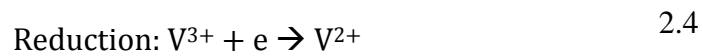
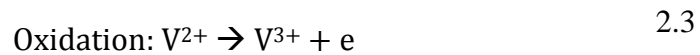
Among numerous RFB metal ion compositions (zinc-cerium, zinc-bromine, magnesium-vanadium, vanadium-polyhalide, vanadium-cerium), the most explored and successful technology is the VRFB, which is the only technology that has reached effective commercial fruition up to date. It consists of vanadium/vanadium redox couple dissolved in aqueous sulfuric acid. The benefit is that, by using the similar metal ions in both electrolytes, the membrane and electrodes are not cross-contaminated and the cell capacity does not lessen with time, allowing for a longer lifespan of battery.

During charging at the positive electrode, tetravalent vanadium within VO^{2+} ions is oxidized to pentavalent vanadium within VO^{2+} ions, whereas at the negative electrode, trivalentions V^{3+} are reduced to bivalentions V^{2+} . The hydrogen ions $2H^+$ penetrates through the membrane to sustain the electrical neutrality of the electrolytes. The equation for the chemical reaction happening inside the storage tank are as follows.

Positive half-cell,



Negative half-cell,



The standard operating cell voltage of a VRFB cell is $E_o = 1.26 \text{ V}$ at $25 \text{ }^\circ\text{C}$, but in fact real cells show $E_o = 1.4 \text{ V}$ due to the correcting Nernst's factors. VRFBs demonstrate a current density in the range of $50 - 80 \text{ mA/cm}^2$. It also has a power density barely reaching 0.1 W/cm^2 , which is much lesser than that of equivalent proton exchange membrane fuel cells (PEMFC) in where this fuel cell combines pure hydrogen fuel with oxygen from the air to produce electrical energy. In addition, VRFBs also stored energy density is in the range of $25 - 35 \text{ Wh/L}$. Active area of cell in the order of 6000 cm^2 and above are needed when managing currents of some hundreds of amperes in a single cell (Alotto et al., 2014).

2.4 Design Consideration of VRFB

In this section, detail discussion focuses on the main component of constructing the cell stack which consists of cell structure and cell characterization. Cell structure emphasizes on the cell design, electrode materials and membrane, whereas cell characterization discusses further emphasizing on membrane and electrolyte concentration.

2.4.1 Cell Structure

There have been several researches conducted on VRFB due to the world's demand on effective energy storage where research were conducted on membrane materials, electrode plate type and electrode thickness. According to the cell structure, a literature review on "*Dramatic Performance Gains in Vanadium Redox Flow Batteries through Modified Cell Architecture*" by (Aaron et al., 2012) would be related to this project. This paper introduces the VRFB performance which comprises of the electrode with cell stack of carbon and is enhanced throughout various electrode thickness. The design proposed by this paper is 5 cm^2 and it is attributed mainly to the architecture of zero gap flow field and thin non-wet proofed porous electrodes that ensure excellent contact between all the

components of the cell and reduces the transport system charge (Aaron et al., 2012). Based on the result, different electrodes (anode and cathode) have different layers of non-wet proofed carbon paper. However, this configuration did not yield satisfactory results since this gave the lowest over potential individually (Aaron et al., 2012). Thus, to have a synchronized over potential yet same layers of carbon are preferred.

Referring to the literature of “*Membrane Stability Studies for Vanadium Redox Cell Applications*” (Sukkar & Skyllas-Kazacos, 2004), the membrane material was discussed with the active area of 25 cm². An ongoing effort in further study was evaluated to find suitable commercial membrane that shows the stability in vanadium electrolytes as well as long cycle life, high performance and low cost for VRFB system. This paper introduces a way to evaluate the membrane performance through their resistance, ion exchange capacity, vanadium ion diffusivity and appearance (Sukkar & Skyllas-Kazacos, 2004). The best membrane performance is selected based on how they are able to maintain their properties in the vanadium electrolytes to provide a long cycle life of the VRFB. Hence, this research is intended to evaluate candidate membranes for the VRFB so as to develop guidelines to the selection and development of suitable membranes for the VRFB and also to gain a better understanding of their behaviour and properties during long-term operation in commercial energy storage systems. A decrease in the conductivity of the membrane during operation will affect the voltage efficiency of the cell, while an increase in the diffusion of the vanadium ions would indicate that the membranes are no longer performing efficiently as ion-selective membranes. An increase in the rate of diffusion of the vanadium ions across the membrane will lead to an increased self-discharge rate and a loss in coulombic efficiency, which is undesirable (Sukkar & Skyllas-Kazacos, 2004).

In addition, the research continues on “*High – Performance Vanadium Redox Flow Batteries with Graphite Felt Electrodes*” by (Davies & Tummino, 2018). Up to date, most commercially available VRFB only uses graphite felt electrodes below comparatively low compression. This prompts in a huge cell ohmic resistance, thus limiting the maximum power density. The excellent performing VRFB is similar to the one used in fuel cells where it uses carbon electrodes, with great compression pressures in the active area of cell. This paper examines the usage of felt electrodes at corresponding compression pressures for active area of cell of 31 cm². Single cells are stacked together by using the compression pressures and tested in a VRFB system. The findings propose that felt

electrodes can challenge with paper electrodes in terms of performance under same compression pressures in which it may lead the electrode development and cell optimization in this important energy storage technology (Davies & Tummino, 2018).

For “A High – Performance Carbon Nanoparticle-decorated Graphite Felt Electrode for Vanadium Redox Flow Batteries” (Wei, Zhao, Zhao, An, & Zeng, 2016), it discusses the increasing performance of VRFB mostly the power density and efficiency of energy which is very significant in order to lower the cost of a system to a level of global commercialization. This paper featured a 4.68 cm² VRFB of a carbon nanoparticle-decorated graphite felt electrode with a structure of flow-field that exhibits a notable decrease in ohmic loss by decreasing the thickness of electrode. It also managed to increase the surface active area and enhanced the activity of electrocatalytic by coating the carbon nanoparticles. In addition, it is shown that the battery with this proposed structure demonstrates a substantially higher capacity retention and rate of capability as contradicted to the normal flow-through the structured battery having thick electrode of graphite felt (Wei et al., 2016).

Other than that, the paper entitled “Performance of A Vanadium Redox Flow Battery with a VANADion Membrane” by (X. L. Zhou, Zhao, An, Zeng, & Zhu, 2016) discussed the conventional VRFB of 3.14 cm² active area employ Nafion 115 that endured from issues connected with high capital cost and ohmic resistance. Thus, a favourable replacement to Nafion 115, which is a commercial membrane (VANADion), is introduced as it consists of a dense Nafion layer and porous layer. In the structure of dual-layer, the porous layer offers a high conductivity of ions and the dense Nafion layer can reduce the convective flow of electrolyte throughout the membrane. The composite membrane is estimated to be particularly cheaper than the conventional Nafion 115 attributable to the fact that the dense Nafion layer is quite thin and the porous layer is relatively cost-effective. The greatest combination of the low cost and preferable performance makes this composite membrane very favourable in the applications of VRFB (X. L. Zhou et al., 2016).

Besides that, the paper “Effects of SOC – dependent Electrolyte Viscosity on Performance of Vanadium Redox Flow Batteries” (Q. Xu et al., 2014) discussed the viscosity of the electrolyte in 4 x 10⁻⁴ m² electrode specific active area of VRFBs that vary

during charge and discharge as the vanadium ions and acid concentration in the electrolyte consecutively change with the state of charge (SOC). In prior model of VRFB, however, the electrolyte has been treated as a constant - viscosity solution. But in this project, an electrochemical and mass-transport model is developed while considering the effect of SOC-dependent electrolyte viscosity. The comparison between the present model and the model with the constant-viscosity simplification specifies that the deliberation of the SOC-dependent electrolyte viscosity allows a more accurate estimations of pumping work, a better realistic simulation of the distributions of overpotential and current density in the electrode and the system efficiency of VRFBs (Q. Xu et al., 2014).

Moving to the next paper entitled “*Performance of a Vanadium Redox Flow Battery With and Without Flow Fields*” by (Q. Xu, Zhao, & Zhang, 2014), this paper discussed the flow field as a vital component for cells to macroscopically scatter reactants onto electrodes. However, it is still unknown whether flow fields are also needed in all VRFBs. In this paper, the performance of a 600 cm² of VRFB with flow fields is compared and analysed with the performance of a VRFB with no flow fields. It can be seen that the battery with flow fields has a higher discharge voltage at higher flow rates, but indicates a huge pressure drop. The utmost power-based efficiency happens at distinct flow rates for the both batteries with and without flow fields. It is also established that the battery with flow fields show 5% higher energy efficiency than the battery without flow fields when running at the flow rates complementary to each battery’s maximum power-based efficiency. Therefore, it can be said that flow fields in VRFB can be a good approach for enhancing the VRFB system efficiency (Q. Xu et al., 2014).

In addition, through “*A Review of Vanadium Electrolytes for Vanadium Redox Flow Batteries*” (Choi et al., 2017) paper, the authors discussed the increasing interest in VRFBs for wide scale-energy storage systems. Vanadium electrolytes, which functions as active material and the electrolyte, are very significant in terms of performance and cost. Although vanadium electrolyte technologies have remarkably progressed during the last few decades, they should be enhanced further with respect to stability, higher vanadium solubility and performance of electrochemical for the design of reliable, energy-dense and cost-effective VRFBs. This paper summarized the vanadium electrolyte technologies as well as their synthesis, thermal stabilities, electrochemical performances and spectroscopic characterizations as well as highlighted the recent problems in the

development of VRFB electrolyte. The disputes that must be tackled in order to facilitate the development of vanadium electrolytes may encourage more researchers to get involved on it (Choi et al., 2017).

Finally, through a review of “*Insights into All-Vanadium Redox Flow Battery: A Case Study on Components and Operational Conditions*” (Boaventura, Monteiro, & Leir, 2018) paper, it discussed regarding VRFB performance depending on the operational components and conditions such as current density, flow rate, membrane and compression of electrode. The performance of battery was analysed based on the graph of charge and discharge, the restricting current was acquired throughout curves of polarization and the ohmic resistance of the battery was acquired by electrochemical impedance spectroscopy (EIS) (Boaventura et al., 2018).

The active area used in this paper was 25 cm² and Figure 2.3 below shows the structure of the VRFB cell stack at mentioned size.

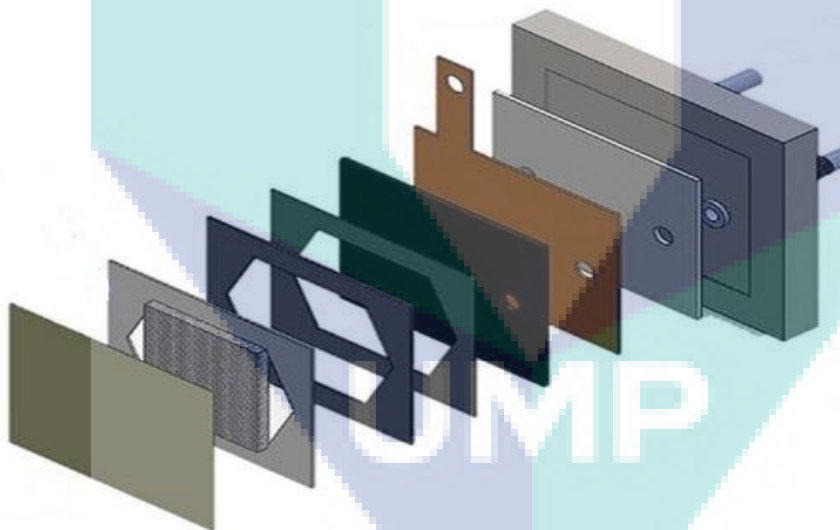


Figure 2.3 : The structure of 25 cm² VRFB cell.

Source: Boaventura et al., (2018).

2.4.2 Cell Characterization

Normally, the characteristics of batteries are analysed based on the charge - discharge of current. The characteristic is shown on the effect of battery in power density and voltage, energy or coulombic efficiency. Few researchers had discussed on the topic of characterization of battery, however, it is only limited to certain parameters. Through the paper of “*Effects of Operating Temperature on The Performance of Vanadium Redox Flow Batteries*” by (Zhang, Zhao, Xu, An, & Zhao, 2015), it discussed the variation in seasons and places that can influence the design of the battery and eventually, its rated capacity and power. Hence, it is essential to characterize the thermal parameter of the battery in order to suit its efficiency and reliability. This paper also discussed the ambient temperatures effect on the overall battery system in a single cell. In addition, it can also be seen that maximizing the performance of battery rely severely on the union of several elements such as side reactions and vanadium crossover, physical and chemical properties of electrolytes, impacts of electrochemical process in the cell stack and both electrode transport and kinetics properties. For this paper, the active area of cell used is 5 cm^2 with an electrolyte volume of 20 ml at both side of the tank, current density of 40 mA/cm^2 and temperature of $25 \text{ }^\circ\text{C}$.

Besides that, the paper “*Advanced Characterization of Lithium Battery Materials with Positrons*” (Ouvrard et al., 2017) discussed on materials of cathode that are important to improve the performance of battery and materials that can conserve stable cycling and high power with a capacity approximate to that of materials of anode. The parameter-free, gradient-corrected model for electron-positron connections predicted that spectroscopies established on annihilation of positron can be utilized to investigate the outcome of lithium intercalation in the oxide matrix of the cathode. The positron characteristic in oxides can be validly computed thus, it can allow a fundamental characterization of lithium battery components concerning annihilation of positron spectroscopy and first-principles calculation. The specific information from the experiment of positron could be helpful in digesting knowledge and optimizing both battery elements and bi-functional catalysts for evolution and oxygen reduction (Ouvrard et al., 2017).

On the other hand, the paper of “*Characterization of Graphite Felt Electrode with Surface Modification for H_2/Br_2 Fuel Cell*” (L. Zhang, Shao, Wang, Yu, & Liu, 2013)

discussed the graphite felt applied as the electrode of bromine in H_2/Br_2 fuel cell, which is surface adjusted by thermal and acidic oxidation in order to improve cell performance. The electrode area used in this paper was 4 cm^2 with electrolyte volume of 40 ml and temperature of $30\text{ }^\circ\text{C}$. The composition, structure, electrochemical performances and properties of the modified electrodes were characterized with scanning electron microscopy, X-ray diffraction and photoelectron spectroscopy, single cell polarization curves and electrochemistry impedance spectroscopy (L. Zhang et al., 2013). The performance of cell was boosted by thermal oxidation and surface modification which exhibits greater performance than acidic oxidation.

Other paper that highlighted the characterization in redox flow battery cell is the paper “*Generalized Characterization Methodology for Performance Modelling of Lithium – Ion Batteries*” by (Stroe, Swierczynski, Stroe, & Kær, 2016). In this paper, the authors discussed the lithium-ion (Li-ion) batteries as a composite storage of energy device with their capability behaviour is very influenced by the operating conditions such as load current, temperature, and state-of-charge (SOC). In order to analyse their techno-economic viability for several application, detailed information on Li-ion battery performance behaviour is needed. Hence, seven-step methodology was introduced for laboratory characterization of Li-ion batteries, in which the performance of battery parameters which consisted of open-circuit voltage (OCV), capacity and impedance were determined and their dependence on the operating conditions are obtained. Furthermore, this project proposed a novel hybrid procedure for parameterizing the batteries’ equivalent electrical circuit (EEC), which is used to emulate the batteries’ dynamic behaviour. In this paper, the temperature used for testing this battery ranged from $15\text{ }^\circ\text{C}$ to $25\text{ }^\circ\text{C}$, $35\text{ }^\circ\text{C}$ and $45\text{ }^\circ\text{C}$. Based on this procedure of parameterization, the performance model of the studied Li-ion battery was built and its reliability was successfully validated for various load profiles, thus verifying the proposed seven-step characterization methodology (Stroe et al., 2016).

Besides that, another paper that highlighted the characterization is the paper “*Particle Based Method and X-ray Computed Tomography for Pore-Scale Flow Characterization in VRFB Electrodes*” (Maggiolo, Zanini, Picano, & Trov, 2018). In this paper, the authors discussed the porous electrodes as a pivotal component of VRFB, which influences few parameters such as the pressure drop losses, power density, activation

overpotentials, bulk and contact resistance, limit current density, as well as ohmic losses. It is useful to quantify the efficiency of fluid-mechanics of porous electrodes, as it is related to the losses of mass transport and it affects the overall performance of battery. Although most studies analysed under the macro homogenous and isotropic behaviour of the fluid mechanics in the porous material and simplifying assumption of linear, this paper introduced an initial approach built on the Lagrange Particle Tracking and Lattice-Boltzmann Method. The methods made use of the pore-scale accurate geometrical data supplied by X-ray computed tomography with the focus of investigating the reaction rates and dispersion of liquid electrolyte reactants in the battery porous electrode. Thus, the comparison between the fluid-dynamic performances provided by a normally applied unconventional material and carbon felt, that was a carbon vitrified foam, was analysed (Maggiolo et al., 2018).

Other than that, more information on the battery characterization has been discussed in the paper of “*Performance of a Vanadium Redox Flow Battery With and Without Flow Fields*” (Q. Xu et al., 2014). In this paper, electrode active area of 1600 cm^2 is used along with 50 ml volume of electrolyte at room temperature. The characterization of battery has been discussed by using the parameters of flow rate, electrode thickness, pumping power and cycling behaviour (Q. Xu et al., 2014). On the other hand, in the paper “*Unit Cell Modelling and Simulation of All Vanadium Redox Flow Battery*” by (Seepana, 2018), the author used 100 cm^2 of electrode active area and conducted the test with different operating parameters of temperature (297 K and 307 K), current densities (800 A/m^2 and 1000 A/m^2) and electrode porosities (0.60, 0.68 and 0.80). It also discussed on the benefits of modelling in which it had the capability to forecast the difficult quantities, and in a few cases impractical, to acquire throughout experiment as well as the demonstrated model in simulation managed to capture the performance at high degree of accuracy (Seepana, 2018).

Through the paper “*Characteristic of a New All – Vanadium Redox Flow Battery*”, the battery performance, life, economical aspect, comparison with other batteries and application were discussed. One of the points in this literature was the large distance between electrodes resulted in low voltage efficiency (M. Rychcik et al., 1988). Hence, with the application of multi-stack of compartments, it is hoped that it can produce zero gaps between the cells for electrolyte flow. Furthermore, it is ensured to have a good

contact between compartments and reduce charge transport distances (M. Rychcik et al., 1988). Excellent performance characteristics have been obtained by using high electrolytes concentration and low resistive membrane. Even though the researchers obtained a good voltage efficiency, the membrane resistivity is still highly considered. So, further improvements in the electric energy efficiency is expected with a less resistive membrane. In addition, the method that can be used to measure resistance area is described by Chieng and Skyllas-Kazacos (Prifti et al., 2012).

In addition, “*A Dynamic Performance Model for Redox – Flow Batteries Involving Soluble Species*” by (Shah & Walsh, 2008) paper discussed the performance of battery at operating parameter of electrolyte concentration (1080 mol/m^3 and 1440 mol/m^3), inlet flow rate (1 ml/s and 2 ml/s) and electrode porosity (0.60, 0.68 and 0.80). The active area used for this experiment is 100 cm^2 with electrolyte volume of 250 ml, temperature of 27°C and current density of 10 A (Shah & Walsh, 2008). On the other hand, the paper “*Characterization Techniques and Electrolyte Separator Performance Investigation for All Vanadium Redox Flow Battery*” (Z. Tang, 2013) discussed regarding the membrane conductivity parameter on a study of uptake behaviour of vanadium/sulfuric acid electrolyte solutions in Nafion. The paper also discussed the effect of composition of bathing solution on conductivity of membrane. In this study, it is found that the conductivity of membrane reduction or enhancement can be reviewed as a trade-off between increase on proton concentration and losses on proton mobility caused by the presence of acid in the battery environment (Z. Tang, 2013).

Finally, for paper entitled “*The Influence of Operational Parameters on The Performance of An Undivided Zinc–Cerium Flow Battery*” (Leung, Leon, & Walsh, 2012) discussed a cell active area of 1.6 cm^2 tested with different operating parameters of current density (0 to 80 mA/cm^2), flow rate (0.64 to 7.0 cm/s) and temperature (20 to 60°C). The efficiency of charge rose at higher current densities and electrolyte flow velocities. Later, after 4 hours of charging the battery, the transformation of Ce(III) to Ce(IV) ions became barely efficient over time attributable to a higher fraction of the current being used in evolution of oxygen. Severe aspects for enhancements in the performance of battery were also reviewed in this paper (Leung et al., 2012).

2.5 Performance Parameter of VRFB

VRFB by now is the most developed and closest battery storage of being commercialized. Since its introduction, VRFB development scores about 20 demonstration systems covering various type of applications as mentioned by Skyllas-Kazacos et al. (Skyllas-kazacos & Kazacos, 2011). To date, the lack of reliable experimental characterization in literature for VRFB system needs to be highlighted. Commonly, the performance characterization of batteries is determined based on the charge and discharge of current as well as its figure of merit which comprised of voltage efficiency, coulombic efficiency and energy efficiency.

Mohamed et al. (Mohamed et al., 2015) brought up that usually all applied current densities will have similar charge-discharge characteristics. Therefore, charge and discharge characteristics could be identified based on current density. Also, Ponce et al. (Le & Walsh, 2006) used these equations for the parameter efficiency that have been mentioned. The efficiency of voltage is the correlation between the voltage of cell of discharge and charge. On the other hand, the term coulombic efficiency refers to the ratio of discharge to charge of electric charge, while energy efficiency is the fraction of energy between discharge and charge process. The measure of figure of merit will also vary due to the charge and discharge process (Simpson, 2011). The equations can be simplified as follows:

Voltage Efficiency, % η_V ;

$$\eta_V = \frac{V_{cell} (discharge)}{V_{cell} (charge)}. \quad 2.5$$

Coulombic Efficiency, % η_C ;

$$\eta_C = \frac{q (discharge)}{q (charge)}. \quad 2.6$$

Energy Efficiency, % ηE ;

$$\eta E = \frac{E (\text{discharge})}{E (\text{charge})}. \quad 2.7$$

Therefore, proper characterization is certainly beneficial to the commercialisation of VRFB applications. Reviews were done and cited with regards to Skyllas- Kazacos et al. (Skyllas-kazacos & Kazacos, 2011) and Teng et al. (Teng, Dai, Bi, & Yin, 2014) on the VRFB performance. In this project, in order to optimize the efficiency of the cell, those three efficiencies mentioned above need to be considered.

2.6 Linearity Study

Linearity can be defined by the ordered systems and straight lines property, distinguished by good behaviour, simple proportions and predictability. It is not a typical factor of the real world and exists mainly in theories. It also can be defined by a condition where a dependent variable has a linear relationship with one or several independent variables and, thus, can be assessed as the linear function of the independent variable(s). After all, linearity is a property of a mathematical function or relationship which explains that it can be represented graphically as a straight line. Linearity is also well known as a data that is a straight line graphically. More technically, a linear function is one that has homogeneity and additivity. Linearity is a necessity for performing linear regression. A linear regression line will not be a line of best fit for data of nonlinear. In order to conduct linear regression on nonlinear data, a nonlinear transformation is needed to change the data into linear form.

Linearity study has been widely used in mathematical field from long ago, and from there it also has been used in medical field such as for gauge linearity, bias study and also communication system such as visual system. One of the papers that discussed the linearity subject is “*Test for Linearity between Continuous Confounder and Binary Outcome First, Run a Multivariate Regression Analysis Second*” (Peter & Jack, 2009). In this paper, it discusses about prior approach in the analysis of multivariate, whether the ongoing confounding variable is linearly related or not to log-odds of the hazard ratios or binary outcome of the time-to-event. If there exists a linear relationship, it is encouraged

that the variables not be dichotomized and the assumption of linearity is examined by restricted cubic splines by using SAS/Stat® procedures (Peter & Jack, 2009).

Next, in the paper *“Improper Use of Linear Reasoning: An In-Depth Study of The Nature and The Irresistibility of Secondary School Students’ Errors”*, (De Bock, 2002) the authors mentioned a few studies among 12–16 years old scholar that inappropriately apply the proportional or linear model in problems of word concerning areas, lengths and volumes of similar solids and plane figures. This paper also analysed the process of thinking underlying scholars’ inappropriate linear reasoning and how this process is influenced by their conceptions of mathematical, habits and beliefs. Results from the discussions yield that the real process of problem solving cause scholars to fall into mechanism behind the ‘linearity trap. Although some scholars seem to genuinely trust that quantities are always linked proportionally, their inappropriate usage of linearity often results from intuitive and superficial reasoning, manipulated by certain conceptions of mathematics, beliefs and habits heading to a limited modelling process (De Bock, 2002).

Another paper that mentioned regarding the linearity is the paper of *“Analysis on Accuracy of Bias, Linearity and Stability of Measurement System in Ball Screw Processes by Simulation”* (Pai, Yeh, & Hung, 2015). In this paper, the author discussed an ideal way for measuring system to have the statistical factor of zero error, but that kind of system could barely presence. Hence, to keep a good standard of the variance that might happen in the process of manufacturing, Measurement system analysis (MSA) is needed for good control of quality. Ball screws, which are a main element in precision machines, have important features as a lead accuracy failures and axial-gap of a ball screw that can induce expensive and negative effects in accuracy of machine positioning. The reliability of a measuring system by using a Monte Carlo simulation to produce probability density function and bias, linearity variance of the normal distribution is assessed. Furthermore, the possible area distribution in the actual case is forecasted so that the measurement capability will be improved. This in return help the users to categorize the measurement system and organize measurement regulations for excellent performance and observing of the ball screw precision (Pai et al., 2015).

In the meanwhile, in redox flow battery field, linearity relationship has been discussed towards the polarization curves among instantaneous current density and

voltage efficiency of a Quinone-Bromide Redox Flow in the paper entitled “*Cycling Analysis of a Quinone-Bromide Redox Flow Battery*” (Q. Chen, Eisenach, & Aziz, 2016). In here, the authors discussed the dependability towards current density of voltage polarization, voltage, current, and energy efficiency and charge capacity for a redox flow cell battery made up of 2, 7-anthraquinone disulfonic and hydrobromic acid as redox-active ions in the electrolytes. Relationships forecasting a few of these figures of merit from the curves of polarization are made and the decline in capacity with rising current density is proclaimed to be a straight result of the interplay of the curves of polarization and the voltage limits forced during cycling. It can also be seen that the linearity of the polarization curves results in an inverse linear relationship among instantaneous current density and voltage efficiency. Hence, current efficiency loss mechanisms are categorized according to whether if they lead directly to cycle capacity loss.

Another paper having similar discussion topic in linearity is the “*Advanced Redox Flow Fuel Cell using Ferric Chloride as Main Catalyst for Complete Conversion From Carbohydrates to Electricity*” (F. Xu, Li, Liu, & Jing, 2017). Liquid catalysed fuel cell (LCFC) is a type of redox flow fuel cell instantaneously transforming carbohydrates to electricity. To increase its efficiency, ferric chloride (FeCl_3) was added as the major catalyst. Long-term continuous operation of the LCFC specified that carbohydrates can be hydrolysed to glucose and then oxidized stepwise to carbon dioxide. At the final stage, there exists a linear relationship among the electron transfer number from glucose to catalyst and the subsequent performance of cell. Based on these results, the contribution of FeCl_3 to LCFC should be acquired from the increased oxidation and hydrolysis of carbohydrates as well as the improved electron transfer from glucose to anode (F. Xu et al., 2017).

In the paper of “*A Membrane – Free Redox Flow Battery with Two Immiscible Redox Electrolytes*” by (Navalpotro, Palma, Anderson, & Marcilla, 2017), the authors focused on a membrane-free redox flow battery that depends on the non-mixing capability of redox electrolytes where vanadium is exchanged by organic molecules. The biphasic system is produced by one acidic solution and ionic liquid, both carrying quinoyl species, which acts as a reversible battery in the absence of any membrane. This membrane-free battery has an open circuit voltage of 1.4 V with a high theoretical energy density of 22.5 WhL/1 and is able to transport 90% of its theoretical capacity while demonstrating good

long-term performance in energy efficiency of 70% and coulombic efficiency of 100%. The polarization curve of this battery also exhibits a small increase in initial discharge voltage than the diluted example (1.4 V vs. 1.2 V), a linear relationship of voltage and current and a power density close to 0.6 mW/cm^2 , approximate to the example with diluted electrolytes (Navalpotro et al., 2017).

Next, the paper “Non - Aqueous Li – Based Redox Flow Batteries” (Hamelet et al., 2012) focused on the outcome of numerous physical or chemical parameters on the performance of the $\text{LiFePO}_4 / \text{LiPF}_6 \text{ EC-DMC} / \text{Li}$ redox flow system. A methodical study on the impact of the flow rate coupled with hydrodynamic and electrochemical characterizations and active material content have been tested and as a result, power density performances were obtained. Also, the feasibility of reaching energy density is demonstrated and it exhibits a linear decrease on the cell voltage with the rising current density, while the power density attains a maximum level. In contrast, the linear decrease in the curve of polarization indicates that various ohmic contributions govern the cell voltage. It is also found that a rise in the KB300 volumetric percent triggers in a decline in the cell voltage. By analysing such results lead to a linear variation of the percolating conduction length where increasing the amount of KB300 results in better kinetics (Hamelet et al., 2012).

In addition, when it comes to the linearity relationship for VRFB itself, there are only a few discussions that has been made and one of it involves the relationship among flow rate and pumping pressure. As for all compression pressures, the relationship between flow rate and pumping pressure is linear, as in agreement with Darcy’s La article of “*High – Performance Vanadium Redox Flow Batteries with Graphite Felt Electrodes*” (Davies & Tummino, 2018). It further studies the usage of felt electrodes at corresponding compression pressures where the peak compression pressure of cell collaborated with a thin Nafion membrane achieved a highest power density and doubled the last good performance from a felt-VRFB. The outcomes recommend that felt electrodes can challenge with paper electrodes in terms of performance during the same compression pressures, which should aid optimization of cell and development of electrode in this significant technology of energy storage (Davies & Tummino, 2018).

Other than that, connection of SOC with the absorbance of the negative electrolyte at some wavelengths has also been discussed through the paper entitled “*Monitoring The State of Charge of Operating Vanadium Redox Flow Batteries*” (Z. Tang, 2012). In this paper, methods for assessment of the SOC of VRFB were described during the experimentation using fuel cell OCV measurements and UV-vis spectrophotometry. The absorbance of the negative electrolyte fluid is linear in SOC for SOC > 0.2. In contrast, the absorbance of the positive electrolyte does not show a linear relationship with SOC, which attributes to the present of an incredible absorbing third ion species. A study on the residue absorbance of the positive electrolyte shows that a complex with 1:1 stoichiometry is established and full-cell OCV measurements are discovered to be an imprecise gauge of the battery state of charge.

In the meantime, other linearity study involving VRFB cell had been discussed through the paper of “*Effects of Operating Temperature on The Performance of Vanadium Redox Flow Batteries*” (C. Zhang et al., 2015). For an operating flow battery system, how the performance of battery differs with ambient temperatures is of practical interest. In here, a laboratory-scale single unit of VRFB is tested by diversifying the operating temperature. The efficiency of voltage of the VRFB is shown to rise when the operating temperature is rose along with the peak discharge power at the similar climb of temperature. The increasing temperature, however, causes a small decline in the coulombic efficiency at the similar increase of temperature. In addition, the studies shows a higher capacity degradation rate at higher temperatures. Thus, at higher temperatures, the involved current can be increased in order to obtain a comparable discharge voltage. From the approximately linear shape of the polarization curve, such a distinct is mostly caused by the change in the ohmic resistance (C. Zhang et al., 2015).

Through the paper entitled “*Mathematical Modeling of Electrolyte Flow Dynamic Patterns and Volumetric Flow Penetrations in The Flow Channel over Porous Electrode Layered System in Vanadium Flow Battery with Serpentine Flow Field Design*” (Xinyou Ke et al., 2016), the pressure in the laminar flow for VRFB with Serpentine Flow Field Design had been discussed. A two-dimensional mathematical model is created to investigate the volumetric flow penetrations and flow patterns in the flow channel through the porous electrode layered system in VRFB with serpentine flow field design. The flow distributions at the interface among the porous electrode and flow channel are studied and

the outcome shows that the non-linear distributions of pressure can differentiate between the ideal parabolic flow inlet boundary conditions and the interface flow distributions under the ideal plug flow. However, the volumetric flow penetration for the electrode cell under the flow channel throughout the integration of interface flow velocity shows that this value is similar for both ideal parabolic flow inlet boundary conditions and ideal plug flow condition. The penetration of volumetric flow through the effect of advection for landing or rib and flow channel are further investigated.

Last but not least, based on previous research by Mohamed, it was only assumed that there is a linear relationship of the electrode compartments by using Faraday's law of electrolysis without any specific research done to prove the assumption (Mohamed, 2013). Thus, it is the main intention of this work to perform the linearity study to investigate the relationship of the different size of electrode compartments towards VRFB cell performances. Hence, based on the linearity characteristics that this research proposes, the result obtained can be used as an attempt to standardize the VRFB cell and help reach battery's commercialization.

2.7 Simulation Method for VRFB

For this project, there are several simulation software available to run the charge and discharge graph of VRFB cell. Some of the software available includes MATLAB and ODE45, ANSYS and COMSOL Multiphysics software.

MATLAB is a high – performance platform for computing technical things where it affiliates visualization, computation, and programming environment (Houcq, 2005). Furthermore, it has an advantage of a cultivated data structures, supports object-oriented programming and accommodates built – in editing and debugging tools. Thus, all these elements make MATLAB software an outstanding tool for research and teaching. On the other hand, ODE45 is one of a few distinct built – in for the numerical result of ordinary differential equations (ODE) available in MATLAB. It is established on an explicit formula of Runge-Kutta and the Dormand-Prince pair which signifies that the numerical solver ODE45 unites a method of fourth-order and a fifth-order, both of which are comparable to the classical fourth-order Runge-Kutta (RK) method (Atkinson, Han, & Stewart, 2009).

The solver ODE45 is fitting for a numerous variety of initial value problems in practical applications and is the greatest function to use as a first try for many problems. An extensive code to resolve the model equations of VRFB can be written in MATLAB and ODE45 which can be applied to solve the differential equations. The charge and discharge curves can be acquired after solving the equations (Seepana, 2018). However, the model has its own disadvantage where it does not examine self – discharge and gas evolving reactions which decreases the efficiency of the cell. Meanwhile for ANSYS, it is a general purpose platform used to simulate interactions between all disciplines of structural, physics, vibration, heat transfer, fluid dynamics, and electromagnetic for engineers. ANSYS has the potential of performing advanced engineering simulations precisely and realistically in nature by several of contact algorithms, and non – linear material models and time dependent simulations. Besides that, it also has the ability of combining numerous physics into one software and conduct the analysis. ANSYS, as a solver, allows robust convergence and a full control on the equations. But on the other side, it is not possible to address every application using this simulation software and not all solution variables or models can be accessed apart from the limitation on nodes and the restriction on the usage.

For COMSOL Multiphysics, it is a platform to simulate devices, designs, and processes in all fields of manufacturing, engineering, and scientific research. This simulation software includes of all the steps in the modelling workflow from defining material properties, geometries and the physics that explain specific phenomena to solving and post processing models for generating trustworthy and accurate results. One of the advantages of using COMSOL is the easiness of setting-up the simulation. With one solver, pre-processor and post-processor, simulation analysts do not require to use a different range of platform in order to get one job done. On top of that, with the fact that COMSOL is having default packages, it limits the errors due to boundary conditions and related to the equations. Even though this simulation software is not very customizable and the solver may have some undesired convergence problems, the majority of VRFB simulation models have been solved using COMSOL Multiphysics. This software also has packages for the solutions of electrochemical models, particularly Tertiary Current Density Distribution on where it is in used for Nernst- Planck equation in electrodes, whereas Secondary Current Density Distribution is used for current and potentials in the

membrane. Thus, COMSOL Software is chosen as the platform to run the simulation model due to advantages of its own compared to the other simulation software available.

2.8 Chapter Conclusion

In this chapter, a comprehensive literature review is presented. Some references are taken as a guide in the development of this project and the main reason VRFB is chosen due to there is no cross-contamination occurs when using vanadium as an electrolyte, has a long life cycle and fast response time. From the review of the journals and some related sources from past research to date, characterization and performance analysis for linearity of multi-stack VRFB is chosen to be investigated because the issue still remains unknown and there is very little discussion in the literature found regarding the linearity study directly related to the VRFB performance analysis and its efficiency. Besides that, the design consideration and performance parameter are also discussed in order to develop a high-efficiency VRFB. By also referring to the literature reviews, ideas on the operation of the VFRB has developed as well as the linearity study.



UMP

CHAPTER 3

METHODOLOGY

3.1 Chapter Overview

This chapter discusses the detail methodology used in this study. For this project, the procedure is based on the activities listed below and by simulating the software part. In this chapter, it also explains the extensive clarification of research methodology within this project field. This chapter begins with the description of the flow process for the whole project followed by the modelling of VRFB cell in the simulation. The numerical details and parameters involved are being discussed as well. Lastly, it focuses on the simulation of the charge and discharge of the VRFB cell.

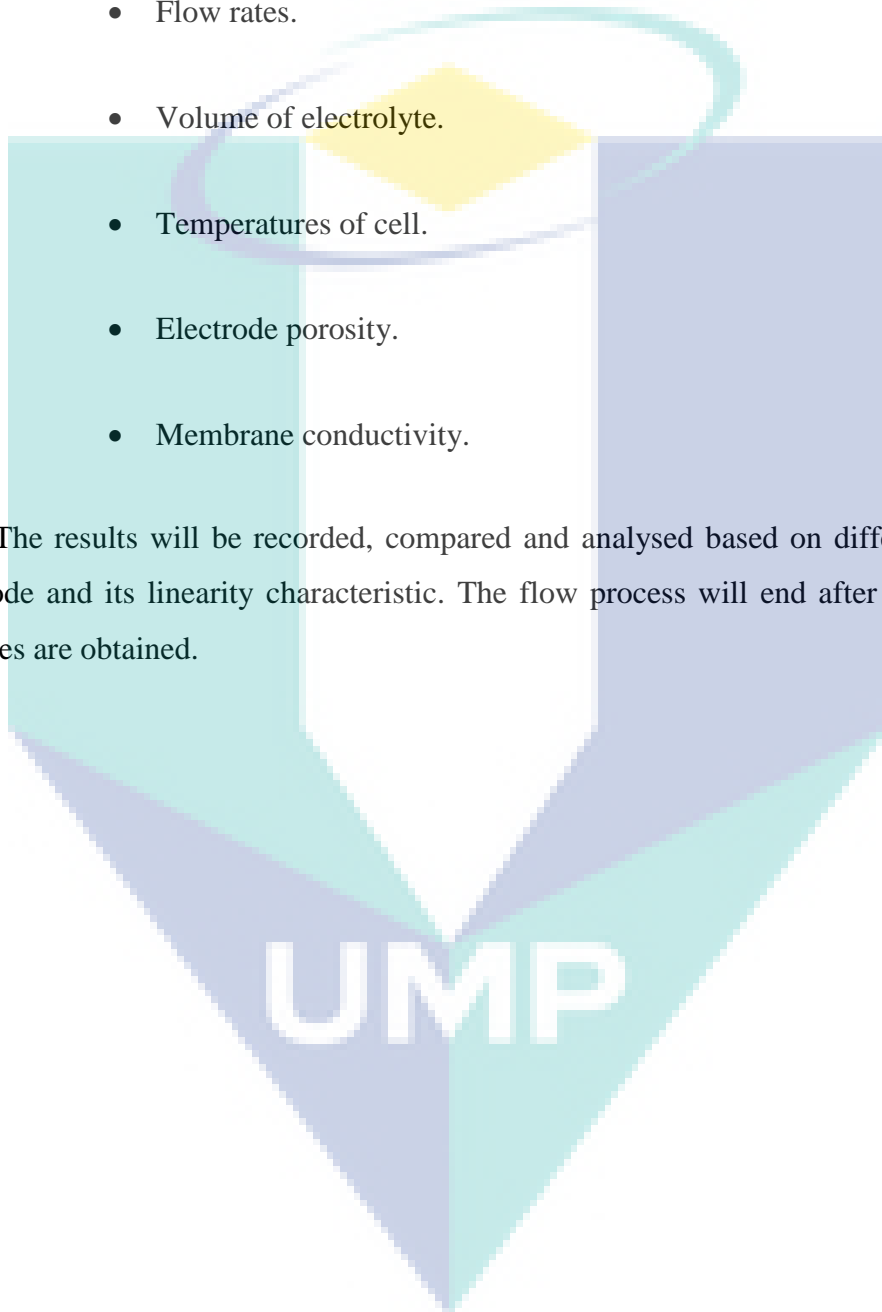
3.2 Flow Process

All procedure could be simplified in the flow process to obtain a clear review regarding this project. Figure 3.1 below illustrates the flow process of the whole project which starts with drawing the VRFB cell model geometry in the COMSOL Multiphysics software based on two dimension (2D). Next step, the parameter and boundary condition are set up and then mesh is created for the geometry to suit the application. After that, the appropriate application mode is selected in order to analyse the efficiency of the battery by using the charge and discharge graph. For this step, it also involves selecting a proper mode for initialization of ion distribution and electrolyte potential before analysing the battery's efficiency. The model design is then simulated with different electrode sizes in order to achieve the results. If the graph of charge and discharge of VRFB is obtained, then a series of analysing the results will be made. Otherwise, if a problem is encountered in obtaining the graph of charge and discharge, then troubleshooting of the model should be made until the final charge and discharge graph is obtained. After the simulation result

is obtained successfully, the next step will be the analyzation of parameter for VRFB characterization. The parameters that will be tested are as follows:

- Current density.
- Flow rates.
- Volume of electrolyte.
- Temperatures of cell.
- Electrode porosity.
- Membrane conductivity.

The results will be recorded, compared and analysed based on different sizes of electrode and its linearity characteristic. The flow process will end after all the result analyses are obtained.



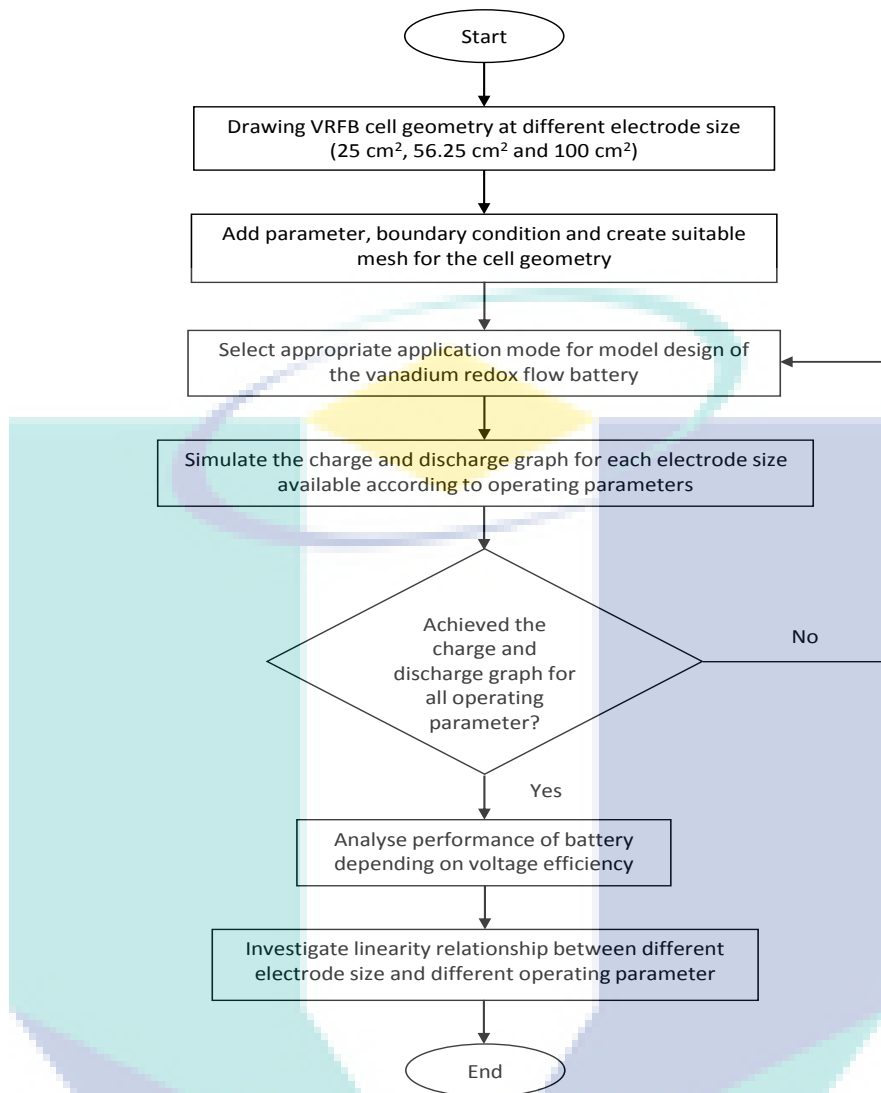


Figure 3.1 Flow Process of the project

3.3 Design and dimension of the cell

This section presents the dimension of the battery in the simulation. The geometry consists of three rectangular with one of it having a different size compared to the other two. The three components involved are positive electrode, negative electrode and membrane where the membrane component is sandwiched in between two electrodes with the same size on both sides as shown in Figure 3.2. The design of the VRFB cell is in two-dimensional space as referred to the model available in the library application for VRFB. The full diagram of the geometry drawing with different size of electrodes (side view) is shown in Figure 3.3, while Figure 3.4 shows full diagram of the geometry in front view.

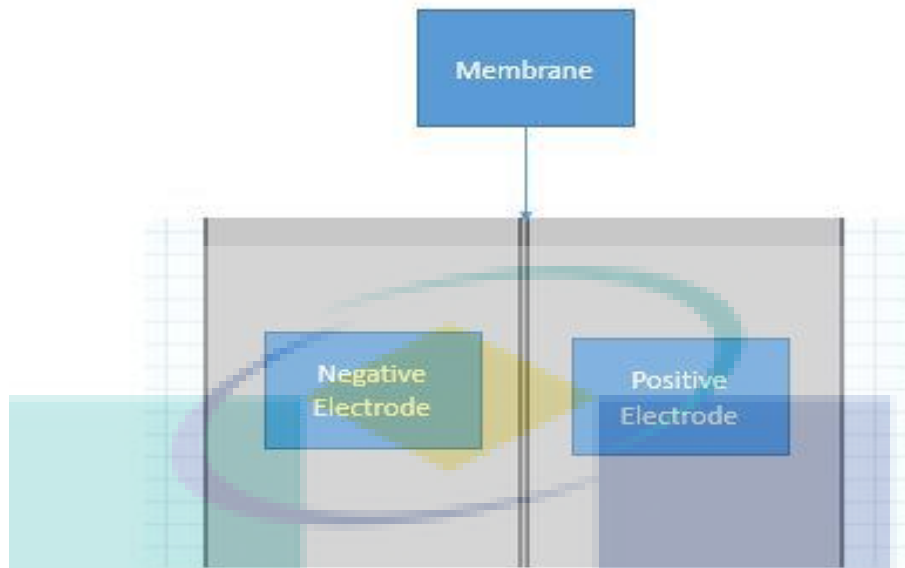


Figure 3.2 Components of battery design

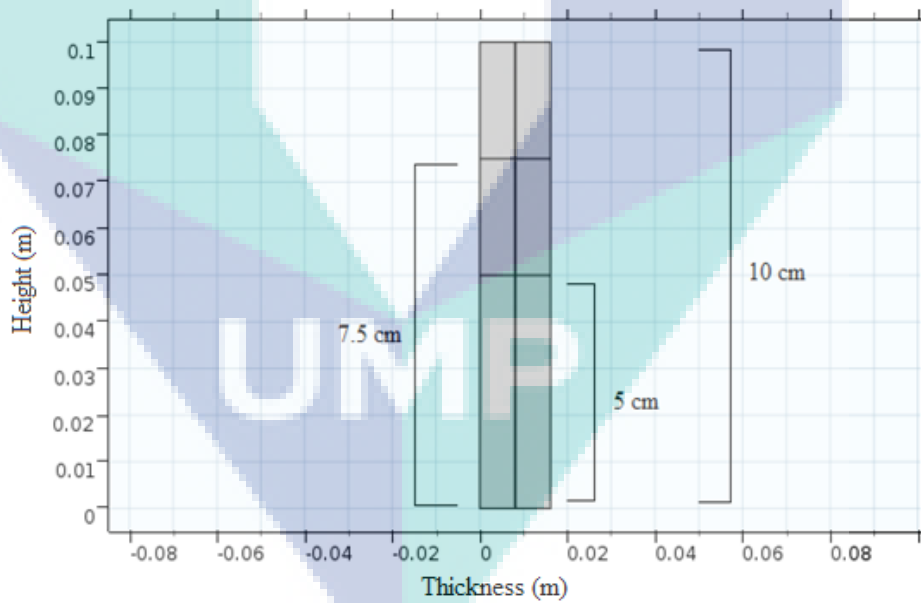


Figure 3.3 Full diagram of geometry drawing with different size of electrodes (side view)

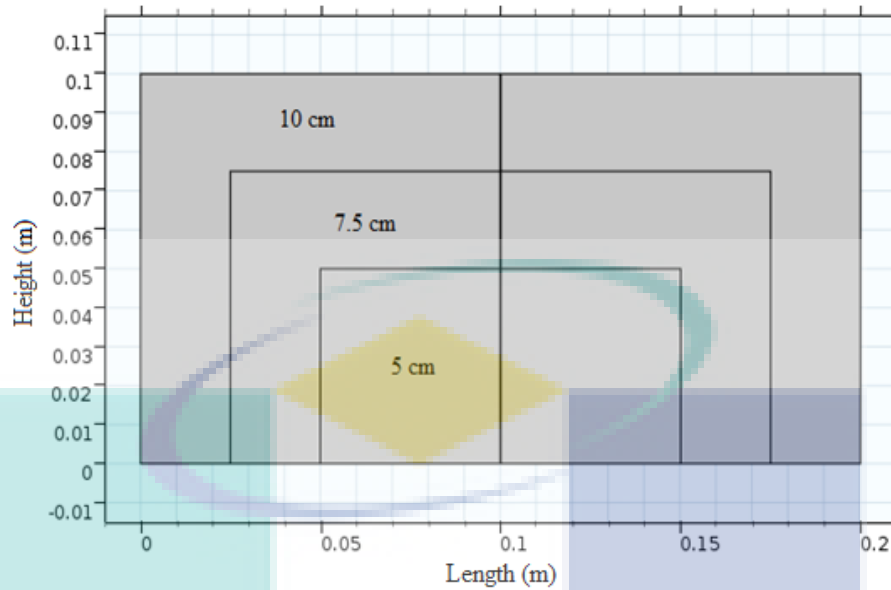


Figure 3.4 Full diagram of geometry drawing with different size of electrodes (front view)

This project focuses on different size of electrodes in order to analyse the VRFB cell linearity. Due to this purpose, three different size of electrodes are proposed for the study which are 5 cm, 7.5 cm and 10 cm. Table 3.1 below shows the full dimension of each component that can be found in the geometry drawing.

Table 3.1 Full dimension of component in VRFB cell

Size of VRFB cell	25 cm ²	56.25 cm ²	100 cm ²
Component	Negative and Positive Electrode		
Length (m)	0.05 m	0.075 m	0.10 m
Height (m)	0.05 m	0.075 m	0.10 m
Thickness (m)	0.008 m	0.008 m	0.008 m
Component	Membrane		
Length (m)	0.05 m	0.075 m	0.10 m
Height (m)	0.05 m	0.075 m	0.10 m
Thickness (m)	1.75E-4 m	1.75E-4 m	1.75E-4 m

3.4 Interfaces and application mode of COMSOL Multiphysics

For COMSOL Multiphysics software, there are a few interfaces available such as electrochemistry, heat transfer, fluid flow, semi – conductor, mathematics and structural mechanics. But for this project, electrochemistry interface is chosen since it suits the VRFB model application. Under electrochemistry, Tertiary Current Distribution, Nernst – Planck is used to define both Negative and Positive electrodes. The Tertiary Current Distribution, Nernst-Planck interface describes the current and potential distribution in an electrochemical cell taking into account the individual transport of charged species (ions) in the electrolyte. The physics interface further assumes that the electroneutrality condition is valid in the electrolyte.

The electrode kinetics for the reaction of charge transfer can be discussed by using arbitrary expressions or by using the predefined Butler-Volmer and Tafel expressions. Note that the electroneutrality condition assumes that all major current – carrying ions are included in the model. This physics interface can be used to model generic electrochemical cells with significant concentration gradients of the current – carrying species (ions). Ohm's law is used in combination with a charge balance to describe the flow of currents in the electrodes. On the other hand, the Nernst-Planck equations are used to portray the transport of charged and neutral species in the electrolyte.

Besides that, Secondary Current Distribution under the electrochemistry interface is chosen to define the membrane compartment. The Secondary Current Distribution interface is similar to that of Primary Current Distribution interface with the difference that it considers for activation overpotentials. The connection between overpotential and charge transfer can be discussed by using arbitrary kinetic expressions, such as Butler-Volmer and Tafel equations. This physics interface can be used for generic modelling of electrochemical cells. It can be combined with interfaces modelling mass transport to describe the concentration dependent (tertiary) current distributions. Ohm's law is also used in combination with a charge balance to describe the conduction of currents in the electrodes and electrolytes.

Other than that, the Global ODEs and DAEs interface under mathematics interface is also used in order to include global space – independent equations that can indicate additional states. The equations can be ODEs, algebraic equations, as well as DAEs.

3.5 Modelling of VRFB

For this subtopic, the modelling of VRFB is discussed. The model consists of two different cell compartments, with different ion compositions and electrode reactions, divided by an ion-exchange membrane. The two cell compartment and membrane are known as the three main domains in the model. Each side of the cell is fed with an electrolyte containing sulfuric acid and a vanadium redox couple that is flowing through the porous electrodes. The liquid enters the cell from the bottom at a steady velocity in the direction of y , corresponding to a few series of flow rate at a cell depth of 0.05 m. A load cycle of 50 s charge, 3 s rest, and 45 s discharge is applied to the cell. During charge or discharge, a constant current density corresponding to a mean current density in the cell is applied.

The potential of electric in the electrodes is reckoned to be space independent. The negative electrode is grounded, while on the positive electrode, an electrode potential is calculated in order to fulfil a current density condition defined by the load cycle (using the Electrode Surface boundary node). The species fluxes are defined on the electrode surfaces according to the electrode reactions. An inflow condition is used at the inlet with the inlet concentrations taken from the tank model. An outflow condition is set at the outlet, while all other boundaries are isolated. The first study will solve for a stationary case in order for the ion concentration to mix while the second study will solve for a time dependent case where charge and discharge graphs of VRFB cell is analysed.

The VRFB model in the COMSOL library relies on the interface of the Batteries and Fuel Cell model which consist of Tertiary current distribution, Nernst-Planck and Secondary current distribution. Tertiary current distribution includes mass, reaction and electric charge transport. It is related to the negative and positive electrodes because the concentrations in the porous electrode domains are of the same order of magnitude and the gradients of the concentrations are not negligible. For the Secondary current distribution, reactions do not occur inside the membrane but is instead related to the

membrane because the negative ions are fixed inside the polymer membrane so their concentration is constant.

There are two main equations that are being used throughout this project which are the Nernst – plank equation and also Butler – Volmer equation. At the beginning, the negative electrolyte carries H^+ , HSO_4^- , SO_4^{2-} , V^{3+} and V^{2+} ions. The negative electrode reaction is:



The equilibrium potential for this reaction is calculated using the Nernst equation (Knehr, Agar, Dennison, & Kalidindi, 2012) given by:

$$E_{eq, neg} = E_{o, neg} + \frac{RT}{F} \ln\left(\frac{aV^{3+}}{aV^{2+}}\right); \quad 3.2$$

where $E_{o, neg}$ is the reference potential for the electrode reaction (SI unit: V), a_i is the chemical activity of species i (dimensionless), R is the molar gas constant (8.31 J/(mol·K)), T is the cell temperature (SI unit: K), and F is Faraday’s constant (96,485 s·A/mol).

On the other hand, the positive electrolyte carries H^+ , HSO_4^- , SO_4^{2-} , VO^{2+} and VO_2^+ ions.

The positive electrode reaction is:



The equilibrium potential calculated according to Nernst Plank equation is:

$$E_{eq, pos} = E_{o, pos} + \frac{RT}{F} \ln\left(\frac{aVO_2^+(aH^+)^2}{aVO^{2+}}\right); \quad 3.4$$

The reversible redox reactions taking place on the surface of the carbon electrode can be expressed by using the Butler-Volmer equation (Dickinson & Hinds, 2019) for the

transfer current densities in both electrode compartments. A Butler-Volmer expression used for the negative electrode reaction is given as follows:

$$i_{neg} = A i_{0,neg} \left(\exp \left(\left(\frac{(1 - a_{neg}) F \eta_{neg}}{RT} \right) \right) - \exp \left(\frac{-a_{neg} F \eta_{neg}}{RT} \right) \right); \quad 3.5$$

$$i_{0,neg} = F k_{neg} (a_{v2+})^{1-a_{neg}} (a_{v3+})^{a_{neg}}. \quad 3.6$$

where A is the specific surface area (SI unit: m^3/m^2) of the porous electrode, a_{neg} is the transfer coefficient (dimensionless), and k_{neg} is the rate constant. The overpotential, η_{neg} (SI unit: V), is defined as

$$\eta = \varphi_s - \varphi_l - E_{eq}; \quad 3.7$$

where φ_s is the electric potential of the solid phase of the electrode (SI unit: V) and φ_l is the electrolyte potential (SI unit: V).

Next, a Butler-Volmer expression used for the positive electrode reaction is given as follows:

$$i_{pos} = A i_{0,pos} \left(\exp \left(\left(\frac{(1 - a_{pos}) F \eta_{pos}}{RT} \right) \right) - \exp \left(\frac{-a_{pos} F \eta_{pos}}{RT} \right) \right); \quad 3.8$$

$$i_{0,pos} = F k_{pos} (a_{vO2+})^{1-a_{pos}} (a_{vO2+})^{a_{pos}}. \quad 3.9$$

For the tank model, the electrolyte flowing out from the cell flows into the tank, undergoes mixing, and then leads into the cell again on the inlet side assuming there will be a good mixing in the tank for the inlet concentrations. The good mixing is governed by the Global ODEs & DAEs physics where when running the first study, the initial

concentration needs to be set as 0 for all ion concentrations in both positive and negative electrode.

3.6 Model Assumption

In order to develop a manageable problem, few assumptions are adopted in the battery model. Firstly, the coulombic efficiency is assumed to be 90% throughout the simulation (Nathan Quill; Robert P. Lynch; Xin Gao and D. Noel Buckley, 2014). Secondly, the model consists of 2 studies. Study 1 is a stationary study which initializes the distribution of each ion and electrolyte potential in order to make sure the ion is mixing well before other simulations are tested. On the other hand, Study 2 is a time dependent study which analyses the charge and discharge of the VRFB model. Lastly, the electrolyte is based on a mixture of vanadium redox couple, sulfuric acid and water, where this model is assumed to dissociate into an electrolyte consisting of a few ions dissolved in a bulk solution of zero-charged species (mainly water). Electroneutrality is assumed locally in the electrolyte. The combination of these assumptions allows the usage of Tertiary Current Distribution, Nernst-Planck interface for modelling the electrolyte transport.

3.7 Chapter Conclusion

This chapter starts with discussing about the chapter overview followed by flow process, and introduction to COMSOL Multiphysics. Next, geometry drawing and the dimension of the cell is mentioned along with defining variables and creating mesh. Later, the modelling of VRFB cell is discussed along with the model assumption for this project. The modelling for the VRFB should continue until the simulation achieves the project's objective.

CHAPTER 4

RESULTS AND DISCUSSION

4.1 Chapter Overview

This chapter starts with discussing few different operating parameters being tested on the VRFB cell. It also explains the graphs obtained after running the simulation and analysing the linearity of each results. Lastly, it focuses on analysing the simulation of the charge and discharge of the VRFB cell based on different size of electrodes.

4.2 Results and discussion

This subchapter is divided into six sections where each section will discuss on the different operating parameters tested in this simulation. The parameters involved are as follows:

- Current density.
- Flow rates.
- Volume of electrolytes.
- Temperature of cell.
- Electrode porosity.
- Membrane conductivity.

For each parameter, the pattern of the graph will be discussed. The performance of the VRFB will also be analysed based on different stacks of electrode compartments. The results obtained from different sizes of electrode compartments can be used to determine and analyse whether they are linear or non-linear. The analyses will continue with different operating parameters being used at different sizes of electrode compartments.

The dissertation of the project is to prove the relationship of VRFB through different sizes of the electrode compartments with the voltage. The larger area of the battery increases the voltage of charge-discharge. Furthermore, based on the objective, the project tends to prove the performance of VRFB depending on different stacks of electrode compartments at different operating parameters which are the current density and flow rate. For the results section, three figures will be shown for each parameter and each figure contains three graphs that represent three different values of controlled parameters. In order to verify the battery performance for each parameter, the voltage efficiency is used. The voltage efficiency can be obtained from the charge – discharge graph by calculating the ratio between charging and discharging of cell potential.

4.3 Results and Analysis of VRFB Modelling

This section will be divided into few parameters being tested which consists of current density, flow rates, volume of electrolytes, temperature, electrode porosity and membrane conductivity.

4.3.1 Current Density

In this section, different results are obtained from the simulation of the VRFB with different values of constant current density applied to different sizes of electrodes in the range of 50 to 100 mA/cm². The other cell parameters such as flow rate of 0.17 cm³/s, volume electrolyte of 10 cm³ and temperature of 298.15 K are kept constant in order to maintain the validity of the result. Figure 4.1, Figure 4.2 and Figure 4.3 show the graph of charge and discharge of VRFB for 25 cm², 56.25 cm² and 100 cm², respectively.

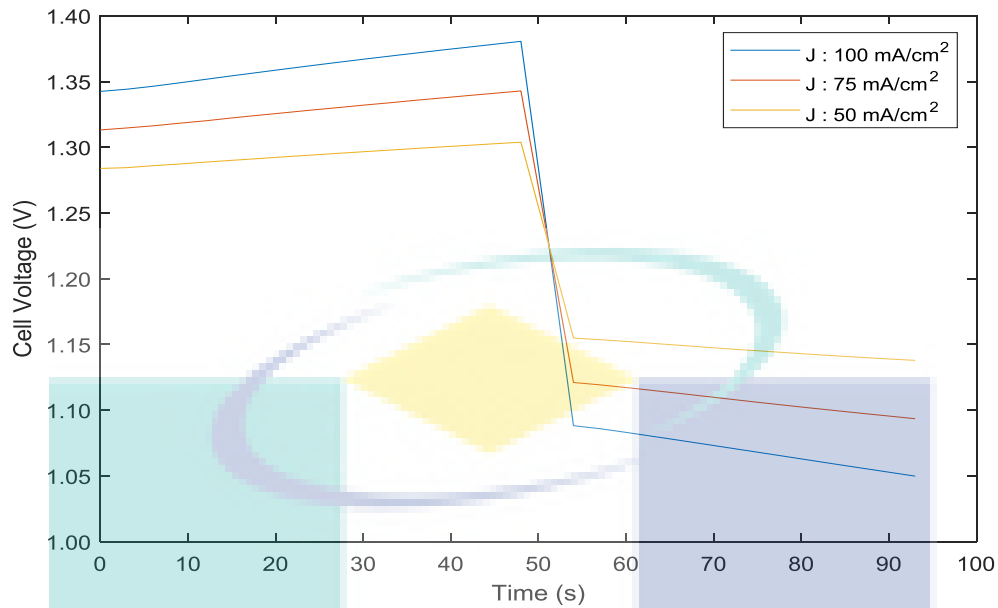


Figure 4.1 Cell voltage vs. time representing charge – discharge characteristics of a 25 cm² VRFB under controlled current density (50, 75 and 100 mA/cm²) for 10 cm³ volume of electrolyte at constant linear flow rate of 0.17 cm³/s, temperature of 298.15 K, electrode porosity of 0.94 and membrane conductivity of 15 S/m.

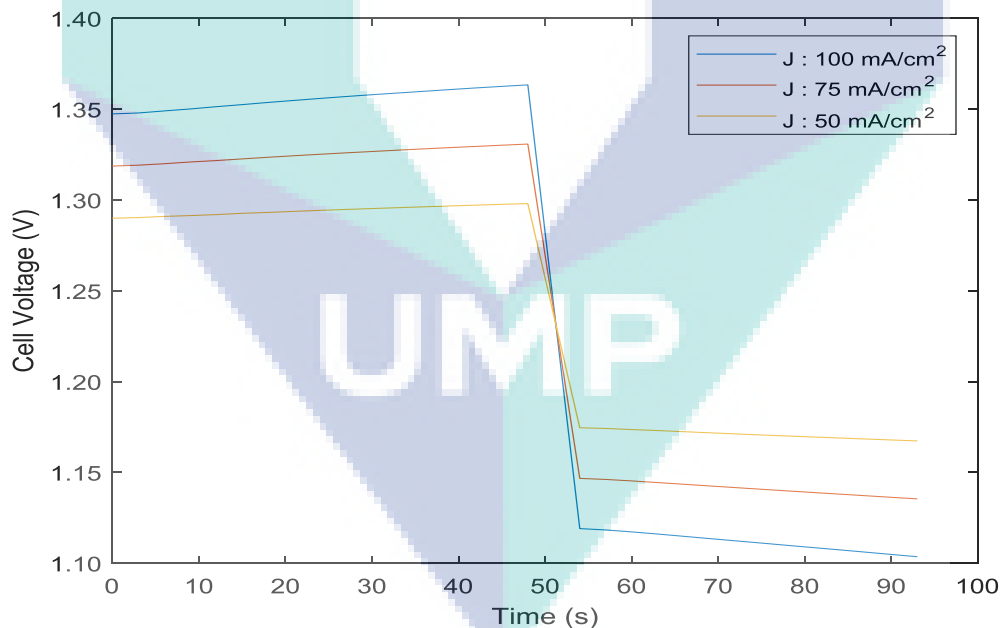


Figure 4.2 Cell voltage vs. time representing charge – discharge characteristics of a 56.25 cm² VRFB under controlled current density (50, 75 and 100 mA/cm²) for 10 cm³ volume of electrolyte at constant linear flow rate of 0.17 cm³/s, temperature of 298.15 K, electrode porosity of 0.94 and membrane conductivity of 15 S/m.

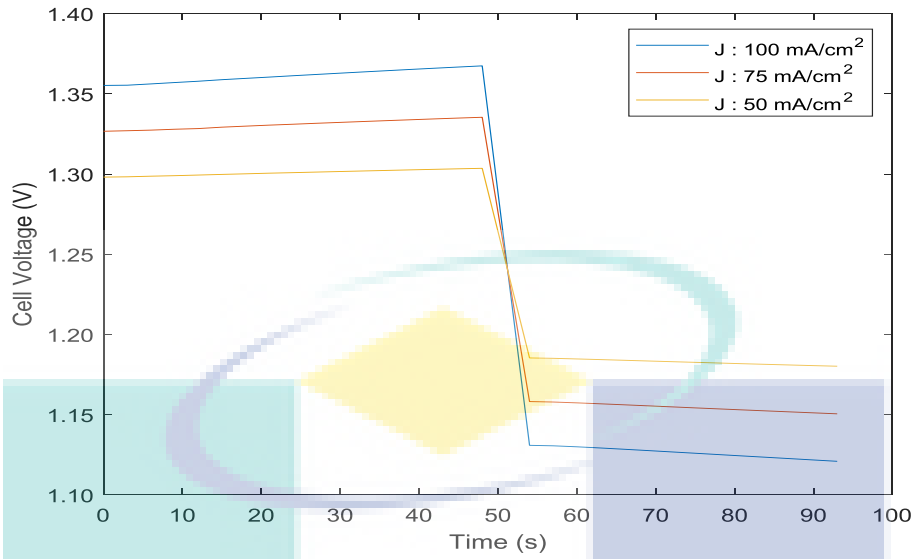


Figure 4.3 Cell voltage vs. time representing charge – discharge characteristics of a 100 cm² VRFB under controlled current density (50, 75 and 100 mA/cm²) for 10 cm³ volume of electrolyte at constant linear flow rate of 0.17 cm³/s, temperature of 298.15 K, electrode porosity of 0.94 and membrane conductivity of 15 S/m.

From the graph of charge and discharge of VRFB, it is clear that all three sizes of electrode possess similar charge-discharge graph characteristics as a result. The data from the simulation is analysed and the voltage efficiency for each graph is tabulated. From Table 4.1 below, it can be seen that the voltage efficiency decreases from 89% to 79% for 25 cm² cell, 90% to 82% for 56.25 cm² and 91% to 83% for 100 cm² as the current density applied on the simulation increases from 50 to 100 mA/cm². Besides that, it can also be seen that voltage efficiency increases from 89% to 91% for 50 mA/cm², 83% to 87% for 75 mA/cm² and 79% to 83% for 100 mA/cm² as the size of electrode increases from 25 cm² to 100 cm².

Table 4.1 Voltage efficiency of VRFB for different current density applied at different electrode size

Current Density / Electrode Size	25 cm ²	56.25 cm ²	100 cm ²
50 mA/cm ²	$\eta_v = 89\%$	$\eta_v = 90\%$	$\eta_v = 91\%$
75 mA/cm ²	$\eta_v = 83\%$	$\eta_v = 86\%$	$\eta_v = 87\%$
100 mA/cm ²	$\eta_v = 79\%$	$\eta_v = 82\%$	$\eta_v = 83\%$

Table 4.2 shows the simulation data for different current densities applied at different electrode sizes in a specific time frame such as starting, peak charge, first discharge, final discharge and IR Drop. From the table, it can be seen that the discharge voltage decreases as current density increases because of the effect of overpotential and IR drop across electrode membrane and electrolyte (Mohamed et al., 2015). Since coulombic efficiency is set at 90% as referred to the optimum value, this means a higher current density will result in a good charge acceptance. This can be credited due to the fact that as current density increases, the reaction rates of the charge-discharge cycle are quicker, hence the time for the active species to penetrate through the membrane is reduces (Mohamed et al., 2015).

Table 4.2 Simulation data for different current densities applied at different electrode sizes in a specific time.

Size of stack	25 cm ²			56.25 cm ²			100 cm ²		
Current Density (mA/cm ²)	50	75	100	50	75	100	50	75	100
Starting Voltage (V)	1.2839	1.3132	1.3425	1.2900	1.3187	1.3474	1.2981	1.3267	1.3553
Peak Charge Voltage (V)	1.3039	1.3428	1.3805	1.2980	1.3308	1.3634	1.3036	1.3354	1.3675
Discharge Voltage (V)	1.1549	1.1211	1.0882	1.1746	1.1467	1.1191	1.1854	1.1582	1.1310
Final Voltage (V)	1.1379	1.0936	1.0499	1.1673	1.1354	1.1036	1.1803	1.1506	1.1210
IR Drop (V)	0.1490	0.2217	0.2923	0.1234	0.1841	0.2443	0.1182	0.1772	0.2365

On the other hand, the efficiency of voltage is depleted with the rise of current density attributable to the big IR drop throughout the discharge cycle where this can be seen as the IR drop increases from 0.1490 to 0.2923 in 25 cm² cell, 0.1234 to 0.2443 in 56.25 cm² and 0.1182 to 0.2365 in 100 cm². The overall efficiency of energy is in the scale of 71% to 82% for current densities between 50 to 100 mA/cm² and it is corresponding to further published VRFB systems.

For linearity study, the mathematical modelling for each graph is calculated by using equation (4.1) since the graph is in exponential mode.

$$y = A_0 e^{kx}; \quad 4.1$$

where A_0 is the value at time zero, e is Euler's constant, k is a constant that determines the difference of variable x , with x being the amount of period considered.

To determine the linearity modelling, equation (4.2) is used:

$$A_n = A_1 + (n-1)d; \quad 4.2$$

where d is the common ratio and n is the n -th term.

For 25 cm² cell, the Table 4.3 below shows linearity equations of graphs and goodness of fitting for each current density value.

Table 4.3 Linearity equations and fitting goodness for 25 cm² of VRFB cell.

Current Density	Linearity Equations	Fitting Goodness
100 mA/cm ²	$y = 1.3425 e^{0.0005x}$	$R^2 = 0.9989$
75 mA/cm ²	$y = 1.3132 e^{0.0004x}$	$R^2 = 0.9994$
50 mA/cm ²	$y = 1.2839 e^{0.0003x}$	$R^2 = 0.9991$

For the intercept, there is an increase of 0.0293 with every increase of 25 mA/cm² current density injected into the system with the minimum value set at 50 mA/cm² and the intercept obtained is 1.2839. While for the difference, there is an increase of 0.0001 with every increase of 25 mA/cm² current density with the minimum value of current density set to 50 mA/cm² and the difference obtained is 0.0003. R-squared (R²) value is also shown for each equations of graph where it shows the goodness-of-fit measure for linear regression model. The closer the line passes through all of the points in the graph, the greater the fit of the regression line, which means the nearer the value to 1.0 digits.

Thus, the linearity modelling obtained for 25 cm² cell is:

$$y = [1.2839 + (n-1)0.0293] e^{[0.0003 + (n-1)0.0001]x}$$

For 56.25 cm² cell, the Table 4.4 below shows linearity equations of graphs and goodness of fitting for each current density value.

Table 4.4 Linearity equations and fitting goodness for 56.25 cm² of VRFB cell.

Current Density	Linearity Equations	Fitting Goodness
100 mA/cm ²	$y = 1.3474 e^{0.00025x}$	R ² = 0.9971
75 mA/cm ²	$y = 1.3187 e^{0.00019x}$	R ² = 0.9972
50 mA/cm ²	$y = 1.2900 e^{0.00013x}$	R ² = 0.9977

For the intercept, there is an increase of 0.0287 with every increase of 25 mA/cm² current density injected into the system with the minimum value set at 50 mA/cm² and the intercept obtained is at 1.2900. While for the difference, there is an increase of 0.00006 with every increase of 25 mA/cm² current density with the minimum value of current density is set to 50 mA/cm² and the difference obtained is 0.00013.

Thus, the linearity modelling obtained for 56.25 cm² cell is as below:

$$y = [1.2900 + (n-1)0.0287] e^{[0.00013 + (n-1)0.00006]x}.$$

Lastly, for 100 cm² cell, the Table 4.5 below shows linearity equations of graphs and goodness of fitting for each current density value.

Table 4.5 Linearity equations and fitting goodness for 100 cm² of VRFB cell.

Current Density	Linearity Equations	Fitting Goodness
100 mA/cm ²	$y = 1.3553 e^{0.00019x}$	$R^2 = 0.9984$
75 mA/cm ²	$y = 1.3267 e^{0.00014x}$	$R^2 = 0.9975$
50 mA/cm ²	$y = 1.2981 e^{0.00009x}$	$R^2 = 0.9991$

For the intercept, there is an increase of 0.0286 with every increase of 25 mA/cm² current density injected into the system with the minimum value set at 50 mA/cm² and the intercept obtained is at 1.2981. While for the difference, there is an increase of 0.00005 with every increase of 25 mA/cm² current density with the minimum value of current density set to 50 mA/cm² and the difference obtained is 0.00009.

Thus, the linearity modelling obtained for 100 cm² cell is:

$$y = [1.2981 + (n-1)0.0286] e^{[0.00009 + (n-1)0.00005]x}.$$

In addition, relationship trend of linearity can be further proven by using Figure 4.4 below for each cell stack size. As per mentioned before, it can be seen that the cell voltage increase linearly with the increase of cell stack size for every 25 mA/cm² increase of current density.

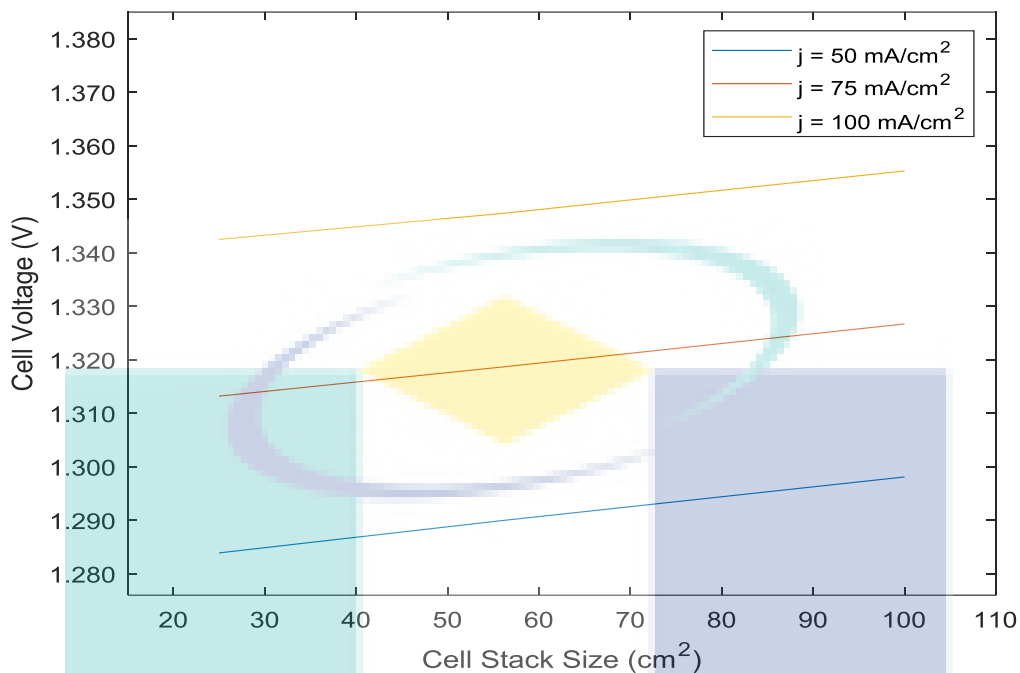


Figure 4.4 Relationship trend between cell voltage vs. different cell stack size (25, 56.25 and 100 cm²) for current density of 50, 75 and 100 mA/cm².

On the other hand, the linearity modelling involving different sizes of cell stack with the same current density cannot be done since it is in non-linear form and there are different ratios produced between each current density value and different cell stack sizes. Thus, it can be concluded that, there exists a linear relationship between different current density value and the same cell stack size but there is no linear relationship between different cell stack size and the same current density value.

Besides that, for comparison purpose, preliminary work for this research is extended and conducted at PCB Laboratory, Universiti Malaysia Pahang. The experiment were set up in order to investigate the performance characterisation of vanadium redox flow battery (VRFB) at cell stack size of 25cm² by applying specific current density of 100 mA/cm² continuously throughout the experiment. The whole process of charging and discharging the battery takes place for approximately 160 minutes. Figure 4.5 shown below is the result of the laboratory experimental work that has been carried out.

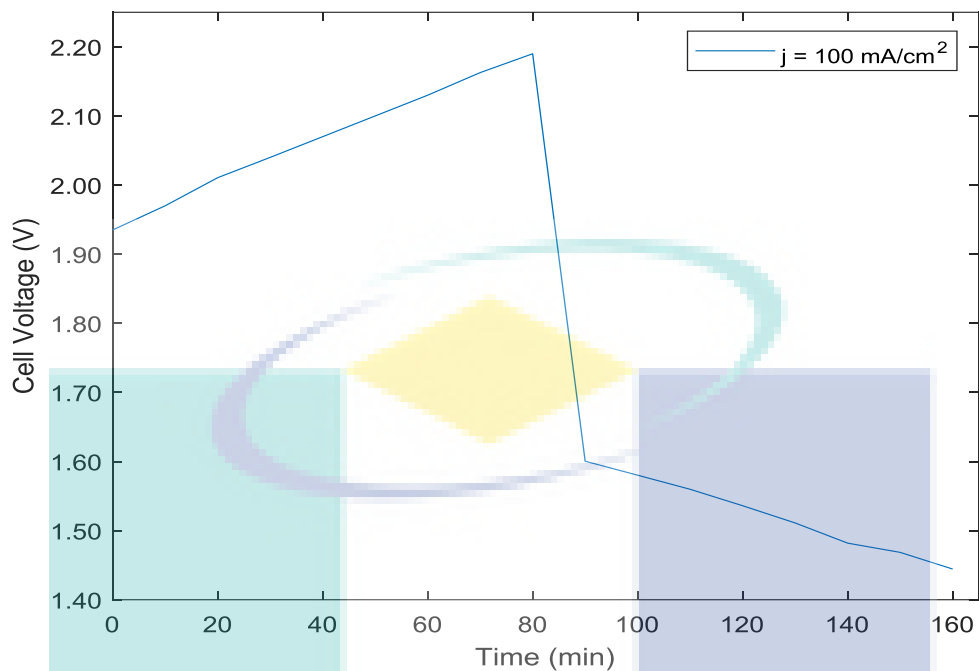


Figure 4.5 Cell voltage vs. time representing charge – discharge characteristics of a 25 cm² VRFB under 100 mA/cm² current density.

Based on the charge and discharge graph from the experimental work, it can be observed that the shape of the graph produced is somewhat similar to the result of this simulation work. There is a linear increase for the charging state and also linear decrease for the discharging state of the battery on where the starting charging voltage read at 1.9350 and the peak charge voltage reach 2.1900. Whereas, for the discharging state, the starting discharge voltage is at 1.6004 and the final discharge voltage is at 1.4444. For the voltage efficiency comparison, this experimental works produced an efficiency of 73% and it is only 6% lesser compared to the simulation results. Lastly, for the coulombic efficiency, it resulted on the 87.5% and it is close to the optimum coulombic efficiency which is 90%. Hence, it can be stated that the simulation result is closely related to the experimental result.

4.3.2 Flow Rates

In this section, the result is achieved via the simulation of the VRFB with different values of constant flow rates applied on different sizes of electrode in the range of 0.17 cm³/s to 0.83 cm³/s. Under constant current density of 50 mA/cm² and temperature of cell of 298.15 K, the effect of the flow velocity of the electrolyte on the battery performance

is studied. Figures below shows the graph of charge and discharge of VRFB for 25 cm^2 , 56.25 cm^2 and 100 cm^2 , respectively. From those three figures, it can be seen that the value and characteristic of the graphs are similar towards each other. This is due to the limitation on the flow rate value that can be tested on COMSOL Multiphysics which is within the small range, thus, resulting on the too little difference obtained among each parameter result. Hence, the charge and discharge graph may seem overlapping towards each other when in fact there is still a little difference available between the three controlled parameters.

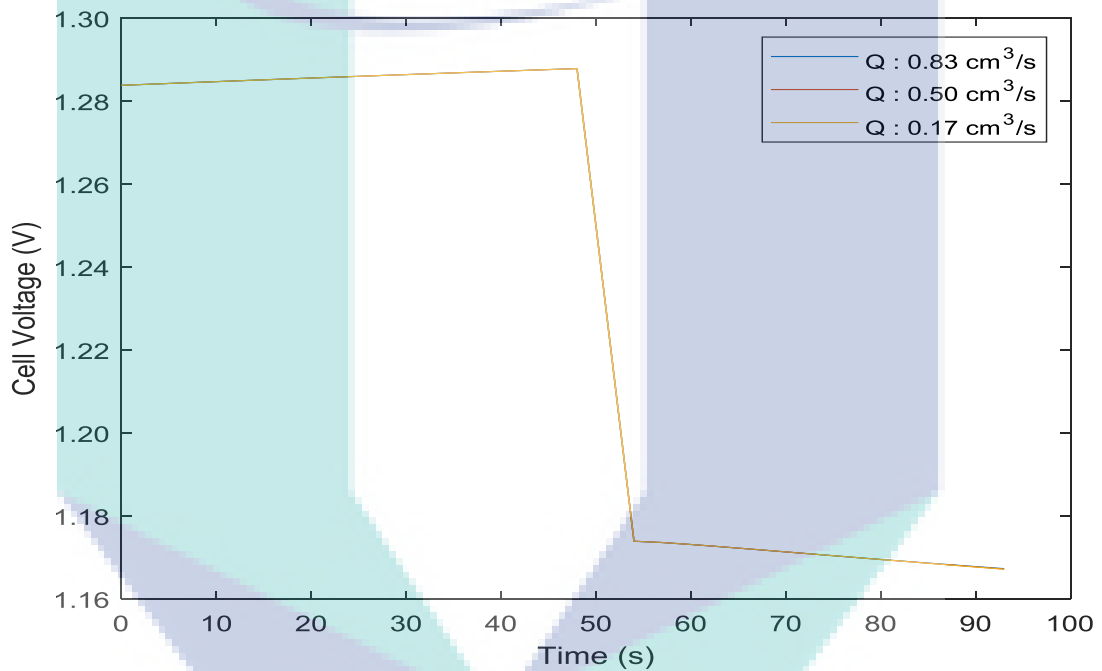


Figure 4.6 Cell voltage vs. time representing charge – discharge characteristics of a 25 cm^2 VRFB at controlled flow rate (0.17 , 0.50 and $0.83 \text{ cm}^3/\text{s}$) for 10 cm^3 volume of electrolyte at constant temperature of 298.15 K , current density of $50 \text{ mA}/\text{cm}^2$, electrode porosity of 0.94 and membrane conductivity of $15 \text{ S}/\text{m}$.

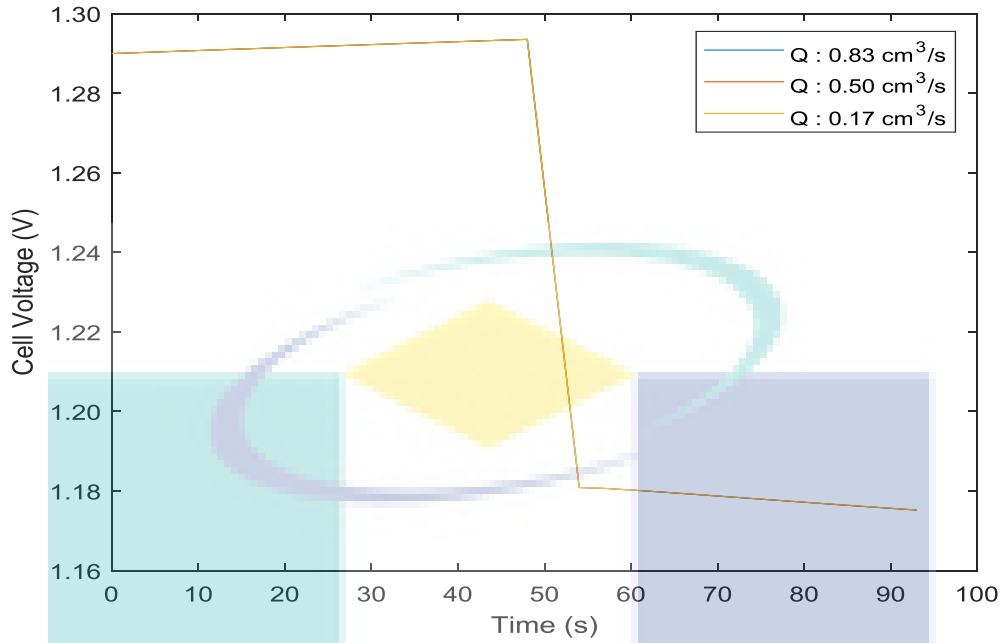


Figure 4.7 Cell voltage vs. time representing charge – discharge characteristics of a 56.25 cm² VRFB at controlled flow rate (0.17, 0.50 and 0.83 cm³/s) for 10 cm³ volume of electrolyte at constant temperature of 298.15 K, constant current density of 50 mA/cm², electrode porosity of 0.94 and membrane conductivity of 15 S/m.

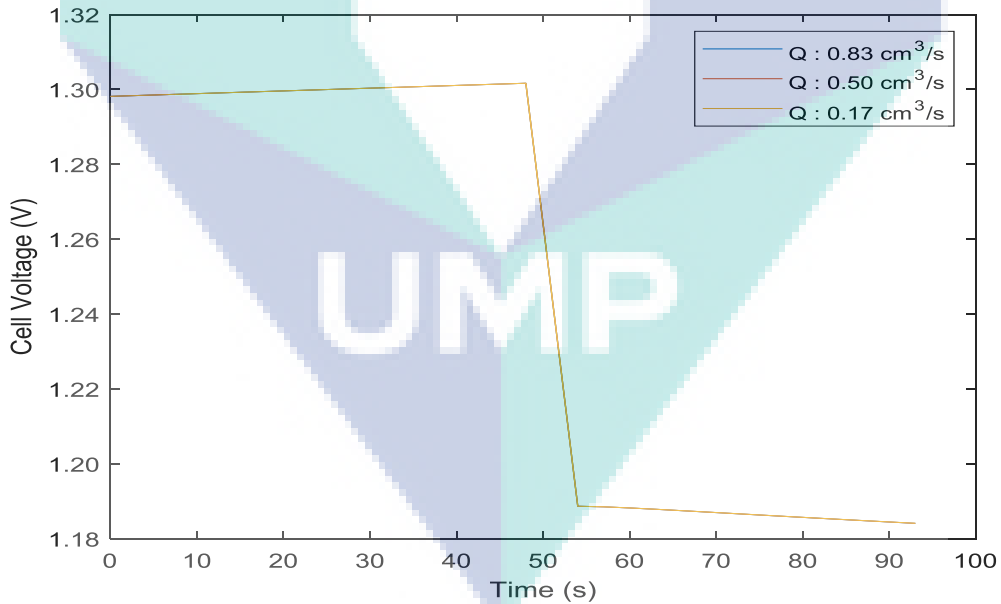


Figure 4.8 Cell voltage vs. time representing charge – discharge characteristics of a 100 cm² VRFB at controlled flow rate (0.17, 0.50 and 0.83 cm³/s) for 10 cm³ volume of electrolyte at constant temperature of 298.15 K, current density of 50 mA/cm², electrode porosity of 0.94 and membrane conductivity of 15 S/m.

From the graph of charge and discharge of VRFB, it can be seen that all three sizes of electrodes possess a similar charge-discharge graph characteristic as a result. The data from the simulation is analysed and the voltage efficiency for each graph is tabulated. From Table 4.6 below, it can be seen that the voltage efficiency decreases slightly from 91.07% to 91.05% for 25 cm² cell, 91.23% to 91.21% for 56.25 cm² and 91.30% to 91.28% for 100 cm² as the flow rates applied on the simulation increases from 0.17 to 0.83 cm³/s.

Besides that, it can also be noticed that voltage efficiency increases slightly from 91.07% to 91.30% for 0.17 cm³/s, 91.06% to 91.29% for 0.50 cm³/s and 91.05% to 91.28% for 0.83 cm³/s as the size of electrode increases from 25 cm² to 100 cm². Low amount of electrolyte flow rates used over the electrode can generate an ineffective flow of electrolyte which develops a non-uniform disperse of ion species inside the electrode itself. However, an elevated amount of electrolyte flow rate, may not grant enough performance considering more power is needed for the pump (Shah & Walsh, 2008).

Table 4.6 Voltage efficiency of VRFB for different flow rates applied at different electrode sizes.

Flow Rates / Electrode Size	25 cm ²	56.25 cm ²	100 cm ²
0.17 cm ³ /s	$\eta_v = 91.07\%$	$\eta_v = 91.23\%$	$\eta_v = 91.30\%$
0.50 cm ³ /s	$\eta_v = 91.06\%$	$\eta_v = 91.22\%$	$\eta_v = 91.29\%$
0.83 cm ³ /s	$\eta_v = 91.05\%$	$\eta_v = 91.21\%$	$\eta_v = 91.280\%$

Table 4.6 shows the simulation data for different flow rates is applied at different electrode size in a specific time frame such as starting, peak charge, first discharge, final discharge and IR Drop. From the table, an increase trend of voltage of cell during the charge cycle is observed and as the flow rates rose, peak cell voltages resolved at 1.287898 V, 1.287907 V, and 1.287916 V, respectively. It is expected that the ion species are not well dispersed inside the cell as the flow rate decreases. This results in the reduction of

the mass transport coefficient and width increment of the Nernst diffusion layer (Mohamed et al., 2015).

The coulombic efficiencies were set to 90% of the optimum cell voltage. On the other hand, efficiency of voltage is recorded in the scale of 91%, where there exists only a small enhancement of efficiency as the flow rate rises. It should also be noted that flow rate does not relay a noticeable effect on the discharge cell voltage in the scale of 0.17 to 0.83 cm³/s. Conversely, discharge cell voltage vaguely plummeted at higher flow velocity as the reaction is no more governed by mass transport. Therefore, an increase in flow velocity is no more fruitful, except when excess power is used to supply the auxiliary components.

Nevertheless, the flow velocity effect can only be significant, mainly at small flow velocity, as additional mass transport of the reactant is required to aid the big reaction rate at bigger discharge current density (Mohamed et al., 2015). If no adequate mass transport of the reactant is supplied for the reactions, side reactions may take place instead causing in even lower discharge cell voltages.

Table 4.7 Simulation data for different flow rates applied at different electrode sizes in a specific time.

Size of stack	25 cm ²			56.25 cm ²			100 cm ²		
	0.17	0.50	0.83	0.17	0.50	0.83	0.17	0.50	0.83
Flow Rates (cm ³ /s)	0.17	0.50	0.83	0.17	0.50	0.83	0.17	0.50	0.83
Starting Voltage (V)	1.283881	1.283882	1.283883	1.289940	1.289941	1.289942	1.298142	1.298143	1.298144
Peak Charge Voltage (V)	1.287898	1.287907	1.287925	1.293508	1.293513	1.293519	1.301600	1.301648	1.301696
Discharge Voltage (V)	1.173963	1.173953	1.173949	1.180907	1.180897	1.180888	1.188679	1.188671	1.188669
Final Voltage (V)	1.167209	1.167245	1.167344	1.175264	1.175221	1.175211	1.184124	1.184103	1.184099
IR Drop (V)	0.113935	0.113954	0.113976	0.112601	0.112618	0.112631	0.112921	0.112977	0.113027

Therefore, the voltage efficiency increases slightly with decreasing flow rates and increasing stack sizes which implies the increase in flow rate, the smaller the number of reactions that will occur (Zimmerman, 2014). There is only a slight change in IR drop during the charge discharge cycle where the IR drop increases from 0.113935 to 0.113976 in 25 cm² cell, 0.112604 to 0.112631 in 56.25 cm² and 0.112921 to 0.113027 in 100 cm². The overall efficiency of energy is around the span of 82% for flow rates of electrolyte between 0.17 to 0.83 cm³/s and it is approximate to other published VRFB systems.

For linearity study, the Table 4.8 below shows linearity equations of graphs and goodness of fitting for each flow rates value for 25 cm² of VRFB cell.

Table 4.8 Linearity equations and fitting goodness for 25 cm² of VRFB cell.

Flow Rates	Linearity Equations	Fitting Goodness
0.83 cm ³ /s	$y = 1.283883 e^{0.0000654x}$	$R^2 = 0.9996$
0.50 cm ³ /s	$y = 1.283882 e^{0.0000652x}$	$R^2 = 0.9996$
0.1d7 cm ³ /s	$y = 1.283881 e^{0.0000650x}$	$R^2 = 0.9996$

For the intercept, there is an increase of 0.000001 with every increase of 0.33 cm³/s flow rates injected into the system with the minimum value set at 0.17 cm³/s and the intercept obtained is at 1.283881. While for the difference, there is an increase of 0.0000002 with every increase of 0.33 cm³/s flow rates with the minimum value of flow rates is set to 0.17 cm³/s and the difference obtained is 0.000065.

Thus, the linearity modelling obtained for 25 cm² cell is:

$$y = [1.283881 + (n-1)0.000001] e^{[0.000065 + (n-1)0.0000002]x}$$

For 56.25 cm² cell, Table 4.9 below shows linearity equations of graphs and goodness of fitting for each flow rates value.

Table 4.9 Linearity equations and fitting goodness for 56.25 cm² of VRFB cell.

Flow Rates	Linearity Equations	Fitting Goodness
0.83 cm ³ /s	$y = 1.289942 e^{0.0000577x}$	$R^2 = 0.9999$
0.50 cm ³ /s	$y = 1.289941 e^{0.0000576x}$	$R^2 = 0.9999$
0.17 cm ³ /s	$y = 1.289940 e^{0.0000575x}$	$R^2 = 0.9999$

For the intercept, there is an increase of 0.000001 with every increase of 0.33 cm³/s flow rates injected into the system with the minimum value set at 0.17 cm³/s and the intercept obtained is at 1.289940. While for the difference, there is an increase of 0.0000001 with every increase of 0.33 cm³/s flow rates with the minimum value of flow rates set to 0.17 cm³/s and the difference obtained is 0.0000575.

Thus, the linearity modelling obtained for 56.25 cm² cell is as shown below:

$$y = [1.289940 + (n-1)0.000001] e^{[0.0000575 + (n-1)0.0000001]x}$$

Lastly, for 100 cm² cell, Table 4.10 below shows linearity equations of graphs and goodness of fitting for each flow rates value.

Table 4.10 Linearity equations and fitting goodness for 100 cm² of VRFB cell.

Flow Rates	Linearity Equations	Fitting Goodness
0.83 cm ³ /s	$y = 1.298144 e^{0.000057x}$	$R^2 = 1.0000$
0.50 cm ³ /s	$y = 1.298143 e^{0.000056x}$	$R^2 = 1.0000$
0.17 cm ³ /s	$y = 1.298142 e^{0.000055x}$	$R^2 = 1.0000$

For the intercept, there is an increase of 0.000001 with every increase of 0.33 cm³/s flow rates injected into the system with the minimum value set at 0.17 cm³/s and the intercept obtained is at 1.298142. While for the difference, there is an increase of 0.000001

with every increase of 0.33 cm³/s flow rates with the minimum value of flow rates set to 0.17 cm³/s and the difference obtained is 0.000055.

Thus, the linearity modelling obtained for 100 cm² cell is as shown below:

$$y = [1.298142 + (n-1)0.000001] e^{[0.000055 + (n-1)0.000001]x}$$

In addition, relationship trend of linearity can be further proven by using Figure 4.9 below for each cell stack size. As per mentioned before, it can be seen that the cell voltage increase linearly with the increase of cell stack size for every 0.33 cm³/s increase of flow rates.

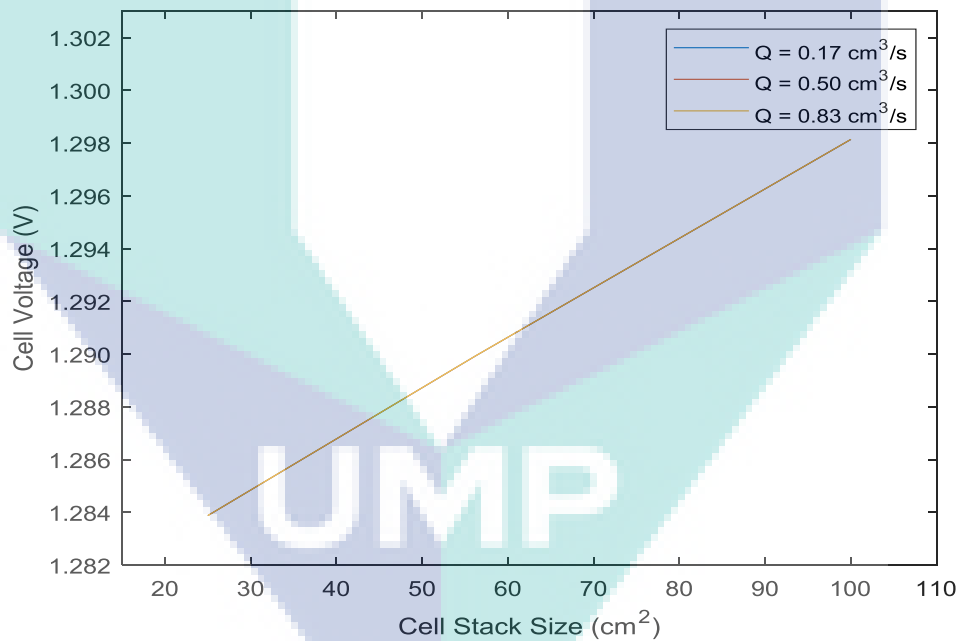


Figure 4.9 Relationship trend between cell voltage vs. different cell stack size (25, 56.25 and 100 cm²) for flow rate of 0.17, 0.50 and 0.83 cm³/s.

On the other hand, the linearity modelling involving different size of cell stacks with the same flow rate value cannot be done since it is in non-linear form and there are different ratios produced between each flow rate value and different cell stack sizes. Thus, it can be concluded that, there is a linear relationship between different flow rate values

and the same cell stack size but there is no linear relationship between different cell stack sizes and the same flow rate value.

4.3.3 Volume of Electrolytes

In this section, we present the results obtained from the simulation of the VRFB with different values of constant volume of electrolytes applied on different size of electrodes in the range of 10 to 50 cm³. The other cell parameter such as current density of 50 mA/cm², flow rate of 0.17 cm³/s, and temperature of 298.15 K is kept constant in order to maintain the validity of the result. Figures below shows the graph of charge and discharge of VRFB for 25 cm², 56.25 cm² and 100 cm², respectively.

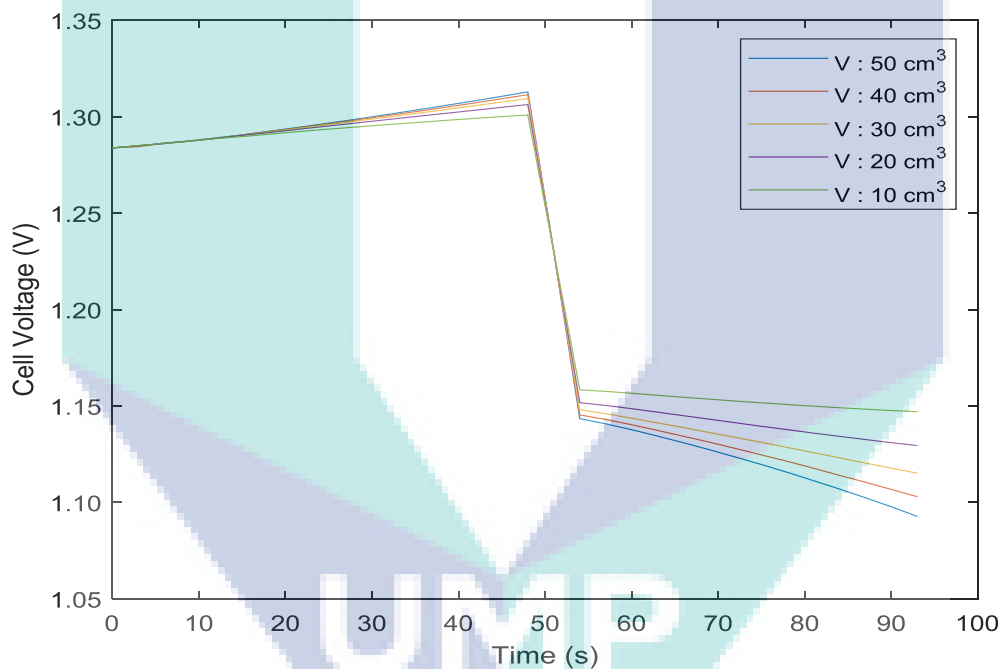


Figure 4.10 Cell voltage vs. time representing charge – discharge characteristics of a 25 cm² VRFB at controlled volume of electrolyte (10, 20, 30, 40 and 50 cm³) at constant flow rate of 0.17 cm³/s, temperature of 298.15 K, current density of 50 mA/cm, electrode porosity of 0.94 and membrane conductivity of 15 S/m.

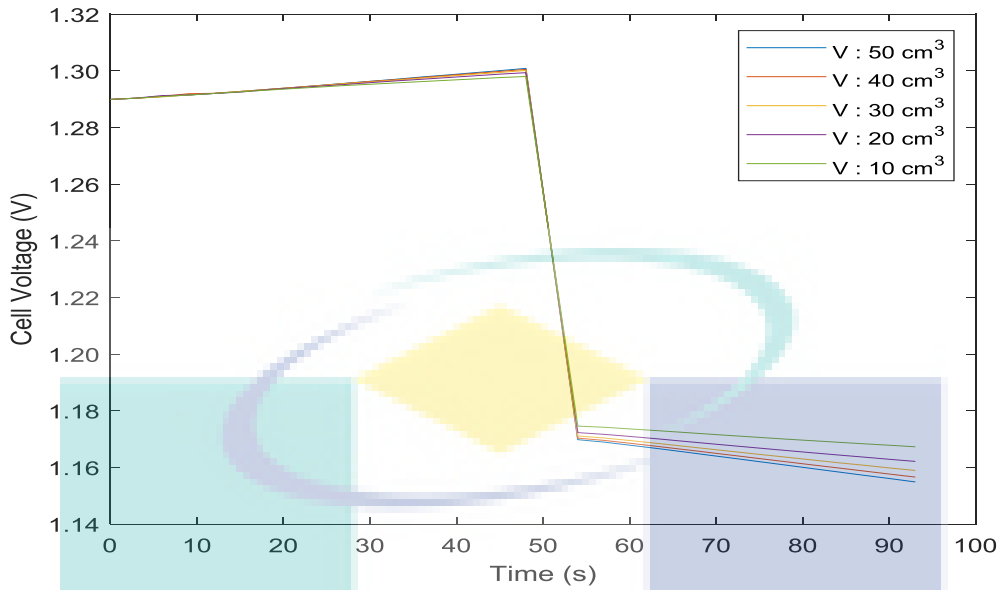


Figure 4.11 Cell voltage vs. time representing charge – discharge characteristics of a 56.25 cm^2 VRFB at controlled volume of electrolyte ($10, 20, 30, 40$ and 50 cm^3) at constant flow rate of $0.17 \text{ cm}^3/\text{s}$, temperature of 298.15 K , current density of $50 \text{ mA}/\text{cm}^2$, electrode porosity of 0.94 and membrane conductivity of $15 \text{ S}/\text{m}$.

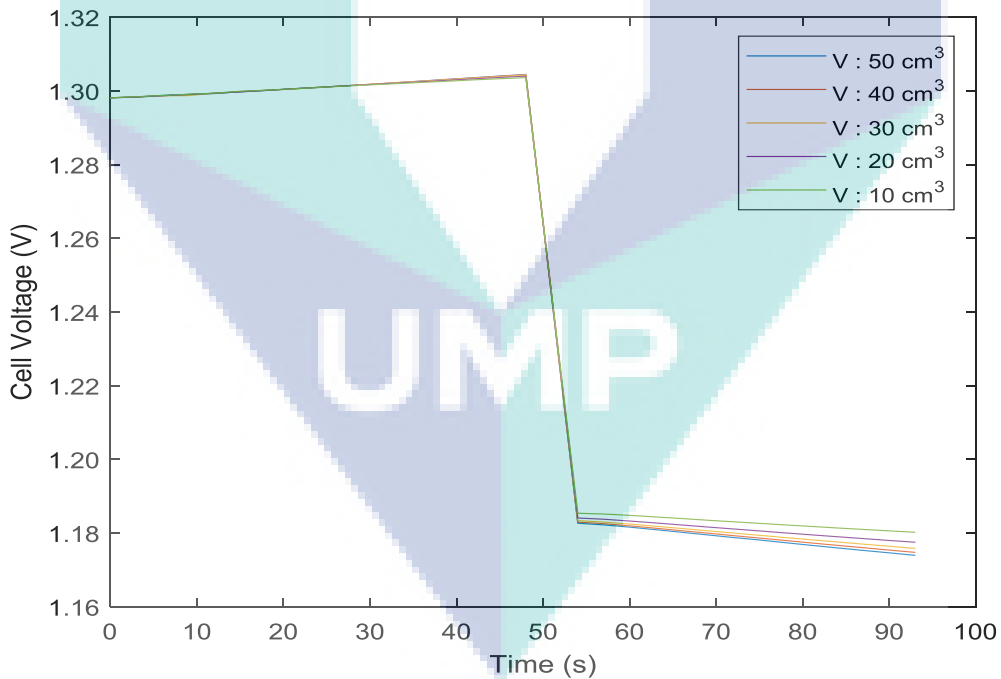


Figure 4.12 Cell voltage vs. time representing charge – discharge characteristics of a 100 cm^2 VRFB at controlled volume of electrolyte ($10, 20, 30, 40$ and 50 cm^3) at constant flow rate of $0.17 \text{ cm}^3/\text{s}$, temperature of 298.15 K , current density of $50 \text{ mA}/\text{cm}^2$, electrode porosity of 0.94 and membrane conductivity of $15 \text{ S}/\text{m}$.

From the graph of charge and discharge of VRFB, the data from the simulation is analysed and the voltage efficiency for each graph is tabulated. From Table 4.11 below, it can be noticed that the efficiency of voltage lessen from 89.1% to 86.7% for 25 cm² cell, 90.5% to 89.8% for 56.25 cm² and 91.0% to 90.5% for 100 cm² as the volume of electrolytes applied on the simulation increases from 10 to 50 cm³. Besides that, it can also be seen that voltage efficiency increases slightly from 89.1% to 91.0% for 10 cm³, 87.5% to 90.7% for 30 cm³ and 86.7% to 90.5% for 50 cm³ as the size of electrode increases from 25 cm² to 100 cm².

Energy and power are distinct of each other in VRFB, where the energy potential is set by the electrolyte volume while the power potential is set by the stack of cell. The larger the volume of reservoirs, the greater the energy is stored in the battery (Weber et al., 2011). This can be seen by an increase in the peak charge voltage as the volume of electrolytes increased from 10 to 50 cm³/s for this simulation. In the experimental level, the volume usually scales between 20 and 1000 mL because of the fact that the vanadium electrolyte is normally dissolved in very acidic solutions such as hydrochloric or sulphuric acid, thus the substance of electrolyte storage need to be chemically inert so that there will be no chemical reaction against the storage tanks itself. Hence, the more energy is stored in the battery, the higher is the IR drop since the discharge graph will decrease and diverge to reach its final voltage during the discharge cycle provided that the discharge time is only fixed to a certain value.

Table 4.11 Voltage efficiency of VRFB for different volumes of electrolyte applied at different electrode sizes.

Volume of electrolyte / Electrode Size	25 cm²	56.25 cm²	100 cm²
10 cm ³	$\eta_v = 89.1\%$	$\eta_v = 90.5\%$	$\eta_v = 91.0\%$
20 cm ³	$\eta_v = 88.2\%$	$\eta_v = 90.2\%$	$\eta_v = 90.8\%$
30 cm ³	$\eta_v = 87.5\%$	$\eta_v = 90.0\%$	$\eta_v = 90.7\%$
40 cm ³	$\eta_v = 87.1\%$	$\eta_v = 89.9\%$	$\eta_v = 90.6\%$
50 cm ³	$\eta_v = 86.7\%$	$\eta_v = 89.8\%$	$\eta_v = 90.5\%$

Table 4.12 shows the simulation data for different volume of electrolytes applied at different electrode sizes in a specific time such as starting, peak charge, first discharge, final discharge and IR Drop. From the table, an upward trend of voltage of cell throughout the charging cycle is observed and as the volume of the electrolyte increased, peak cell voltages reported at 1.3009 V, 1.3043 V, and 1.3090 V for 25 cm², 1.3020 V, 1.3060 V, and 1.3106 V for 56.25 cm², and 1.3041 V, 1.3094 V, and 1.3150 V for 100 cm², respectively. On the other hand, there is a slight increase on IR drop throughout the charge and discharge cycle where the IR drop increases from 0.1425 to 0.1655 in 25 cm² cell, 0.1274 to 0.1408 in 56.25 cm² cell and 0.1187 to 0.1323 in 100 cm² cell. The overall energy efficiency is still in the scale of 78% to 82% for volume of electrolytes between 10 to 50 cm³/s and it is similar to other reported VRFB systems.

Table 4.12 Simulation data for different volumes of electrolyte applied at different electrode sizes at a specific time.

Size of stack	25 cm ²			56.25 cm ²			100 cm ²		
	10	30	50	10	30	50	10	30	50
Volume of electrolytes (cm ³)	10	30	50	10	30	50	10	30	50
Starting Voltage (V)	1.2838	1.2839	1.2840	1.2898	1.2899	1.2900	1.2979	1.2980	1.2981
Peak Charge Voltage (V)	1.3009	1.3043	1.3090	1.3020	1.3060	1.3106	1.3041	1.3094	1.3150
Discharge voltage (V)	1.1584	1.1481	1.1435	1.1746	1.1711	1.1698	1.1854	1.1834	1.1827
Final Voltage (V)	1.1471	1.1152	1.0928	1.1673	1.1589	1.1549	1.1802	1.1759	1.1740
IR Drop (V)	0.1425	0.1562	0.1655	0.1274	0.1349	0.1408	0.1187	0.1260	0.1323

For linearity study, Table 4.13 shows linearity equations and fitting goodness for each volume of electrolyte value for 25 cm² of VRFB cell.

Table 4.13 Linearity equations and fitting goodness for 25 cm² of VRFB cell.

Volume of electrolyte	Linearity Equations	Fitting Goodness
50 cm ³	$y = 1.2840 e^{0.00046x}$	$R^2 = 0.9931$
30 cm ³	$y = 1.2839 e^{0.00041x}$	$R^2 = 0.9973$
10 cm ³	$y = 1.2838 e^{0.00028x}$	$R^2 = 0.9971$

For the intercept, there is an increase of 0.0001 with every increase of 20 cm³ volume of electrolyte injected into the system with the minimum value is set at 10 cm³ and the intercept obtained is at 1.2838. While for the difference, there is an increase of 0.00013 & 0.00005, respectively, with every increase of 20 cm³ volume of electrolyte with the minimum value of volume of electrolyte is set to 10 cm³. Thus, it can be concluded that the modelling obtained for 25 cm² cell is non-linear since the difference is not the same.

For 56.25 cm² cell, Table 4.14 shows linearity equations and fitting goodness for each volume of electrolyte value.

Table 4.14 Linearity equations and fitting goodness for 56.25 cm² of VRFB cell.

Volume of electrolyte	Linearity Equations	Fitting Goodness
50 cm ³	$y = 1.2900 e^{0.00018x}$	$R^2 = 0.9967$
30 cm ³	$y = 1.2899 e^{0.00017x}$	$R^2 = 0.9986$
10 cm ³	$y = 1.2898 e^{0.00013x}$	$R^2 = 0.9981$

For the intercept, there is an increase of 0.0001 with every increase of 20 cm³ volume of electrolyte injected into the system with the minimum value is set at 10 cm³ and the intercept obtained is at 1.2898. While for the difference, there is an increase of 0.00004 and 0.00001, respectively, with every increase of 20 cm³ volume of electrolyte with the minimum value of electrolyte volume is set to 10 cm³. Thus, it can be concluded that the modelling obtained for 56.25 cm² cell is non-linear since the difference is not the

same. Lastly, for 100 cm² cell, Table 4.15 below shows linearity equations of graphs and goodness of fitting for each volume of electrolytes value.

Table 4.15 Linearity equations and fitting goodness for 100 cm² of VRFB cell.

Volume of electrolyte	Linearity Equations	Fitting Goodness
50 cm ³	$y = 1.2981 e^{0.000102x}$	$R^2 = 0.9960$
30 cm ³	$y = 1.2980 e^{0.000101x}$	$R^2 = 0.9963$
10 cm ³	$y = 1.2979 e^{0.000099x}$	$R^2 = 0.9992$

For the intercept, there is an increase of 0.0001 with every increase of 20 cm³ volume of electrolyte injected into the system with the minimum value set at 10 cm³ and the intercept obtained is at 1.2979. While for the difference, there is an increase of 0.000002 and 0.000001, respectively, with every increase of 20 cm³ volume of electrolyte with the minimum value of electrolyte volume is set to 10 cm³. Thus, it can be concluded that the modelling obtained for 100 cm² cell is non-linear since the difference is not the same.

In addition, relationship trend of linearity can be further proven by using Figure 4.13 below for each cell stack size. As per mentioned before, it can be seen that the cell voltage value increase in non-linear form as the cell stack size value increase for every 20 cm³ increase of volume of electrolyte.

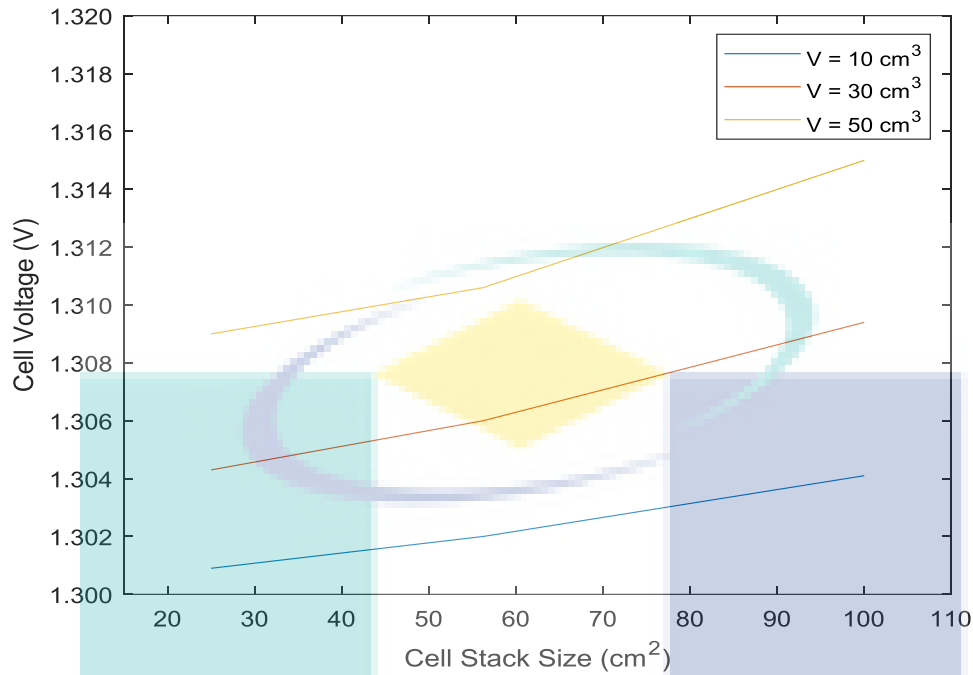


Figure 4.13 Relationship trend between cell voltage vs. different cell stack size (25, 56.25 and 100 cm²) for volume of electrolyte of 10, 30 and 50 cm³.

On the other hand, the linearity modelling involving different sizes of cell stack with the same volume of electrolyte value cannot be performed since it is in non-linear form and there are difference in the ratio produce between each volume of electrolyte value and different cell stack sizes. Thus, it can be concluded that, there is no linear relationship between different volumes of electrolyte value with the same cell stack size and between different cell stack sizes with the same volume of electrolyte value.

4.3.4 Temperature of cell

In this section, the results obtained from the simulation of the VRFB is based on different values of temperature of cell applied on different sizes of electrode in the range of 288.15 to 298.15 K. This range of temperature is chosen due to the limitation that exists in the COMSOL simulation as the value can be in a certain range of number only and if the number is out of the range, it will results in an error as the maximum iteration number is reached and convergence issue will occur. The other cell parameter such as current density of 50 mA/cm², flow rate of 0.17 cm³/s, and electrolyte volume of 10 cm³ is kept constant in order to achieve a valid result. Figures below shows the graph of charge and discharge of VRFB for 25 cm², 56.25 cm² and 100 cm², respectively.

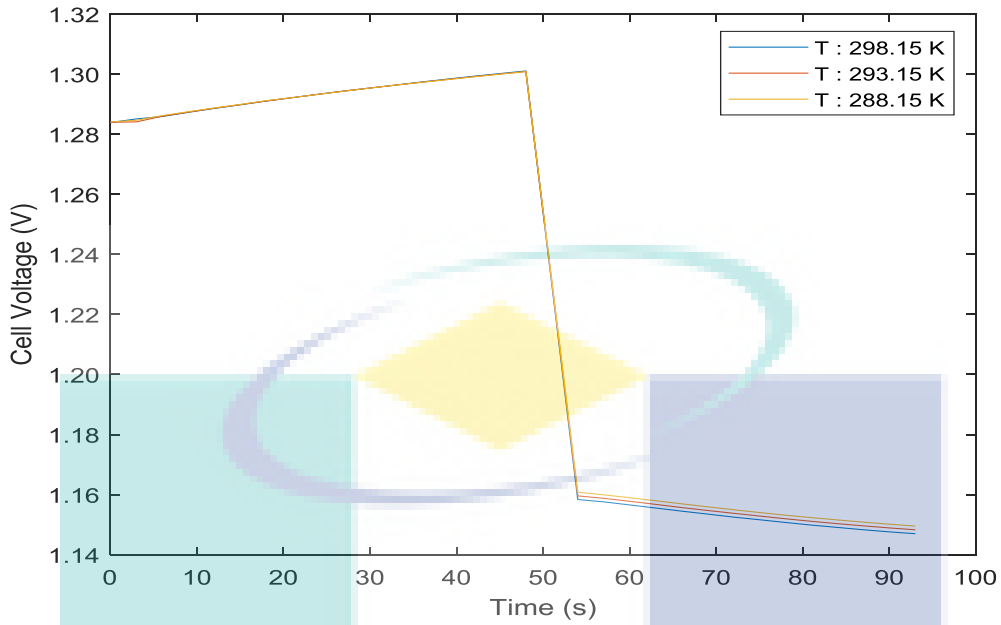


Figure 4.14 Cell voltage vs. time representing charge – discharge characteristics of a 25 cm^2 VRFB under controlled temperatures (288.15, 293.15 and 298.15 K) for 10 cm^3 volume of electrolyte at constant linear flow rate of $0.17 \text{ cm}^3/\text{s}$, current density of $50 \text{ mA}/\text{cm}^2$, electrode porosity of 0.94 and membrane conductivity of $15 \text{ S}/\text{m}$.

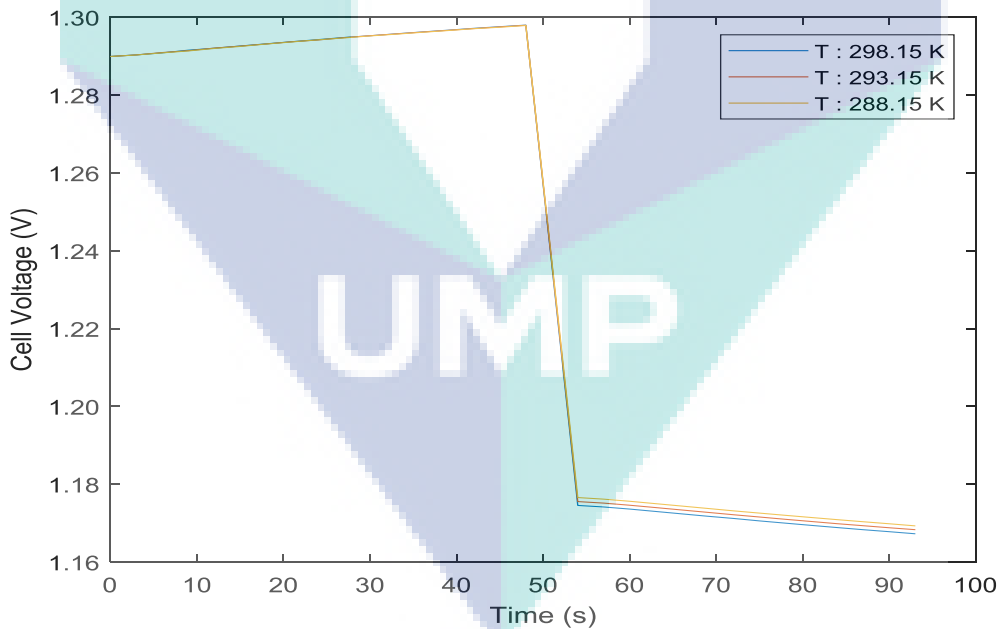


Figure 4.15 Cell voltage vs. time representing charge – discharge characteristics of a 56.25 cm^2 VRFB under controlled temperatures (288.15, 293.15 and 298.15 K) for 10 cm^3 volume of electrolyte at constant linear flow rate of $0.17 \text{ cm}^3/\text{s}$, current density of $50 \text{ mA}/\text{cm}^2$, electrode porosity of 0.94 and membrane conductivity of $15 \text{ S}/\text{m}$.

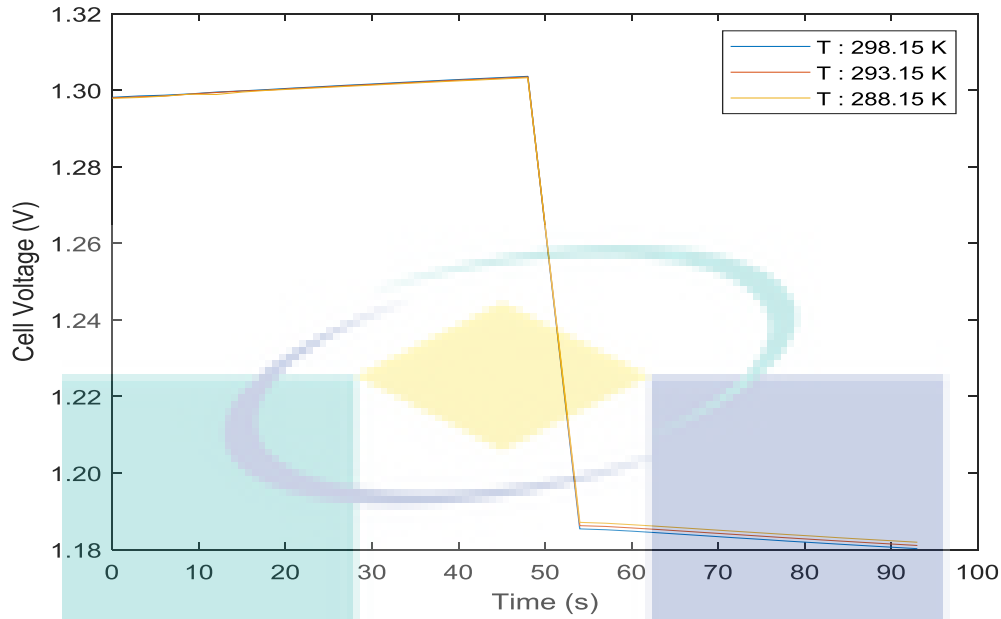


Figure 4.16 Cell voltage vs. time representing charge – discharge characteristics of a 100 cm^2 VRFB under controlled temperatures (288.15, 293.15 and 298.15 K) for 10 cm^3 volume of electrolyte at constant linear flow rate of $0.17 \text{ cm}^3/\text{s}$, current density of $50 \text{ mA}/\text{cm}^2$, electrode porosity of 0.94 and membrane conductivity of $15 \text{ S}/\text{m}$.

From the graph of charge and discharge of VRFB, all three sizes of electrode possess similar charge-discharge graph characteristic as a result. The data from the simulation is analysed and the voltage efficiency for each graph is tabulated. From Table 4.16 below, it can be noticed that the voltage efficiency drops from 89.3% to 89.1% for 25 cm^2 cell, 90.7% to 90.5% for 56.25 cm^2 cell and 91.1% to 90.9% for 100 cm^2 cell as the temperature of the cell applied on the simulation increases from 288.15 to 298.15 K. Besides that, it can also be seen that voltage efficiency increases from 89.3% to 91.1% for 288.15 K, 89.2% to 91.0% for 293.15 K and 89.1% to 90.9% for 298.15 K as the size of electrode increases from 25 cm^2 to 100 cm^2 .

Table 4.16 Voltage efficiency of VRFB for different temperatures of cell applied at different electrode sizes.

Temperature of cell / Electrode Size	25 cm ²	56.25 cm ²	100 cm ²
288.15 K	$\eta_v = 89.3\%$	$\eta_v = 90.7\%$	$\eta_v = 91.1\%$
293.15 K	$\eta_v = 89.2\%$	$\eta_v = 90.6\%$	$\eta_v = 91.0\%$
298.15 K	$\eta_v = 89.1\%$	$\eta_v = 90.5\%$	$\eta_v = 90.9\%$

For vanadium battery model, it is highlighted that VRFB has the capability of operating at nearly room temperature, which allows avoiding complex and costly thermal control systems (Trovò, Marini, Sutto, Alotto, & Giomo, 2019). Due to this advantage, the temperature's effect on a vanadium cell is studied under various temperatures of cell settings close to room temperature for this project. The voltage of cell follows an identical pattern of the charge and discharge characteristic as the cell efficiency decreases with increasing temperature. However, this is only true up to 55 °c since the permeability of vanadium ions species across the membrane will rise at higher temperatures, not only triggering a fall in the coulombic efficiency but also a faster capacity decay (C. Zhang et al., 2015). It is also suggested that thermal management of an actual operating VRFB is necessary in guaranteeing that the battery runs at the optimal thermal condition to reach the most productive and dependable operation.

Nevertheless, From the Table 4.17, it is observed that the charging voltages are almost the same for all 3 settings of temperature ranging from 1.3005 V to 1.3011 V for 25 cm² cell, 1.2978 V to 1.2980 V for 56.25 cm² cell and 1.3034 V to 1.3036 V for 100 cm² cell, respectively. Cell running under the ambient temperature decelerate the conductivity of ions, hence, lowering the reaction kinetics rate and vanadium species diffusion (Mohamed et al., 2015). This could later increase an extreme heat in the stack of the cell, causing thermal precipitation in the positive electrolyte, thus, heighten the cell overpotential throughout charging cycle, but further adding to premature voltage cut-off during discharge cycle (A. Tang, Bao, & Skyllas-kazacos, 2012). This can be seen at slightly different voltages achieved during the discharge voltage as a result. The

coulombic efficiency is set to 90% throughout the simulation. On the other hand, improved results are noticed at the temperature of 288.15 K with efficiency of voltages recorded at 89.31% for 25 cm², 90.65% for 56.25 cm² and 91.10% for 100 cm², respectively.

Table 4.17 Simulation data for different temperatures of cell applied at different electrode sizes in a specific time.

Size of stack	25 cm ²				56.25 cm ²			100 cm ²	
	288.15	293.15	298.15	288.15	293.15	298.15	288.15	293.15	298.15
Temperature (K)	288.15	293.15	298.15	288.15	293.15	298.15	288.15	293.15	298.15
Starting Voltage (V)	1.2841	1.2840	1.2839	1.2901	1.2900	1.2899	1.2981	1.2980	1.2979
Peak Charge Voltage (V)	1.3005	1.3008	1.3011	1.2978	1.2979	1.2980	1.3034	1.3035	1.3036
Discharge Voltage (V)	1.1608	1.1596	1.1584	1.1766	1.1756	1.1746	1.1871	1.1862	1.1854
Final Voltage (V)	1.1495	1.1483	1.1470	1.1693	1.1683	1.1673	1.1820	1.1811	1.1802
IR Drop (V)	0.1397	0.1412	0.1427	0.1212	0.1223	0.1234	0.1163	0.1173	0.1182

For linearity study, the Table 4.18 below shows linearity equations of graphs and goodness of fitting for each temperature of cell value for 25 cm² of VRFB cell.

Table 4.18 Linearity equations and fitting goodness for 25 cm² of VRFB cell.

Temperature of cell	Linearity Equations	Fitting Goodness
298.15 K	$y = 1.2839 e^{0.00028x}$	$R^2 = 0.9953$
293.15 K	$y = 1.2840 e^{0.00027x}$	$R^2 = 0.9967$
288.15 K	$y = 1.2841 e^{0.00026x}$	$R^2 = 0.9934$

For the intercept, there is a decrease of 0.0001 with every increase of 5 K temperature of cell injected into the system with the minimum value set at 288.15 K and the intercept obtained is at 1.2841. While for the difference, there is an increase of 0.00001 with every increase of 5 K temperature of cell with the minimum value of temperature of cell set at 288.15 K and the difference obtained is 0.00026.

Thus, the linearity modelling obtained for 25 cm² cell is:

$$y = [1.2841 - (n-1)0.0001] e^{[0.00026 + (n-1)0.00001]x}$$

For 56.25 cm² cell, Table 4.19 below shows linearity equations of graphs and goodness of fitting for each temperature of cell value.

Table 4.19 Linearity equations and fitting goodness for 56.25 cm² of VRFB cell.

Temperature of cell	Linearity Equations	Fitting Goodness
298.15 K	$y = 1.2899 e^{0.000130x}$	$R^2 = 0.9977$
293.15 K	$y = 1.2900 e^{0.000127x}$	$R^2 = 0.9978$
288.15 K	$y = 1.2901 e^{0.000124x}$	$R^2 = 0.9975$

For the intercept, there is a decrease of 0.0001 with every increase of 5 K temperature of cell injected into the system with the minimum value set at 288.15 K and the intercept obtained is at 1.2901. While for the difference, there is an increase of 0.000003 with every increase of 5 K temperature of cell with the minimum value of temperature of cell is set at 288.15 K and the difference obtained is 0.000124.

Thus, the linearity modelling obtained for 56.25 cm² cell is:

$$y = [1.2901 - (n-1)0.0001] e^{[0.000124 + (n-1)0.000003]x}$$

Lastly, for 100 cm² cell, Table 4.20 below shows linearity equations of graphs and goodness of fitting for each temperature of cell value.

Table 4.20 Linearity equations and fitting goodness for 100 cm² of VRFB cell.

Temperature of cell	Linearity Equations	Fitting Goodness
298.15 K	$y = 1.2979 e^{0.000091x}$	$R^2 = 0.9992$
293.15 K	$y = 1.2980 e^{0.000088x}$	$R^2 = 0.9987$
288.15 K	$y = 1.2981 e^{0.000085x}$	$R^2 = 0.9966$

For the intercept, there is a decrease of 0.0001 with every increase of 5 K temperature of cell injected into the system with the minimum value set at 288.15 K and the intercept obtained is at 1.2981. While for the difference, there is an increase of 0.000003 with every increase of 5 K temperature of cell with the minimum value of temperature of cell is set at 288.15 K and the difference obtained is 0.000085.

Thus, the linearity modelling obtained for 100 cm² cell is:

$$y = [1.2981 - (n-1)0.0001] e^{[0.000085 + (n-1)0.000003]x}$$

In addition, relationship trend of linearity can be further proven by using Figure 4.17 below for each cell stack size. As per mentioned before, it can be seen that the cell voltage increase linearly with the increase of cell stack size for every 5 K increase of temperature of cell.

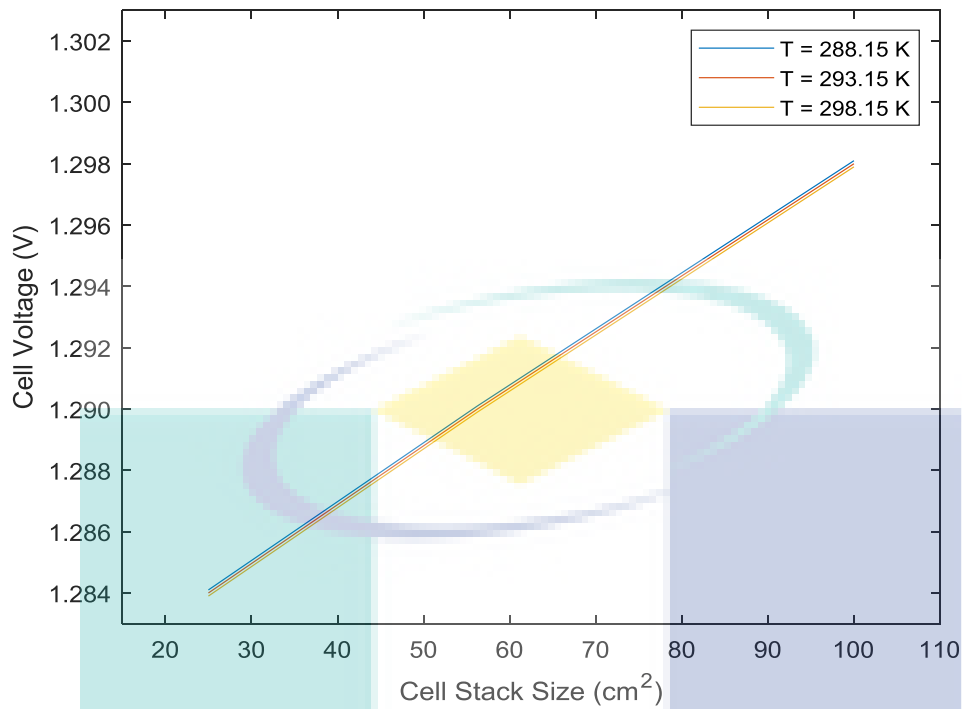


Figure 4.17 Relationship trend between cell voltage vs. different cell stack size (25, 56.25 and 100 cm²) for temperature of cell of 288.15, 293.15 and 298.15 K.

On the other hand, the linearity modelling involving different sizes of cell stack with the same temperature of cell value cannot be performed since it is in non-linear form and there exists difference in the ratio produced between each temperature of cell value and different cell stack sizes. Thus, it can be concluded that, there is a linear relationship between different temperatures of cell value with the same cell stack sizes but there is no linear relationship between different cell stack sizes with the same temperature of cell value.

4.3.5 Electrode Porosity

In this section, the result is obtained from the simulation of the VRFB with different values of constant electrode porosity applied to different sizes of electrode in the range of 0.92 to 0.94. Other cell parameters such as current density of 50 mA/ cm², flow rate of 0.17 cm³/s, volume of electrolyte of 10 cm³ and temperature of 298.15 K is kept constant in order to maintain the validity of the result. Figures below shows the graph of charge and discharge of VRFB for 25 cm², 56.25 cm² and 100 cm².

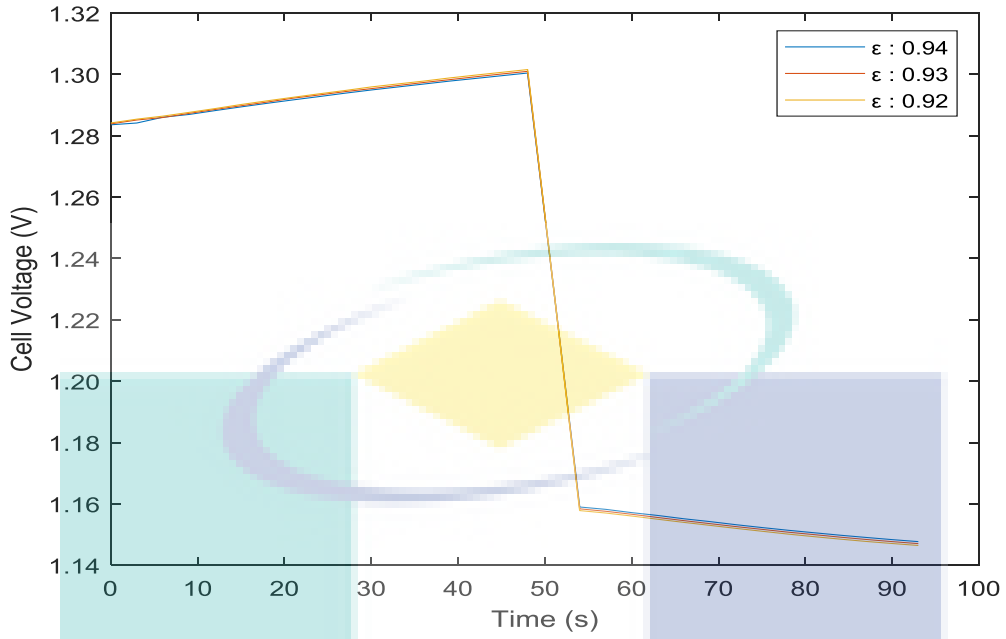


Figure 4.18 Cell voltage vs. time representing charge – discharge characteristics of a 25 cm² VRFB at controlled electrode porosity (0.92, 0.93 and 0.94) with constant flow rate of 0.17 cm³/s, volume of 10 cm³, temperature of 298.15 K, membrane conductivity of 15 S/m and current density of 50 mA/cm².

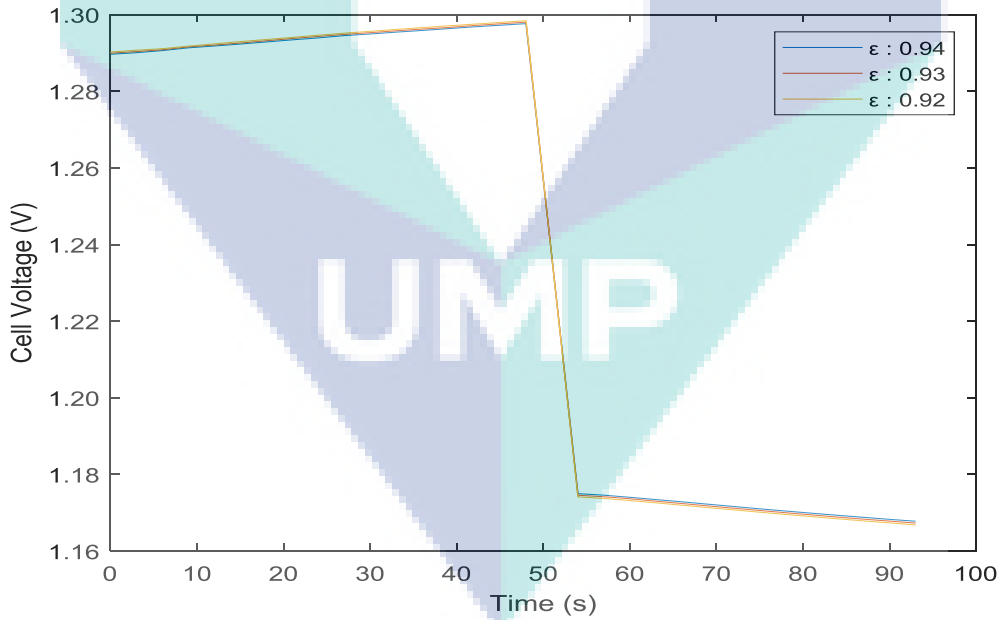


Figure 4.19 Cell voltage vs. time representing charge – discharge characteristics of a 56.25 cm² VRFB at controlled electrode porosity (0.92, 0.93 and 0.94) with constant flow rate of 0.17 cm³/s, volume of 10 cm³, temperature of 298.15 K, membrane conductivity of 15 S/m and current density of 50 mA/cm².

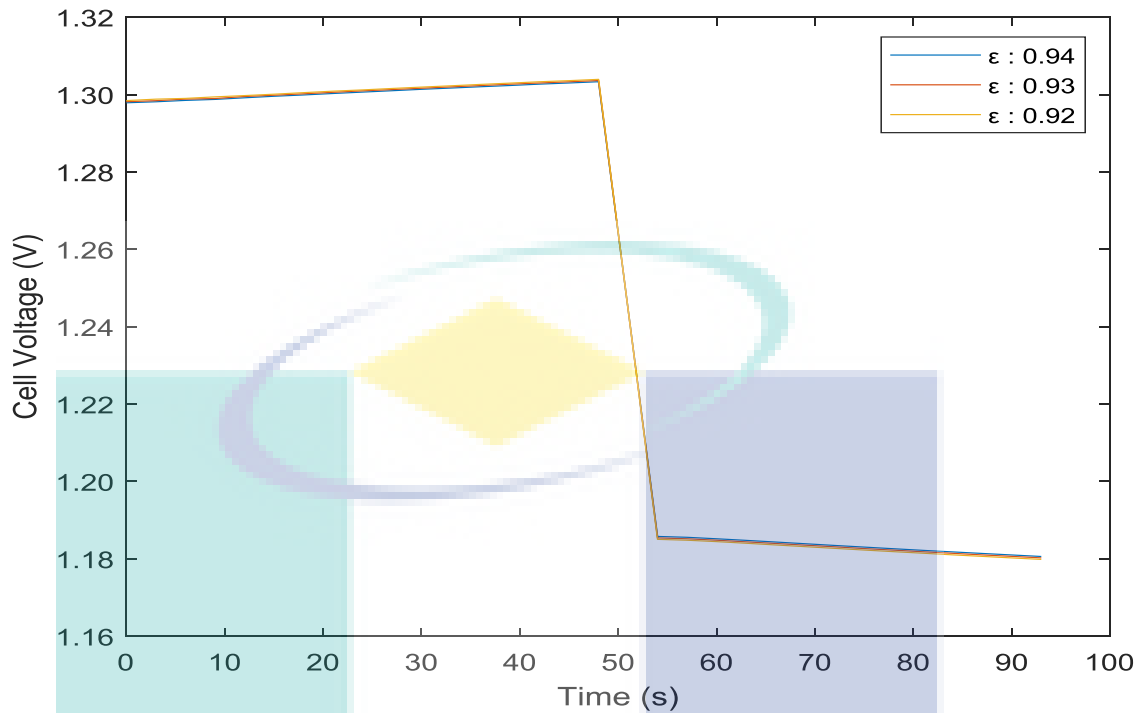


Figure 4.20 Cell voltage vs. time representing charge – discharge characteristics of a 100 cm^2 VRFB at controlled electrode porosity (0.92, 0.93 and 0.94) with constant flow rate of $0.17 \text{ cm}^3/\text{s}$, volume of 10 cm^3 , temperature of 298.15 K , membrane conductivity of 15 S/m and current density of 50 mA/cm^2 .

From the graph of charge and discharge of VRFB, all three sizes of electrode possess a similar charge-discharge graph characteristic as a result. The data from the simulation is analysed and the voltage efficiency for each graph is tabulated. From Table 4.21 below, the voltage efficiency increases from 89.0% to 89.2% for 25 cm^2 cell, 90.4% to 90.6% for 56.25 cm^2 cell and 90.8% to 91.0% for 100 cm^2 cell as the electrode porosity applied on the simulation increases from 0.92 to 0.94 epsilon. Besides that, it can also be seen that the voltage efficiency increases slightly from 89.0% to 90.8% for 0.92 epsilon, 89.1% to 90.9% for 0.93 epsilon and 89.2% to 91.0% for 0.94 epsilon as the size of electrode increases from 25 cm^2 to 100 cm^2 .

Table 4.21 Voltage efficiency of VRFB for different electrode porosities applied at different electrode sizes.

Electrode Porosity / Electrode Size	25 cm ²	56.25 cm ²	100 cm ²
0.92	$\eta_v = 89.0\%$	$\eta_v = 90.4\%$	$\eta_v = 90.8\%$
0.93	$\eta_v = 89.1\%$	$\eta_v = 90.5\%$	$\eta_v = 90.9\%$
0.94	$\eta_v = 89.2\%$	$\eta_v = 90.6\%$	$\eta_v = 91.0\%$

When selecting the electrode material, there are few criteria that need to be taken into consideration, such as electrical conductivity, specific surface area and resistance to corrosion. The simulated charge and discharge graphs for these three value of porosity show a relatively small difference in porosity among themselves. On the other hand, there are a few effects linked with an increment of porosity which are reduced conductivity of bulk, greater electrolyte volume in the electrolyte, rose in bulk diffusion coefficients and increased permeability (Shah & Walsh, 2008). At a lower electrode porosity, the overpotential is slightly higher compared to the others and the decreased in bulk conductivity leads to a higher polarization. An increase porosity would therefore leads to a rise in side reaction rate in the cell stack during the charging process, thus voltage efficiency increases with the increasing electrode porosity and increasing stack size.

Table 4.22 Simulation data for different electrode porosities applied at different electrode sizes at a specific time.

Size of stack	25 cm ²			56.25 cm ²			100 cm ²		
Electrode porosity	0.92	0.93	0.94	0.92	0.93	0.94	0.92	0.93	0.94
Starting Voltage (V)	1.2842	1.2839	1.2836	1.2901	1.2899	1.2897	1.2983	1.2981	1.2979
Peak Charge Voltage (V)	1.3016	1.3010	1.3005	1.2984	1.2980	1.2976	1.3040	1.3036	1.3032
Discharge Voltage (V)	1.1578	1.1584	1.1590	1.1742	1.1746	1.1750	1.1850	1.1854	1.1858
Final Voltage (V)	1.1464	1.1470	1.1477	1.1668	1.1673	1.1678	1.1799	1.1802	1.1806
IR Drop (V)	0.1438	0.1426	0.1415	0.1242	0.1234	0.1226	0.1190	0.1182	0.1174

Table 4.22 shows the simulation data for different electrode porosities applied at different electrode sizes in a specific time such as starting, peak charge, first discharge, final discharge and IR Drop. From the table, a downward trend of cell voltage during the charge cycle is observed and as the electrode porosity rises, peak cell voltages are recorded at 1.3016 V, 1.3010 V, and 1.3005 V for 25 cm², 1.2984 V, 1.2980 V, and 1.2976 V for 56.25 cm², and 1.3040 V, 1.3036 V, and 1.3032 V for 100 cm², respectively. It has been assumed that the higher the rate of side reactions during charging leads to the increasing of voltage efficiency (Shah & Walsh, 2008). There is a small IR drop throughout the charge and discharge cycle which can be seen that the IR drop decreases from 0.1438 to 0.1415 in 25 cm² cell, 0.1242 to 0.1226 in 56.25 cm² and 0.1190 to 0.1174 in 100 cm². The overall energy efficiency is on the scale of 80% to 82% for electrode porosity between 0.92 to 0.94 epsilon and it is similar to other reported VRFB systems (Shah & Walsh, 2008).

For linearity study, Table 4.23 below shows linearity equations of graphs and goodness of fitting for each electrode porosity value for 25 cm² of VRFB cell.

Table 4.23 Linearity equations and fitting goodness for 25 cm² of VRFB cell.

Electrode porosity	Linearity Equations	Fitting Goodness
0.94	$y = 1.2836 e^{0.000272x}$	$R^2 = 0.9969$
0.93	$y = 1.2839 e^{0.000276x}$	$R^2 = 0.9964$
0.92	$y = 1.2842 e^{0.000280x}$	$R^2 = 0.9958$

For the intercept, there is a decrease of 0.0003 with every increase of 0.01 electrode porosity inserted into the system with the minimum value set at epsilon 0.92 and the intercept obtained is at 1.2842. While for the difference, there is a decrease of 0.000004 with every increase of 0.01 electrode porosity with the minimum value of electrode porosity set to epsilon 0.92 and the difference obtained is 0.000280.

Thus, the linearity modelling obtained for 25 cm² cell is:

$$y = [1.2842 - (n-1)0.0003] e^{[0.000280 - (n-1)0.000004]x}$$

For 56.25 cm² cell, Table 4.24 shows linearity equations of graphs and goodness of fitting for each electrode porosity value.

Table 4.24 Linearity equations and fitting goodness for 56.25 cm² of VRFB cell.

Electrode porosity	Linearity Equations	Fitting Goodness
0.94	$y = 1.2897 e^{0.000127x}$	$R^2 = 0.9975$
0.93	$y = 1.2899 e^{0.000130x}$	$R^2 = 0.9974$
0.92	$y = 1.2901 e^{0.000133x}$	$R^2 = 0.9976$

For the intercept, there is a decrease of 0.0002 with every increase of 0.01 electrode porosity inserted into the system with the minimum value set at epsilon 0.92 and the intercept obtained is at 1.2901. While for the difference, there is a decrease of 0.000003

with every increase of 0.01 electrode porosity with the minimum value of electrode porosity set to epsilon 0.92 and the difference obtained is 0.000133.

Thus, the linearity modelling obtained for 56.25 cm² cell is:

$$y = [1.2901 - (n-1)0.0002] e^{[0.000133 - (n-1)0.000003]x}$$

Lastly, for 100 cm² cell, Table 4.25 shows linearity equations of graphs and goodness of fitting for each electrode porosity value.

Table 4.25 Linearity equations and fitting goodness for 100 cm² of VRFB cell.

Electrode porosity	Linearity Equations	Fitting Goodness
0.94	$y = 1.2979 e^{0.000085x}$	$R^2 = 0.9993$
0.93	$y = 1.2981 e^{0.000088x}$	$R^2 = 0.9989$
0.92	$y = 1.2983 e^{0.000091x}$	$R^2 = 0.9993$

For the intercept, there is a decrease of 0.0002 with every increase of 0.01 electrode porosity inserted into the system with the minimum value set at epsilon 0.92 and the intercept obtained is at 1.2983. While for the difference, there is a decrease of 0.000003 with every increase of 0.01 electrode porosity with the minimum value of electrode porosity set to epsilon 0.92 and the difference obtained is 0.000091.

Thus, the linearity modelling obtained for 100 cm² cell is:

$$y = [1.2983 - (n-1)0.0002] e^{[0.000091 - (n-1)0.000003]x}$$

In addition, relationship trend of linearity can be further proven by using Figure 4.21 below for each cell stack size. As per mentioned before, it can be seen that the cell voltage increase linearly with the increase of cell stack size for every 0.01 increase of electrode porosity.

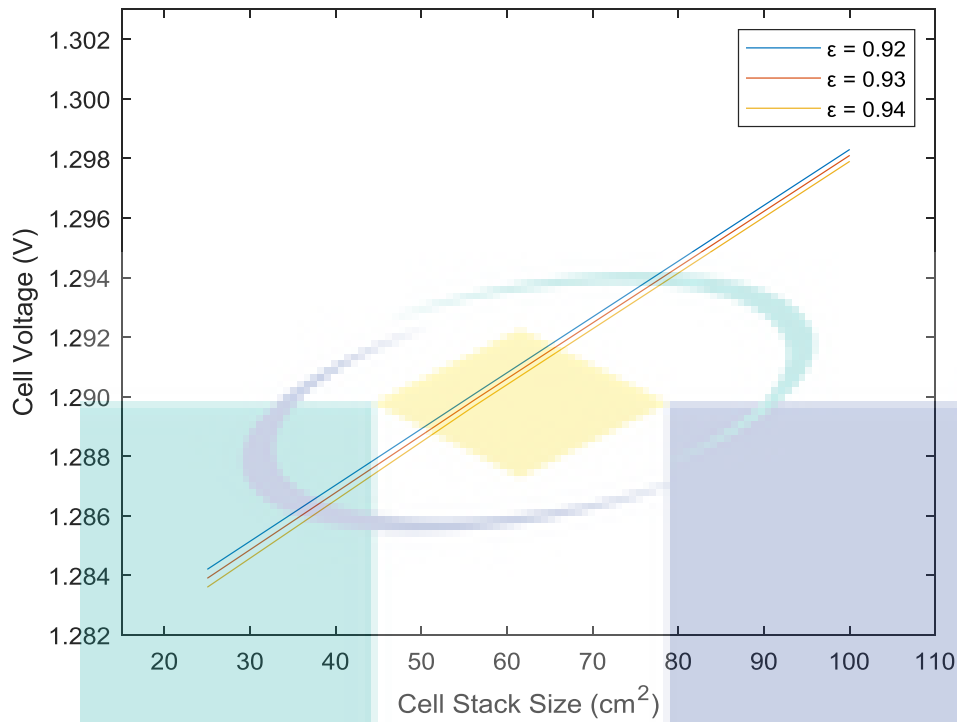


Figure 4.21 Relationship trend between cell voltage vs. different cell stack size (25, 56.25 and 100 cm²) for electrode porosity of 0.92, 0.93 and 0.94.

On the other hand, the linearity modelling involving different sizes of cell stack with the same electrode porosity value cannot be performed since it is in non-linear form and there are different ratios produced between each electrode porosity value and different cell stack size. Thus, it can be concluded that, there is a linear relationship between different electrode porosity values with the same cell stack size but there is no linear relationship between different cell stack sizes with the same electrode porosity value.

4.3.6 Membrane Conductivity

In this section of the chapter, the result is obtained from the simulation of the VRFB with different values of constant membrane conductivity applied on different sizes of electrode in the range of 5 to 15 S/m. The other cell parameters such as current density of 50 mA/cm², flow rate of 0.17 cm³/s, volume of electrolyte of 10 cm³ and temperature of 298.15 K are kept constant in order to maintain the validity of the result. Figures below shows the graph of charge and discharge of VRFB for 25 cm², 56.25 cm² and 100 cm², respectively.

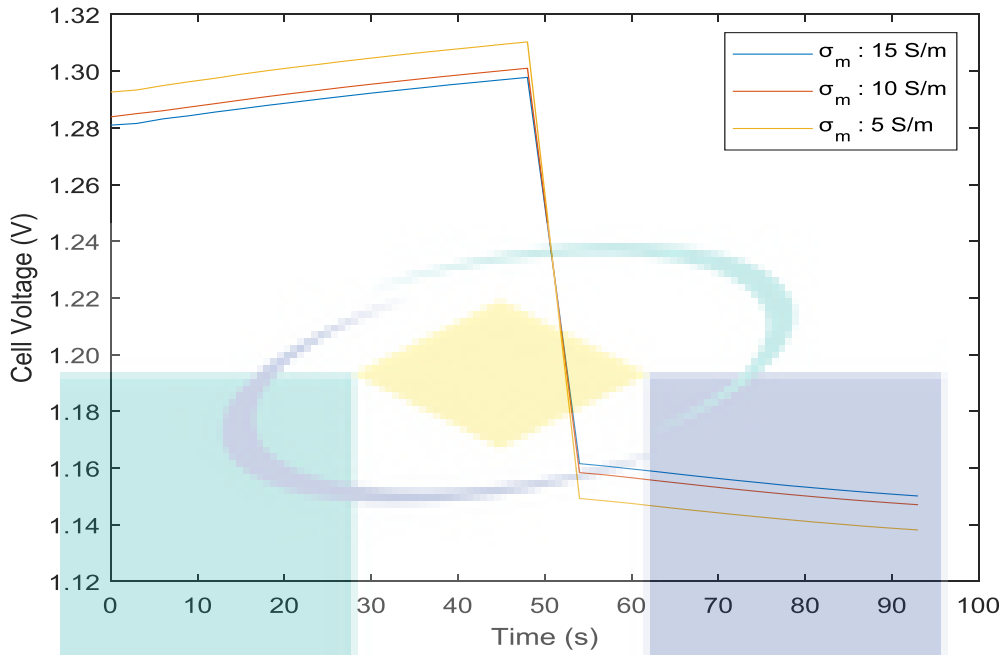


Figure 4.22 Cell voltage vs. time representing charge – discharge characteristics of a 25 cm² VRFB at controlled membrane conductivity (5, 10 and 15 S/m) with constant flow rate of 0.17 cm³/s, volume of 10 cm³, temperature of 298.15 K, electrode porosity of 0.94 and current density of 50 mA/cm².

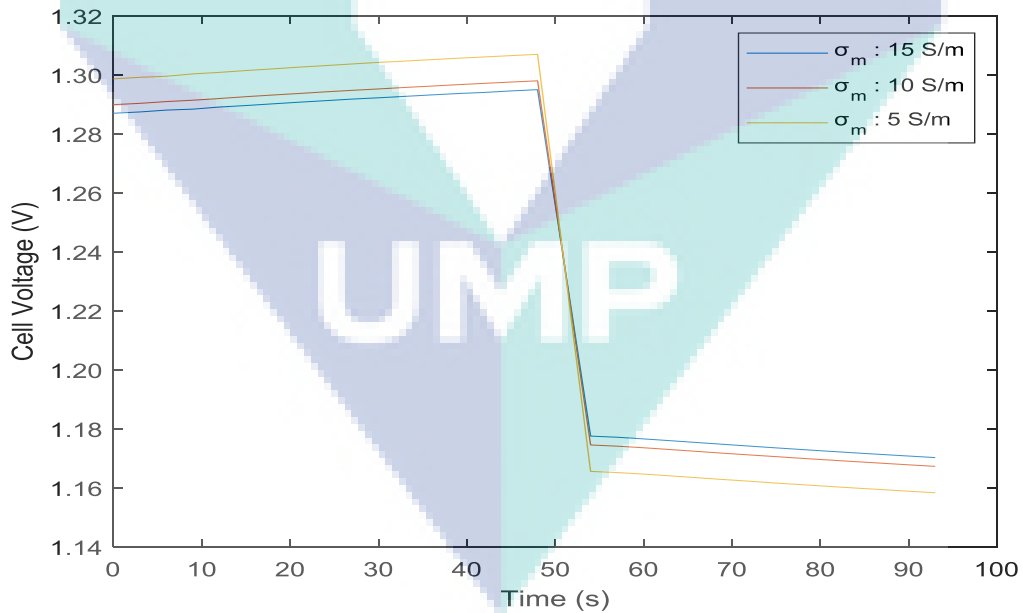


Figure 4.23 Cell voltage vs. time representing charge – discharge characteristics of a 56.25 cm² VRFB at controlled membrane conductivity (5, 10 and 15 S/m) with constant flow rate of 0.17 cm³/s, volume of 10 cm³, temperature of 298.15 K, electrode porosity of 0.94 and current density of 50 mA/cm².

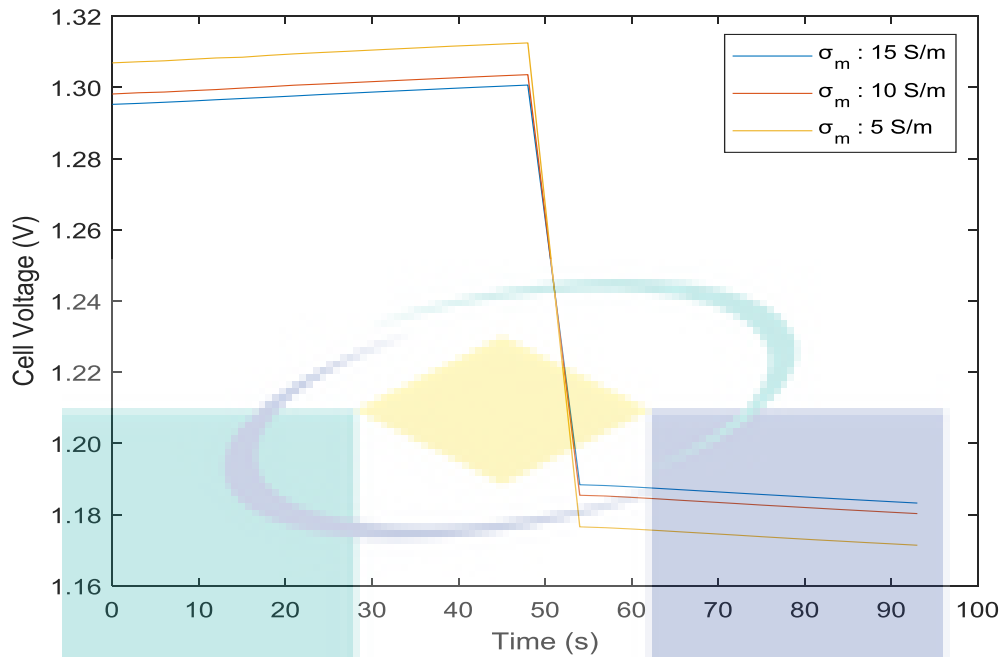


Figure 4.24 Cell voltage vs. time representing charge – discharge characteristics of a 100 cm² VRFB at controlled membrane conductivity (5, 10 and 15 S/m) with constant flow rate of 0.17 cm³/s, volume of 10 cm³, temperature of 298.15 K, electrode porosity of 0.94 and current density of 50 mA/cm².

From the graph of charge and discharge of VRFB, all three sizes of electrode possess similar charge-discharge graph characteristic as a result. The data from the simulation is analysed and the voltage efficiency for each graph is tabulated. From Table 4.26 below, it can be seen that the voltage efficiency increases from 87.8% to 89.6% for 25 cm² cell, 89.2% to 90.9% for 56.25 cm² cell and 89.7% to 91.4% for 100 cm² cell as the membrane conductivity applied on the simulation increases from 5 to 15 S/m. Besides that, it can also be seen that voltage efficiency increases slightly from 87.8% to 89.7% for 5 S/m, 89.1% to 90.9% for 10 S/m and 89.6% to 91.4% for 15 S/m as the size of electrode increases from 25 cm² to 100 cm².

Table 4.26 Voltage efficiency of VRFB for different membrane conductivities applied on different electrode sizes.

Membrane Conductivity / Electrode Size	25 cm ²	56.25 cm ²	100 cm ²
5 S/m	$\eta_v = 87.8\%$	$\eta_v = 89.2\%$	$\eta_v = 89.7\%$
10 S/m	$\eta_v = 89.1\%$	$\eta_v = 90.5\%$	$\eta_v = 90.9\%$
15 S/m	$\eta_v = 89.6\%$	$\eta_v = 90.9\%$	$\eta_v = 91.4\%$

The conductivity of membrane improvement or reduction can be assessed as a trade-off between concentration of proton increment and mobility of proton losses caused by the presence of acid in the environment (Z. Tang et al., 2013). In membrane, the sulfuric acid can supply extra protons by its ionization, while it also can lower the water content of the membrane. A wide range of membranes for the VRFB have been investigated over the years and many of them show promising results, however, fulfilling the economic needs for commercialization is still a challenge. Membrane is a critical material in VRFB which prevents the cross-contamination of negative and positive electrolytes and the short circuiting of the porous electrodes, while permitting the transport of ions to complete the current circuit (Chng Mei Lin, 2018). Ideally, there are three conditions the membrane should possess to be considered a good membrane which are: high ionic conductivity to minimize the resistance, a high proton to vanadium selectivity to prevent diffusion of active vanadium species which reduce cell efficiency such as coulombic, voltage, and energy efficiency as well as an excellent chemical stability in strong acidic environment and highly oxidative pentavalent vanadium ions in the positive half-cell electrolyte in VRFB. One approach to reduce cost of membrane is by reducing the membrane thickness which lowers the membrane's area resistance and hence, increases the efficiency of voltage (Chng Mei Lin, 2018).

However, thin membrane experiences a higher crossover rate which reduces the coulombic efficiency. Voltage efficiency increases with the increasing electrode porosity and stack size. By differentiating the results of these three membrane conductivities, it is noticed that the voltage efficiency increases when there is an increase in the membrane conductivity with both the porosity of membrane and the concentration being fixed throughout the simulation. It can also be deduced that, an appropriate rise in the porosity of membrane helps to increase the membrane conductivity and overall improving the battery performance. On the other hand, the defined concentration should also be cautiously changed to prevent a severe deterioration of electrolyte disparity and a rigorous reduction of coulombic efficiency. Therefore, in this simulation, the concentration of electrolyte and coulombic efficiency has been fixed throughout the simulation.

Table 4.27 Simulation data for different membrane conductivities applied at different electrode sizes in a specific time.

Size of stack	25 cm ²			56.25 cm ²			100 cm ²		
	5	10	15	5	10	15	5	10	15
Membrane conductivity (S/m)									
Starting Voltage (V)	1.2926	1.2839	1.2810	1.2986	1.2899	1.2870	1.3069	1.2981	1.2952
Peak Charge Voltage (V)	1.3103	1.3010	1.2978	1.3070	1.2980	1.2950	1.3125	1.3036	1.3006
Discharge Voltage (V)	1.1493	1.1584	1.1616	1.1656	1.1746	1.1776	1.1766	1.1854	1.1883
Final Voltage (V)	1.1382	1.1471	1.1502	1.1584	1.1673	1.1703	1.1714	1.1803	1.1832
IR Drop (V)	0.1610	0.1426	0.1362	0.1414	0.1234	0.1184	0.1359	0.1182	0.1123

Table 4.27 shows the simulation data for different membrane conductivity applied at different electrode sizes in a specific time such as starting, peak charge, first discharge, final discharge and IR Drop. From the table, a downward trend of cell voltage during the charge cycle is observed. As the membrane conductivity rose, peak cell voltages are recorded at 1.3103 V, 1.3010 V, and 1.2978 V for 25 cm², 1.3070 V, 1.2980 V, and 1.2950 V for 56.25 cm², and 1.3125 V, 1.3036 V, and 1.3006 V for 100 cm², respectively. There is a small IR drop throughout the charge and discharge cycle where the IR drop decreases from 0.1610 to 0.1362 in 25 cm² cell, 0.1414 to 0.1134 in 56.25 cm² cell and 0.1359 to 0.1123 in 100 cm² cell. The overall energy efficiency is in the span of 80% to 82% for membrane conductivity between 5 to 15 S/m and it is approximate to other published VRFB systems.

For linearity study, Table 4.28 below shows linearity equations of graphs and goodness of fitting for each membrane conductivity value for 25 cm² of VRFB cell.

Table 4.28 Linearity equations and fitting goodness for 25 cm² of VRFB cell.

Membrane conductivity	Linearity Equations	Fitting Goodness
15 S/m	$y = 1.2810 e^{0.000270x}$	$R^2 = 0.9947$
10 S/m	$y = 1.2839 e^{0.000275x}$	$R^2 = 0.9967$
5 S/m	$y = 1.2926 e^{0.000280x}$	$R^2 = 0.9962$

For the intercept, it can be seen that there is a decrease of 0.0087 and 0.0029 with the increase from 5 to 15 S/m value of membrane conductivity inserted into the system with the value of intercept obtained at 1.2926 at membrane conductivity of 5 S/m. While for the difference, there is a decrease of 0.000005 with the increase from 5 to 15 S/m value of membrane conductivity with the minimum value of difference obtained is at 0.000288 at membrane conductivity of 5 S/m. Therefore, it can be concluded that there is no linear relationship for membrane conductivity at 25 cm² cell stack.

For 56.25 cm² cell, Table 4.29 shows linearity equations of graphs and goodness of fitting for each membrane conductivity value.

Table 4.29 Linearity equations and fitting goodness for 56.25 cm² of VRFB cell.

Membrane conductivity	Linearity Equations	Fitting Goodness
15 S/m	$y = 1.2870 e^{0.000129x}$	$R^2 = 0.9968$
10 S/m	$y = 1.2899 e^{0.000130x}$	$R^2 = 0.9980$
5 S/m	$y = 1.2986 e^{0.000134x}$	$R^2 = 0.9980$

For the intercept, it can be seen that there is a decrease of 0.0087 and 0.0029 with the increase from 5 to 15 S/m value of membrane conductivity inserted into the system with the value of intercept obtained at 1.2986 at membrane conductivity of 5 S/m. While for the difference, there is a decrease of 0.000004 and 0.000001 with the increase from 5 to 15 S/m value of membrane conductivity with the minimum value of difference obtained at 0.000134 at membrane conductivity of 5 S/m. Therefore, it can be concluded that there is no linear relationship for membrane conductivity at 56.25 cm² cell stack.

Lastly, for 100 cm² cell, Table 4.30 shows linearity equations of graphs and goodness of fitting for each membrane conductivity value.

Table 4.30 Linearity equations and fitting goodness for 100 cm² of VRFB cell.

Membrane conductivity	Linearity Equations	Fitting Goodness
15 S/m	$y = 1.2952 e^{0.000086x}$	$R^2 = 0.9987$
10 S/m	$y = 1.2981 e^{0.000088x}$	$R^2 = 0.9989$
5 S/m	$y = 1.3069 e^{0.000089x}$	$R^2 = 0.9996$

For the intercept, it can be seen that there is a decrease of 0.0088 and 0.0029 with the increase from 5 to 15 S/m value of membrane conductivity inserted into the system with the value of intercept obtained at 1.3069 at membrane conductivity of 5 S/m. While for the difference, there is a decrease of 0.000001 and 0.000002 respectively between membrane conductivity of 5 S/m and membrane conductivity of 15 S/m with the initial value of difference obtained at 0.000089 at membrane conductivity of 5 S/m. Therefore,

it can be concluded that there is no linear relationship for membrane conductivity at 100 cm² cell stack.

In addition, relationship trend of linearity can be further proven by using Figure 4.25 below for each cell stack size. As per mentioned before, it can be seen that the cell voltage value increase in non-linear form as the cell stack size value for every 5 S/m increase of membrane conductivity.

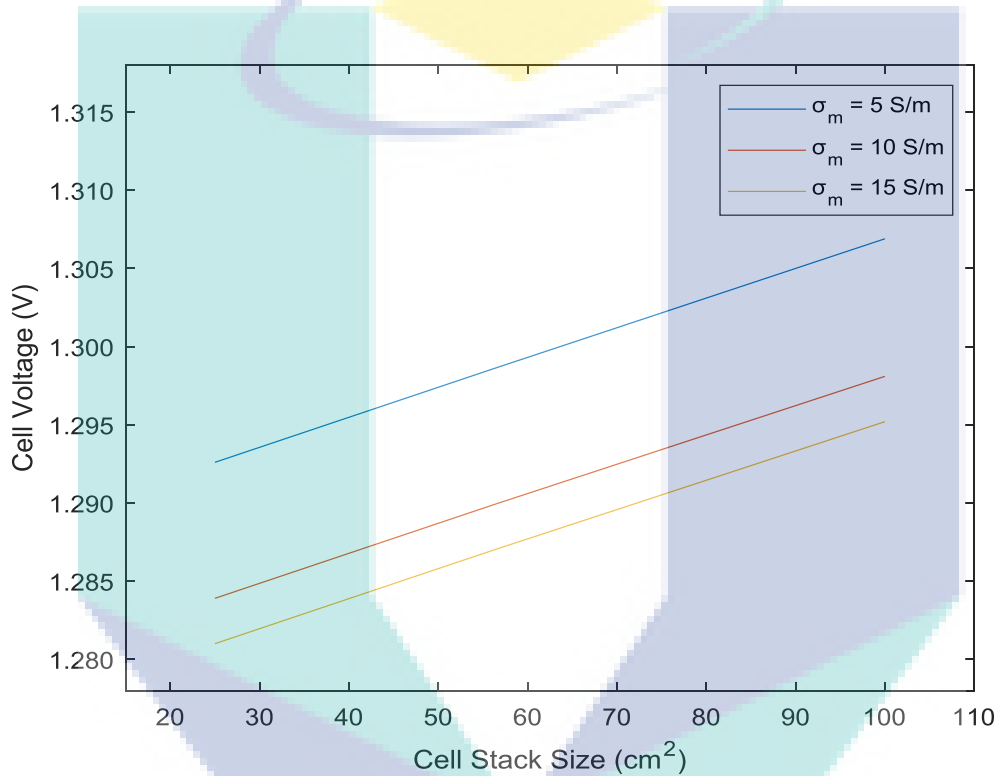


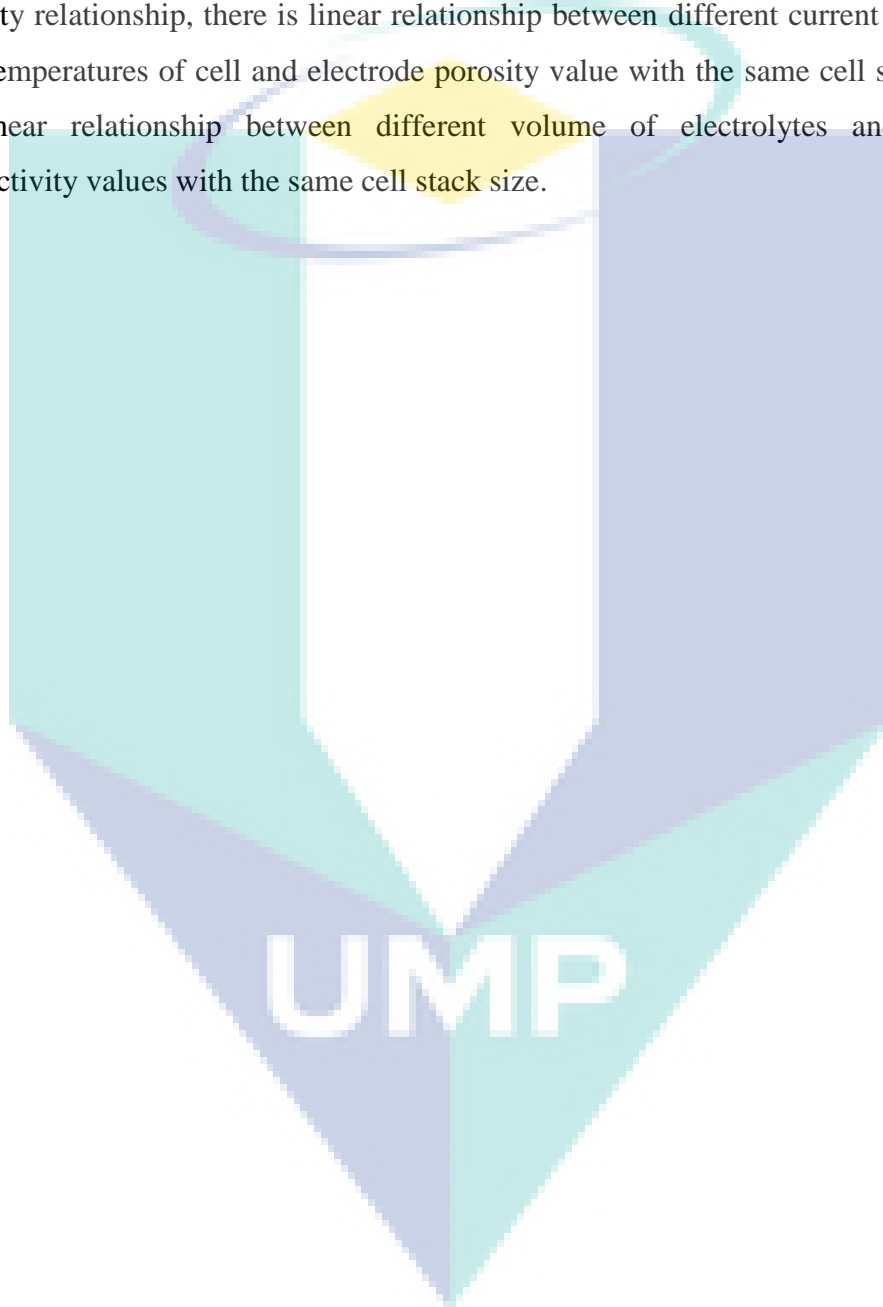
Figure 4.25 Relationship trend between cell voltage vs. different cell stack size (25, 56.25 and 100 cm²) for membrane conductivity of 5, 10 and 15 S/m.

On the other hand, the linearity modelling involving different sizes of cell stack with the same membrane conductivity value cannot be performed since it is in non-linear form and there are different ratios produced between each membrane conductivity value and different cell stack size. Thus, it can also be concluded that, there is no linear relationship between different cell stack sizes with the same membrane conductivity value.

4.4 Chapter Conclusion

As a conclusion, the lower the current density value, the higher the voltage efficiency of the VRFB. The higher the flow rate, volume of electrolyte and temperature

of cell value, the lower the voltage efficiency of cell. The increment in electrode porosity, membrane conductivity and size of cell stack increases the voltage efficiency. Hence, the best cell design for this project is 100 cm² with current density of 50 mA/cm², flow rate of 0.17 cm³/s, volume of electrolyte of 10 cm³, temperature of cell of 288.15 K, electrode porosity of 0.94 epsilon and membrane conductivity of 15 S/m. On the other hand, for linearity relationship, there is linear relationship between different current density, flow rate, temperatures of cell and electrode porosity value with the same cell stack size and no linear relationship between different volume of electrolytes and membrane conductivity values with the same cell stack size.



CHAPTER 5

CONCLUSION

5.1 Chapter Overview

This chapter presents the conclusion and recommendations made according to the results collected and discussed in the previous chapter. In this chapter, the conclusion will be discussed in the sub-chapter according to the objectives, while the following sub-chapter will discuss on the recommendations for the improvement of the VRFB system.

5.2 Conclusion

As a conclusion, the performance of VRFB depending on the different stack sizes (25 cm², 56.25 cm² and 100 cm²) of electrode compartments at different operating parameters (current density, flow rate, volume of electrolyte, temperature of cell, electrode porosity and membrane conductivity) is analysed by using COMSOL Multiphysics software. For current density parameter, the voltage efficiency decreased as current density increased from 50 mA/cm² to 100 mA/cm² and increased when the cell stack size increased from 25 cm² to 100 cm². For flow rates parameter, it is concluded that the voltage efficiency decreased slightly as the flow rate increased from 0.17 cm³/s to 0.83 cm³/s and increased slightly when the cell stack size increased from 25 cm² to 100 cm². For volume of electrolytes, it is also concluded that the voltage efficiency decreased slightly as the volume of electrolyte increased from 10 cm³ to 50 cm³ and increased slightly when the cell stack size increased from 25 cm² to 100 cm².

On the other hand, for temperature of cell parameter, it is found that the voltage efficiency decreased slightly as the cell temperature increased from 288.15 K to 298.15 K and increased when the cell stack size increased from 25 cm² to 100 cm². However, for

flow rates, volume of electrolytes and temperature of cell parameter, this result might only be true up to certain value only as there is another factor that can affect this. For electrode porosity, the voltage efficiency increased as the epsilon increased from 0.92 to 0.94 and increased when the cell stack size increased from 25 cm² to 100 cm². Finally, for the membrane conductivity parameter, the voltage efficiency increased as the membrane conductivity increased from 5 S/m to 15 S/m and increased when the cell stack size increased from 25 cm² to 100 cm².

The relationship between voltage efficiency and all operating parameter can further be simplified as Table 5.1 below:

Table 5.1 Relationship between voltage efficiency and operating parameter.

η_v decrease with increasing X, but η_v increase with increasing X and increase with increasing stack size for : increasing stack size for :

Current Density	Electrode Porosity
Flow Rates	Membrane Conductivity
Volume of electrolytes	
Temperature of Cell	

In where η_v is the voltage efficiency and X is the operating parameter.

Besides that, the relationship trend of VRFB at different sizes of electrode compartments were also investigated involving different operating parameter values which are current density, flow rate, volume of electrolytes, temperatures of cell, electrode porosity and membrane conductivity. For current density, flow rate, temperature of cell and electrode porosity parameter, it yielded a linear result as there existed same ratio produced between each operating parameter but with the same size of cell stack value. Thus, it can be concluded that, there was a linear relationship only between different current density, flow rate, temperatures of cell and electrode porosity value with the same cell stack size but there was no linear relationship between different cell stack sizes with the same current density, flow rate, temperatures of cell and electrode porosity value. On the other hand, the linearity modelling involving operating parameters of volume of

electrolytes and membrane conductivity with the cell stack size yields a non-linear result in either way. Thus, it can be concluded that, there was no linear relationship between different volume of electrolytes and membrane conductivity values with the same cell stack size and between different cell stack sizes with the same volume of electrolytes and membrane conductivity value.

The relationship trend between linearity and all operating parameter can also be further simplified as below:

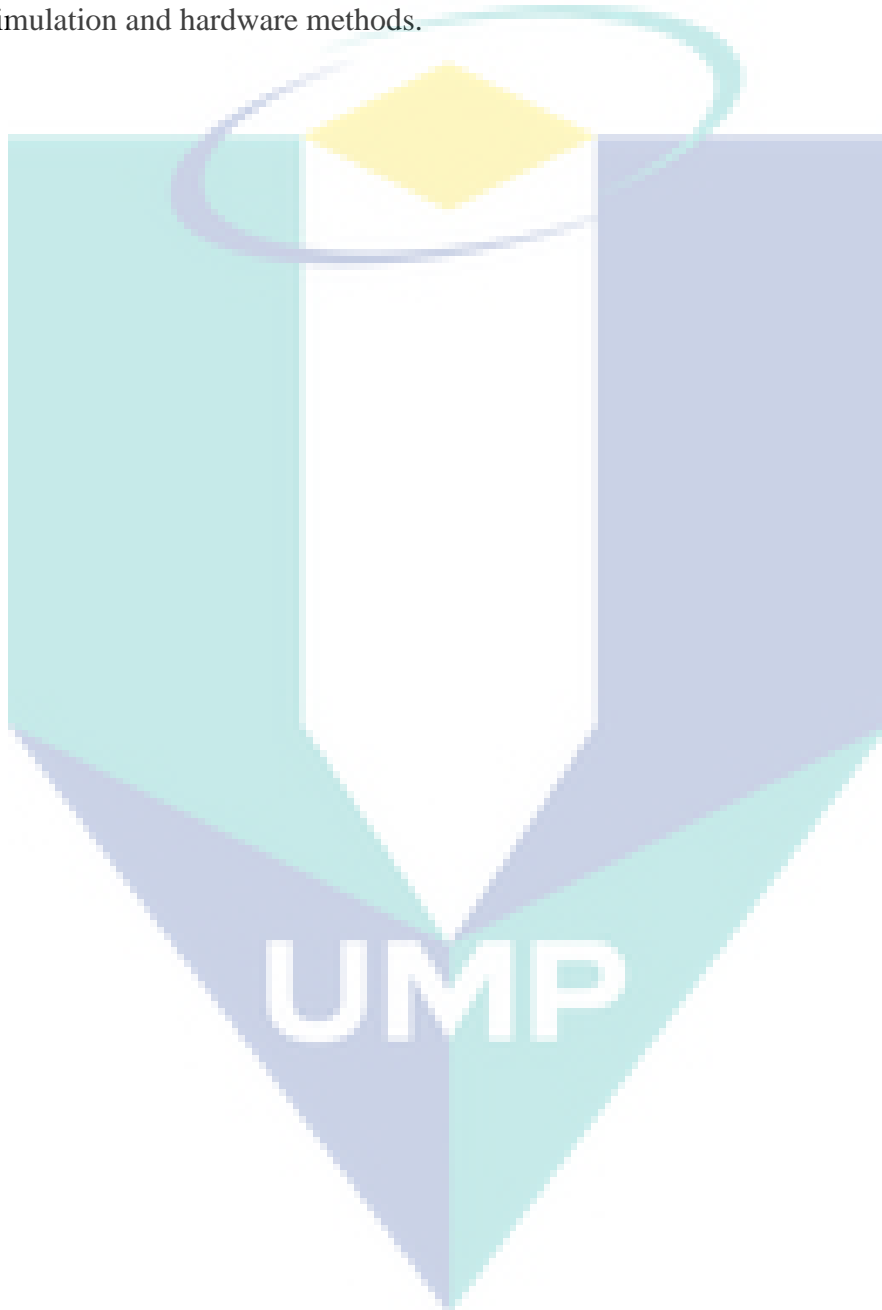
Table 5.2 Relationship trend between operating parameter and different stack size.

There is a linear relationship only between different X with the same stack size for :	There is no linear relationship between different X with the same stack size for :
Current Density	Volume of electrolytes
Flow Rates	Membrane Conductivity
Temperature of Cell	
Electrode Porosity	

5.3 Recommendation

This VRFB project is a promising platform for future research and experiments in this area. There are various chances for future growth of the VRFB in areas such as material selection, mechanical engineering, chemistry, electrochemistry and spectroscopy. A few topics that could potentially captivate researcher's interest is explained below. Although most of the effort in this area was dedicated to observe SOC of electrolyte using UV-Vis response technique, many other systems presence could possibly be faster and simpler. The electrolytes are noticed to have a different concentration of proton as the SOC changes, which makes it a prospective way to utilize electrolyte's pH of electrolyte as a benchmark. In addition, the electrolyte conductivity and OCV of battery changes linearly with SOC, making them a practical choice in monitoring the SOC. One of many electrochemical energy conversion technologies

presence is the VRFB. More research on organic and metal electrolytes also should be done. Presently, there are lots of research focusing on the development of new organic RFB such as quinone that could challenge with metal-base systems. Other than that, other recommendation for future work is to repeat the same experiment for this simulation but by using hardware implementation to see if the results obtained would be the same for both simulation and hardware methods.



REFERENCES

- Aaron, D. S., Liu, Q., Tang, Z., Grim, G. M., Papandrew, a. B., Turhan, a., ... Mench, M. M. (2012). Dramatic performance gains in vanadium redox flow batteries through modified cell architecture. *Journal of Power Sources*, 206, 450–453. <https://doi.org/10.1016/j.jpowsour.2011.12.026>
- Abbas A. Akhil, Georgianne Huff, Aileen B. Currier, Benjamin C. Kaun, D. M. R., & Stella Bingqing Chen, Andrew L. Cotter, Dale T. Bradshaw, and W. D. G. (2013). DOE/EPRI 2013 Electricity **Storage Handbook** in Collaboration with NRECA.
- Alotto, P., Guarnieri, M., & Moro, F. (2014). Redox flow batteries for the storage of renewable energy : A review. *Renew Sustain Energy Rev*, 29, 325–335. <https://doi.org/10.1016/j.rser.2013.08.001>
- Atkinson, K., Han, W., & Stewart, D. (2009). Numerical Solution of Ordinary Differential Equations. John Wiley & Sons Inc. <https://doi.org/10.1002/9781118164495>
- Barsukov, Y. (2013). Flow batteries get popular... again. Retrieved from https://e2e.ti.com/blogs_/archives/b/fullycharged/archive/2013/09/20/flow-batteries-get-popular-again-part-1
- Boaventura, M., Monteiro, R., & Leir, J. (2018). Insights into all-vanadium redox flow battery : A case study on components and operational conditions. *Electrochimica Acta*, 267, 80–93. <https://doi.org/10.1016/j.electacta.2018.02.054>
- Chen, H., Ngoc, T., Yang, W., Tan, C., & Li, Y. (2009). Progress in electrical energy storage system : A critical review. *Progress in Natural Science*, 19(3), 291–312. <https://doi.org/10.1016/j.pnsc.2008.07.014>
- Chen, Q., Eisenach, L., & Aziz, M. J. (2016). Cycling Analysis of a Quinone-Bromide Redox Flow Battery. *Journal of the Electrochemical Society*, 163(1), 5057–5063. <https://doi.org/10.1149/2.0081601jes>
- Chng Mei Lin. (2018). Membranes for Redox Flow Batteries. ScholarBank@NUS Repository. Retrieved from <http://scholarbank.nus.edu.sg/handle/10635/139096>
- Choi, C., Kim, S., Kim, R., Choi, Y., Kim, S., Jung, H., ... Kim, H. (2017). A review of vanadium electrolytes for vanadium redox flow batteries. *Renewable and Sustainable Energy Reviews*, 69(March), 263–274. <https://doi.org/10.1016/j.rser.2016.11.188>
- Climate Change – The Science. (2014). Retrieved January 11, 2016, from <http://www.world-nuclear.org/info/Energy-and-Environment/Climate-Change---The-Science/>
- Davies, T. J., & Tummino, J. J. (2018). High-Performance Vanadium Redox Flow

- Batteries with Graphite Felt Electrodes. *C Journal of Carbon Research*, 4(1), 8.
<https://doi.org/10.3390/c4010008>
- De Bock, D. . V. D. W. J. D. et al. (2002). Improper use of linear reasoning: an in-depth study of the nature and the irresistibility of secondary school students' errors. *Educational Studies in Mathematics*, (50), 311–334.
<https://doi.org/https://doi.org/10.1023/A:1021205413749>
- Dekka, A., Ghaffari, R., & Venkatesh, B. B. W. (2015). A Survey on Energy Storage Technologies in Power Systems. *Proc 2015, IEEE Electrical Power and Energy Conference (EPEC)*, London, UK, 105–111.
- Denholm, P., Ela, E., Kirby, B., & Milligan, M. (2010). *The Role of Energy Storage with Renewable Electricity Generation*. Golden, CO: National Renewal Energy Laboratory, (January).
- Dickinson, E. J. F., & Hinds, G. (2019). The Butler-Volmer Equation for Polymer Electrolyte Membrane Fuel Cell (PEMFC) Electrode Kinetics : A Critical Discussion, 166(4). <https://doi.org/10.1149/2.0361904jes>
- European Commission Directorate-General for Energy. (2013). *The future role and challenges of Energy Storage*, 1–36. Retrieved from http://ec.europa.eu/energy/infrastructure/doc/energy-storage/2013/energy_storage.pdf
- Fessler, D. (2015). *The Fastest-Growing Energy Sector of 2015 and Beyond*. Retrieved January 12, 2016, from <http://www.investментu.com/article/detail/46174/solar-wind-renewables-fastest-growing-energy-sector#.VpNshPI97IU>
- General Dr. Mohamed ElBaradei. (2014). *Nuclear Power: Looking to the Future*. Retrieved December 20, 2015, from <https://www.iaea.org/newscenter/statements/nuclear-power-looking-future-0>
- Hamelet, S., Tzedakis, T., Leriche, J.-B., Larcher, D., Taberna, P., & Simon, P. (2012). Non-Aqueous Li-Based Redox Flow Batteries. *Journal of the Electrochemical Society*, 159, A1360–A1367. <https://doi.org/10.1149/2.071208jes>
- Hasan, M. H. (2014). A review of available methods and development on energy storage ; Technology update. *Renewable and Sustainable Energy Reviews*, 33(May), 532–545. <https://doi.org/10.1016/j.rser.2014.01.068>
- Houcque, D. (2005). *Introduction to Matlab for Engineering Students*, (August).
- Hsieh, W., Leu, C., Wu, C., & Chen, Y. (2014). Measurement of local current density of all-vanadium redox flow batteries. *Journal of Power Sources*, 271, 245–251.
<https://doi.org/10.1016/j.jpowsour.2014.06.081>
- Huang, K., Li, X., Liu, S., Tan, N., & Chen, L. (2008). Research progress of vanadium redox flow battery for energy storage in China. *Renewable Energy*, Elsevier,

33(2), 186–192. <https://doi.org/10.1016/j.renene.2007.05.025>

International Energy Agency. (2014). *Technology Roadmap - Energy Storage* (40th ed.).

Knehr, K. W., Agar, E., Dennison, C., & Kalidindi, A. R. (2012). A Transient Vanadium Flow Battery Model Incorporating Vanadium Crossover and Water Transport through the Membrane [Email alerting service](#). *The Electrochemical Society*, 159(9), A1446–A1459. <https://doi.org/10.1149/2.017209jes>

L.H. Thaller. (1974). Electrically rechargeable redox flow cells. In *Proceedings of the 9th Intersociety Energy Conversion Engineering Conference*. San Francisco, California, U.S.A.

Le, C. P. De, & Walsh, F. C. (2006). Redox flow cells for energy conversion. *Journal of Power Sources*, 160, 716–732. <https://doi.org/10.1016/j.jpowsour.2006.02.095>

Leung, P. K., Leon, C. P. De, & Walsh, F. C. (2012). *Electrochimica Acta* The influence of operational parameters on the performance of an undivided zinc – cerium flow battery. *Electrochimica Acta*, 80, 7–14. <https://doi.org/10.1016/j.electacta.2012.06.074>

Luo, X., Wang, J., Dooner, M., & Clarke, J. (2015). Overview of current development in electrical energy storage technologies and the application potential in power system operation. *Applied Energy*, 137, 511–536. <https://doi.org/10.1016/j.apenergy.2014.09.081>

Maggiolo, D., Zanini, F., Picano, F., & Trov, A. (2018). Particle based method and X-ray computed tomography for pore-scale flow characterization in VRFB electrodes. *Energy Storage Materials*, 16(April), 91–96. <https://doi.org/10.1016/j.ensm.2018.04.021>

Massachusetts Institute of Technology. (2003). *The Future of Nuclear Power, 2020*, 1–28. Retrieved from <http://web.mit.edu/nuclearpower/pdf/nuclearpower-full.pdf>

Milena Gonzales and Matt Lucky. (2013). *Fossil Fuels Dominate Primary Energy Consumption*. Retrieved January 10, 2016, from <http://www.worldwatch.org/fossil-fuels-dominate-primary-energy-consumption-1>

Mohamed, M. R. (2013). *Experimental Characterisation and Modeling of a Vanadium Redox Flow Battery*. Universiti Malaysia Pahang (UMP). Retrieved from <http://umpir.ump.edu.my/id/eprint/4934/>

Mohamed, M. R., Leung, P. K., & Sulaiman, M. H. (2015). Performance characterization of a vanadium redox flow battery at different operating parameters under a standardized test-bed system. *Applied Energy*, 137, 402–412.

<https://doi.org/10.1016/j.apenergy.2014.10.042>

- Nathan Quill; Robert P. Lynch; Xin Gao and D. Noel Buckley. (2014). Coulombic Efficiency of Negative and Positive Half-Cells in a Vanadium Redox Flow Cell. *The Electrochemical Society*, 14–01, 389.
- Navalpotro, P., Palma, J., Anderson, M., & Marcilla, R. (2017). A Membrane-Free Redox Flow Battery with Two Immiscible Redox Electrolytes. *Angewandte Chemie International Edition*, 57(15), 12460–12465.
<https://doi.org/10.1002/anie.201704318>
- Ouvrard, G., Bourgeon, N., Bieda, M., Kawalko, J., Machacek, J. R., & Tattersall, W. (2017). Advanced characterization of lithium battery materials with positrons. *Journal of Physics Conference Series*, 791(1), 012016.
<https://doi.org/10.1088/1742-6596/755/1/011001>
- Pai, F., Yeh, T., & Hung, Y. (2015). Analysis on Accuracy of Bias, Linearity and Stability of Measurement System in Ball screw Processes by Simulation. *Sustainable Engineering and Science*, 7(11), 15464–15486.
<https://doi.org/10.3390/su71115464>
- Parasuraman, A., Mariana, T., Menictas, C., & Skyllas-kazacos, M. (2013). Electrochimica Acta Review of material research and development for vanadium redox flow battery applications. *Electrochimica Acta*, 101, 27–40.
<https://doi.org/10.1016/j.electacta.2012.09.067>
- Peter, C., & Jack, V. (2009). SAS Global Forum 2009 Statistics and Data Analysis Test for linearity between continuous confounder and binary outcome first , run a multivariate regression analysis second Jiming Fang , Peter C . Austin , Jack V . Tu SAS Global Forum 2009, 1–8.
- Poullikkas, A. (2017). A comparative overview of large-scale battery systems for electricity storage. *Renewable and Sustainable Energy Reviews*, 27(January 2013), 778–788. <https://doi.org/10.1016/j.rser.2013.07.017>
- Prifti, H., Parasuraman, A., Winardi, S., Lim, T. M., & Skyllas-Kazacos, M. (2012). Membranes for Redox Flow Battery Applications. *Membranes*, 2(4), 275–306.
<https://doi.org/10.3390/membranes2020275>
- Rosin, A., & Tallinn, V. (2012). Energy storages.
- Schaber, Christopher & Mazza, Patrick & Hammerschlag, R. (2004). Utility-Scale Storage of Renewable Energy. *The Electricity Journal*, Elsevier, 17(6)(July), 21–29.
- Seepana, M. M. (2018). Unit Cell Modelling and Simulation of All Vanadium Redox Flow Battery. *Chemical Product and Process Modeling*, 13(1), 1–11.
<https://doi.org/10.1515/cppm-2017-0014>

- Shafie, S. M., Mahlia, T. M. I., Masjuki, H. H., & Andriyana, A. (2011). Current energy usage and sustainable energy in Malaysia: A review. *Renewable and Sustainable Energy Reviews*, 15(9), 4370–4377. <https://doi.org/10.1016/j.rser.2011.07.113>
- Shah, A. A., & Walsh, F. C. (2008). A dynamic performance model for redox-flow batteries involving soluble species. *Electrochimica Acta*, 53(27), 8087–8100. <https://doi.org/10.1016/j.electacta.2008.05.067>
- Shi, F. (2014). *Reactor and Process Design in Sustainable Energy Technology 1st Edition*.
- Shigematsu, T. (2011). Redox flow battery for energy storage. *SEI Technical Review*, (73), 4–13. <https://doi.org/10.1149/1.3492325>
- Simpson, C. (2011). *Characteristics of Rechargeable Batteries*. (T. I. Incorporated, Ed.). <https://doi.org/http://www.ti.com/lit/an/snva533/snva533.pdf>
- Skyllas-kazacos, M., & Kazacos, M. (2011). State of charge monitoring methods for vanadium redox flow battery control. *Journal of Power Sources*, 196(20), 8822–8827. <https://doi.org/10.1016/j.jpowsour.2011.06.080>
- Skyllas Kazacos M, Chakrabarti MH, Hajimolona SA, Mjalli FS, S. M. (2011). Progress in Flow Battery Research and Development. *J Electrochemistry Society*, 55–79.
- Stroe, D., Swierczynski, M., Stroe, A., & Kær, S. K. (2016). Generalized Characterization Methodology for Performance Modelling of Lithium-Ion Batteries. *Batteries*, 2(4), 37. <https://doi.org/10.3390/batteries2040037>
- Sukkar, T., & Skyllas-Kazacos, M. (2004). Membrane stability studies for vanadium redox cell applications. *Journal of Applied Electrochemistry*, 34, 137–145. <https://doi.org/10.1023/B:JACH.0000009931.83368.dc>
- Tang, A., Bao, J., & Skyllas-kazacos, M. (2012). Thermal modelling of battery configuration and self-discharge reactions in vanadium redox flow battery. *Journal of Power Sources*, 216, 489–501. <https://doi.org/10.1016/j.jpowsour.2012.06.052>
- Tang, Z. (2012). Monitoring the State of Charge of Operating Vanadium Redox Flow Batteries Zhijiang Tang. *Journal of the Electrochemical Society*, 41(23), 1–9.
- Tang, Z. (2013). *Characterization Techniques and Electrolyte Separator Performance Investigation for All Vanadium Redox Flow Battery*. University of Tennessee - Knoxville. Retrieved from https://trace.tennessee.edu/utk_graddiss/2620
- Tang, Z., Svoboda, R., Lawton, J. S., Aaron, D. S., Papandrew, A. B., & Zawodzinski, T. A. (2013). Composition and Conductivity of Membranes Equilibrated with Solutions of Sulfuric Acid and Vanadyl Sulfate. *The Electrochemical Society*, 160(9), 1040–1047. <https://doi.org/10.1149/2.083309jes>

- Teng, X., Dai, J., Bi, F., & Yin, G. (2014). Ultra-thin polytetra fluoroethene / Nafion / silica composite membrane with high performance for vanadium redox flow battery. *Journal of Power Sources*, 272, 113–120. <https://doi.org/10.1016/j.jpowsour.2014.08.060>
- Trovò, A., Marini, G., Sutto, A., Alotto, P., & Giomo, M. (2019). Standby thermal model of a vanadium redox flow battery stack with crossover and shunt-current effects Standby thermal model of a VRFB stack with crossover and shunt-current effects Introduction, (March). <https://doi.org/10.1016/j.apenergy.2019.02.067>
- U.S. Energy Information Agency. (2013). *International Energy Outlook 2013*. Outlook 2013, 312. [https://doi.org/EIA-0484\(2013\)](https://doi.org/EIA-0484(2013))
- Verma, H., Gambhir, J., & Goyal, S. (2013). Energy Storage : A Review. *International Journal of Innovative Technology and Exploring Engineering (IJITEE)*, 3(1), 63–69.
- Walsh, F. C., & Zhang, C. (2011). The performance of a soluble lead-acid flow battery and its comparison to a static lead-acid battery. *Energy Conversion and Management*, (November 2011), 3391–3398. <https://doi.org/10.1016/j.enconman.2011.07.006>
- Weber, A. Z., Mench, M. M., Meyers, J. P., Ross, P. N., Gostick, J. T., & Liu, Q. (2011). Redox flow batteries : a review. *Journal of Applied Electrochemistry*, 41, 1137–1164. <https://doi.org/10.1007/s10800-011-0348-2>
- Wei, L., Zhao, T. S., Zhao, G., An, L., & Zeng, L. (2016). A high-performance carbon nanoparticle-decorated graphite felt electrode for vanadium redox flow batteries. *Applied Energy*, 176(C), 74–79. <https://doi.org/10.1016/j.apenergy.2016.05.048>
- Wei Wang, Qingtao Luo, Bin Li, Xiaoliang Wei, Liyu Li, Z. Y. (2013). Recent progress in Redox Flow Battery Research and Development. *Advanced Functional Materials*, 23, 970–986.
- World Energy Needs and Nuclear Power. (2015). Retrieved January 10, 2016, from <http://www.world-nuclear.org/info/Current-and-Future-Generation/world-Energy-Needs-and-nuclear-power/>
- Xinyou Ke; Joseph M. Prael; J.Iwan D. Alexander; Robert F. Savinell. (2016). Mathematical Modeling of Electrolyte Flow Dynamic Patterns and Volumetric Flow Penetrations in the Flow Channel over Porous Electrode Layered System in Vanadium Flow Battery with Serpentine Flow Field Design. *Electrochimica Acta*, 223, 124–134. Retrieved from <https://ui.adsabs.harvard.edu/abs/2016arXiv161006171K>
- Xu, F., Li, H., Liu, Y., & Jing, Q. (2017). Advanced redox flow fuel cell using ferric chloride as main catalyst for complete conversion from carbohydrates to electricity. *Scientific Reports*, (May), 1–9. <https://doi.org/10.1038/s41598-017-05535-2>

- Xu, Q., Zhao, T. S., & Zhang, C. (2014a). Effects of SOC-dependent electrolyte viscosity on performance of vanadium redox flow batteries. *Applied Energy*, 130, 139–147. <https://doi.org/10.1016/j.apenergy.2014.05.034>
- Xu, Q., Zhao, T. S., & Zhang, C. (2014b). Performance of a vanadium redox flow battery with and without flow fields. *Electrochimica Acta*, 142, 61–67. <https://doi.org/10.1016/j.electacta.2014.07.059>
- Zeng, Y. K., Zhao, T. S., An, L., Zhou, X. L., & Wei, L. (2015). A comparative study of all-vanadium and iron-chromium redox flow batteries for large-scale energy storage. *Journal of Power Sources*, 300, 438–443. <https://doi.org/10.1016/j.jpowsour.2015.09.100>
- Zhang, C., Zhao, T. S., Xu, Q., An, L., & Zhao, G. (2015). Effects of operating temperature on the performance of vanadium redox flow batteries. *Applied Energy*, 155, 349–353. <https://doi.org/10.1016/j.apenergy.2015.06.002>
- Zhang, L., Shao, Z., Wang, X., Yu, H., & Liu, S. (2013). The characterization of graphite felt electrode with surface modification for H₂ / Br₂ fuel cell. *Journal of Power Sources*, 242, 15–22. <https://doi.org/10.1016/j.jpowsour.2013.05.049>
- Zhao, P., Zhang, H., Zhou, H., & Yi, B. (2005). Nickel foam and carbon felt applications for sodium polysulfide / bromine redox flow battery electrodes. *Electrochimica Acta*, 51, 1091–1098. <https://doi.org/10.1016/j.electacta.2005.06.008>
- Zhou, H., Zhang, H., Zhao, P., & Yi, B. (2006). A comparative study of carbon felt and activated carbon based electrodes for sodium polysulfide / bromine redox flow battery. *Electrochimica Acta*, 51, 6304–6312. <https://doi.org/10.1016/j.electacta.2006.03.106>
- Zhou, X. L., Zhao, T. S., An, L., Zeng, Y. K., & Zhu, X. B. (2016). Performance of a vanadium redox flow battery with a VANADion membrane. *Applied Energy*, 180, 353–359. <https://doi.org/10.1016/j.apenergy.2016.08.001>
- Zimmerman, N. (2014). Sizing of VRB in electrified heavy construction equipment. Mälardalen University. Retrieved from <http://www.diva-portal.org/smash/record.jsf?pid=diva2%3A772090&dswid=5378>

APPENDIX A

INTRODUCTION TO COMSOL MULTIPHYSICS

For this section, the software used in this project will be discussed. COMSOL Multiphysics is a general purpose platform software for modelling engineering applications. There are a few add-on modules available for this software such as structural mechanics, electromagnetics, fluid flow, acoustics, heat transfer, and chemical engineering behaviour. When simulating a design, the core module from library application can be used. Otherwise, another way for simulating the design is by combining a few add-on modules to create a new modelling with its own functionality. There are up to 40 versions that has been released for COMSOL software from 1998 up to date, however, for this project, COMSOL Multiphysics 5.2a version is used as there is an easy access available for it and also with the fact that it is among the newest version of COMSOL available.

The modelling process in this software consists of seven main steps which are: drawing the model geometry based on a two-dimensional space, adding the parameters, functions and variable needed before defining it to the geometry sketch, selecting the appropriate material and mesh for the geometry, adding suitable Multiphysics application mode needed for the project, inserting a suitable study involved for analysing the application, setting up the subdomain equations and boundary conditions, and solving the convergence issue before post processing the results.

Figure A1 shows the front panel of the COMSOL Multiphysics. The model builder includes parameters of VRFB cell, materials, components involved and study section located on the most left part with the properties and setting section in the middle, while graphics section that shows the geometry and graphs positioned in the rightest section.

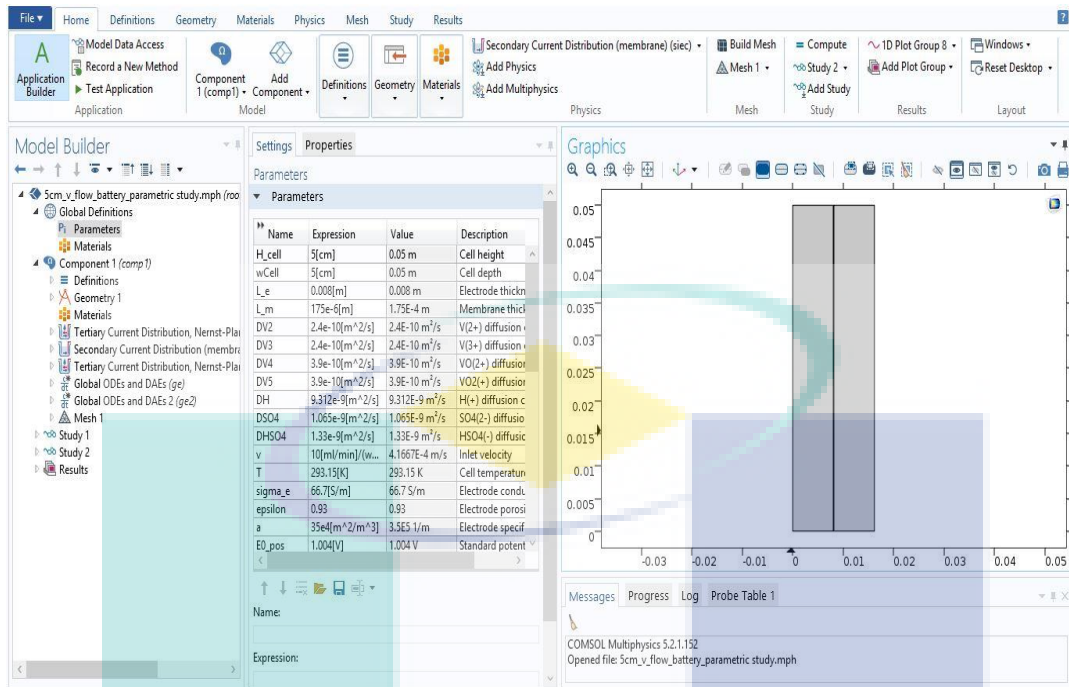
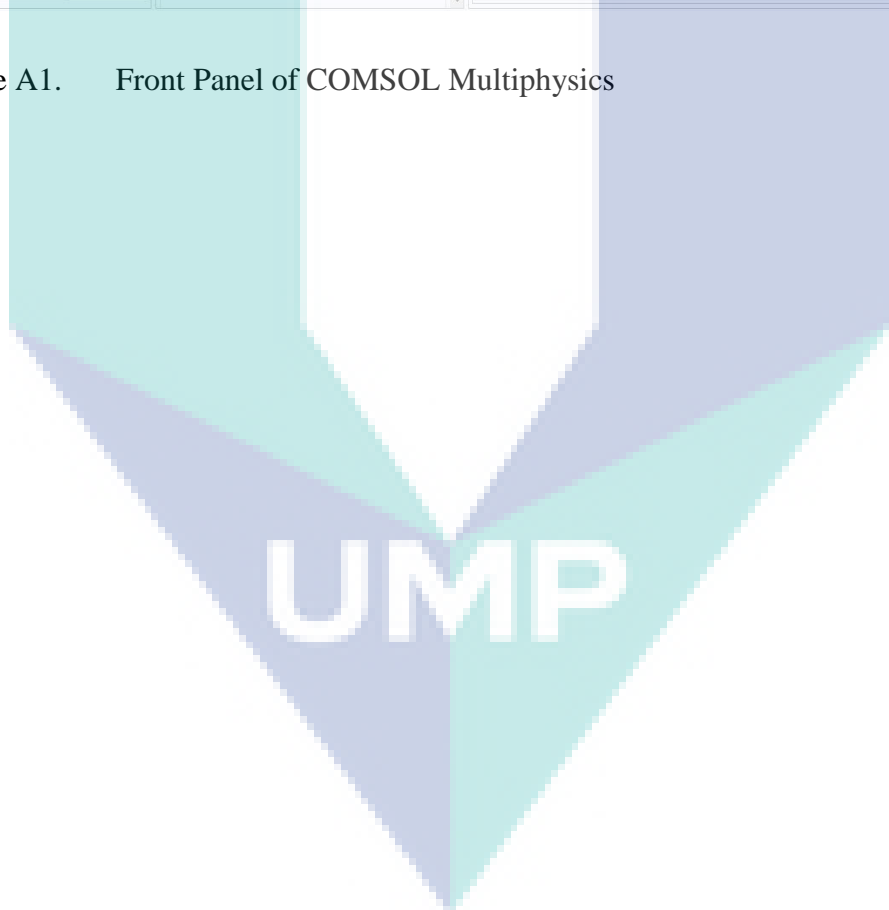


Figure A1. Front Panel of COMSOL Multiphysics



APPENDIX B

GEOMETRY DRAWING

For the steps to draw the geometry, note that the geometry will be a union of three rectangles, the two porous electrodes and the membrane domains. Firstly, on the toolbar of Geometry, choose Primitives section and click on Rectangle as shown in Figure .

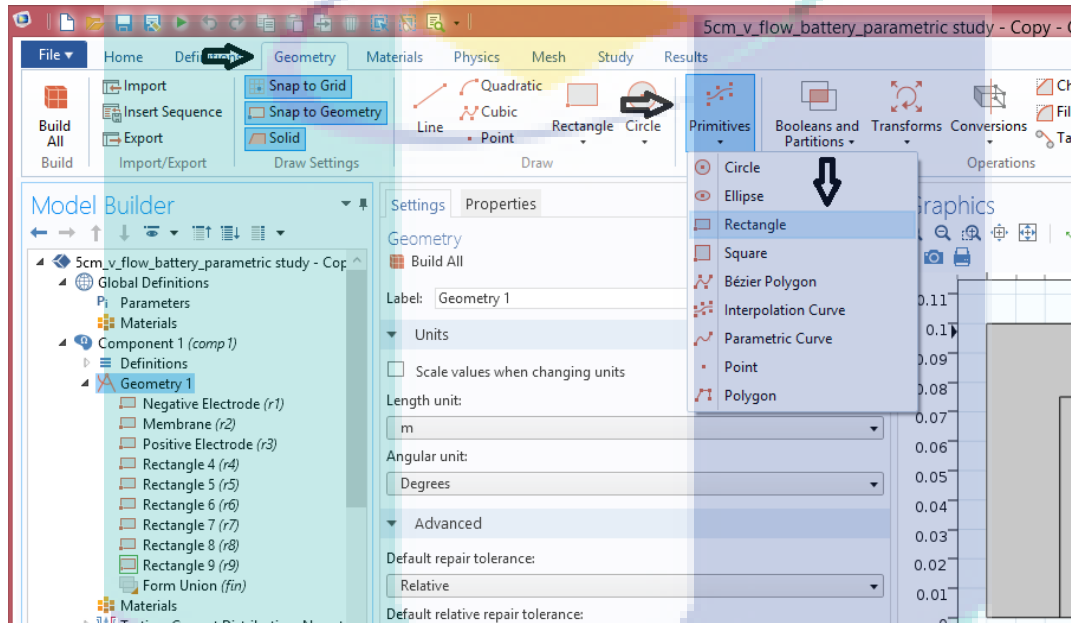


Figure B1. Step to draw cell geometry

In the Rectangle Settings window, find the Size and Shape component and add the measurement required for electrode geometry and membrane geometry. Next, find the section of Selections of Resulting Entities and click on the Resulting objects selection box as shown in Figure .

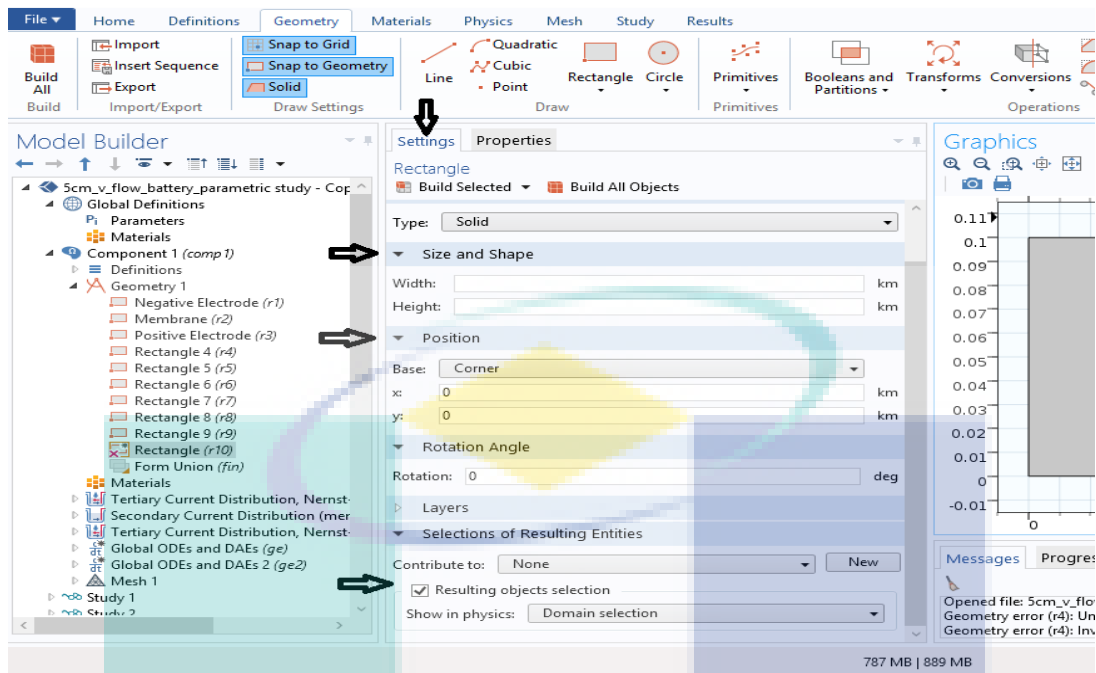


Figure B2. Step to insert measurement of cell geometry

Following from there, the rectangle can be labelled as Negative Electrode. Repeat the same step for the second and third rectangle but rename it with membrane and Positive Electrode.

UMP

APPENDIX B

ADDING PARAMETERS, BOUNDARY CONDITION AND MESH

For section of global definitions, the parameter model from a text file is added. To do that, firstly, on the toolbar of Home, click on Parameters. Next, in the Parameters Settings window, spot the Parameters part. After that, click on Load from File and browse to the application's Application Libraries folder and select the filev_flow_battery_parameters.txt. to add the file into the parameter section as in Figure .

For definitions of each component of the battery, similar steps are applied, however, only the file uploaded in here is for analytic function for the negative electrode, membrane and positive electrode.

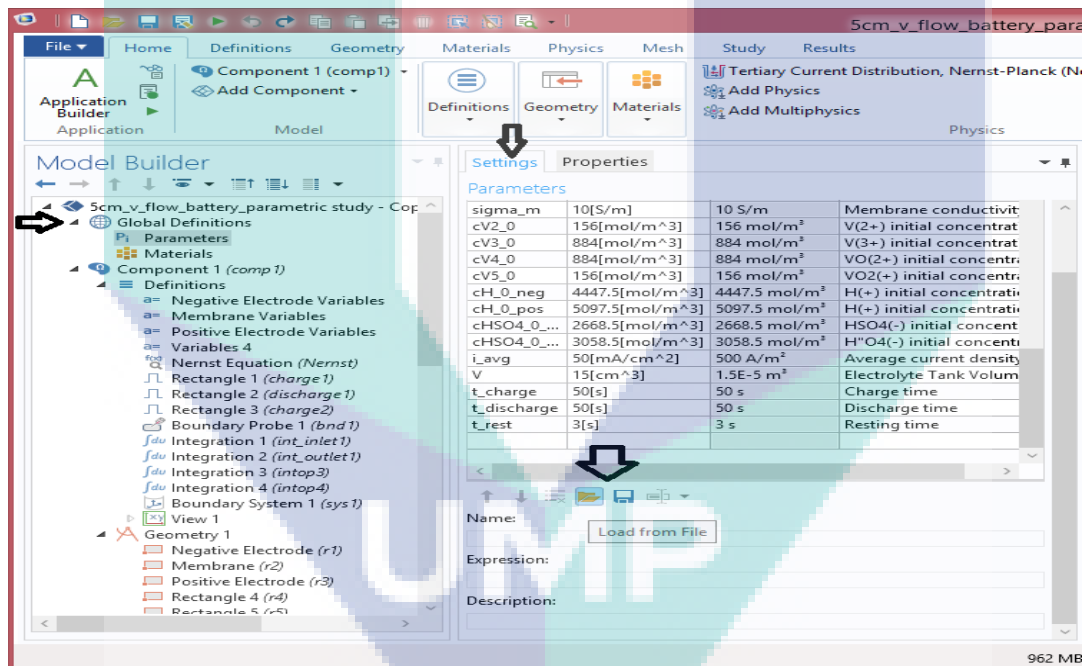


Figure C1. Step to upload the parameters of VRFB from model library

After that, in order to create a mapped mesh with higher resolution in the porous electrodes toward the membrane, in the window of Model Builder under Component 1 (comp1), right-click Mesh 1 and select Mapped component as shown in Figure .

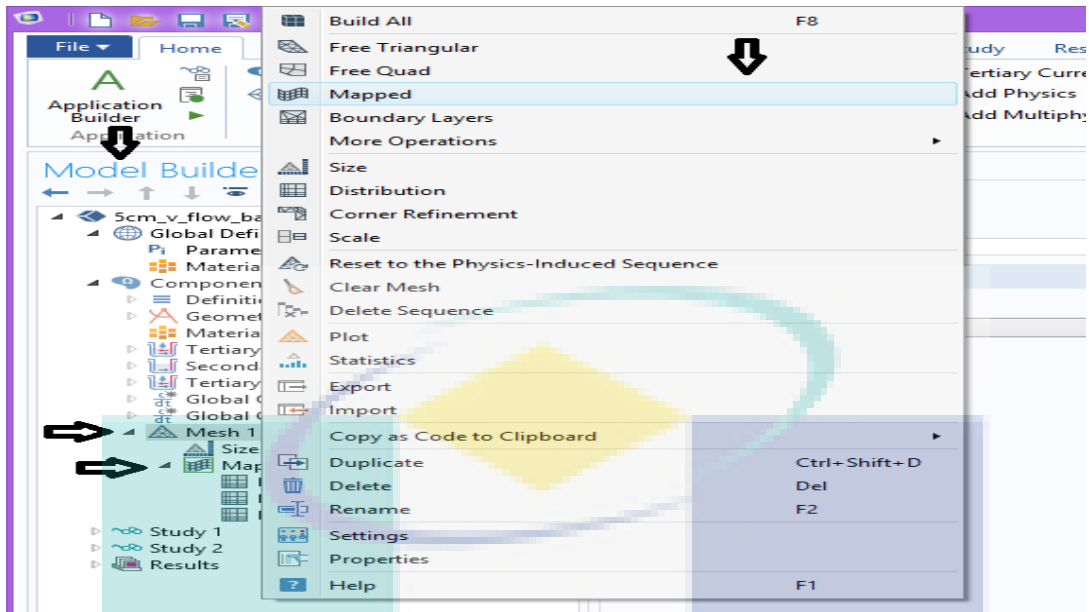


Figure C2. Step to create mesh for VRFB

Next, for Mapped 1 subsection, in the window of Model Builder, repeat the same steps as before but only under Component 1 (comp1) > Mesh 1, select Mapped 1 and click Distribution. After that, under distribution 1 subsection, choose only Boundaries 5 and 6. In the Distribution Settings window, spot the Distribution component and the Number of elements text field, type 3 as in Figure .

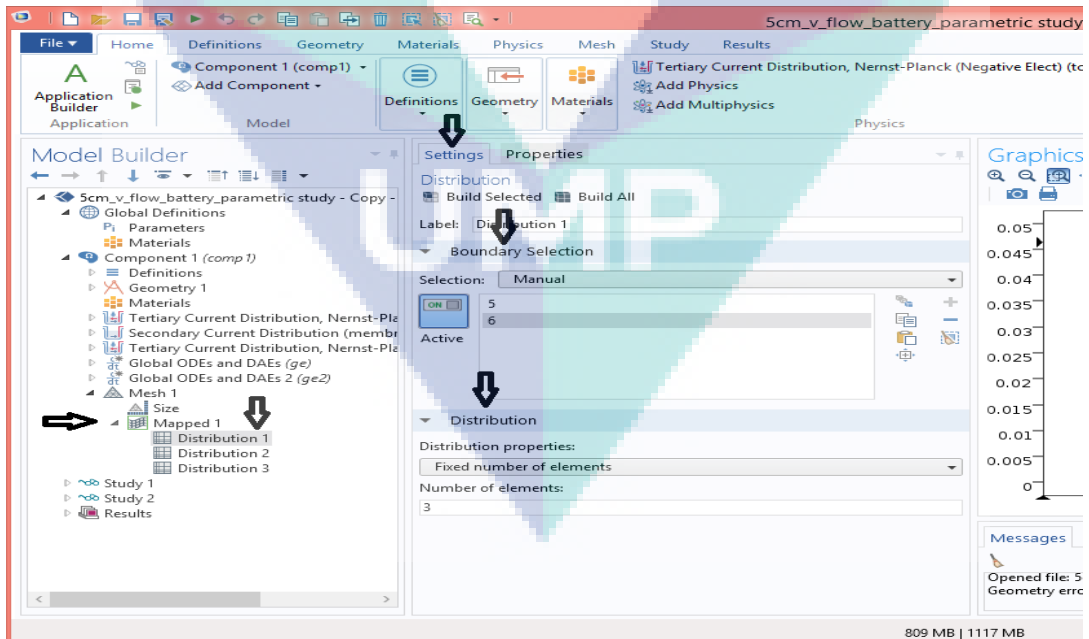


Figure C4. Step to add boundary conditions in mesh for VRFB

For Distribution 2 subsection, steps similar to Distribution 1 subsection are repeated but only Boundaries 2 and 3 are selected in the boundary selection. Next, Distribution section is located and Predefined distribution type is chosen instead. In the Number of elements text field, enter 40 while in the Element ratio text field, enter 20. For Distribution 3 subsection, duplicate Distribution 2 and in the Boundary Selection section, select Boundaries 8 and 9 only. Spot the section of Distribution as well and click on the Reverse direction box. Lastly, click build all to build the mesh for the geometry.

